심리학박사 학위논문

Neural Activities of Monkey Primary Visual Cortex: Contextual Modulation and Roles for Initiation of Saccadic Eye Movements

원숭이 1차시각피질의 신경활동: 맥락에 따른 활동수준조절과 안구운동 발생에서의 역할

2015 년 8 월

서울대학교 대학원

심리학과 생물심리 전공

김 가 연

Neural Activities of Monkey Primary Visual Cortex: Contextual Modulation and Roles for Initiation of Saccadic Eye Movements

지도 교수 이 춘 길

이 논문을 심리학박사 학위논문으로 제출함

2015 년 8 월

서울대학교 대학원

심리학과 생물심리 전공

김 가 연

김가연의 심리학박사 학위논문을 인준함

2015 년 8 월

위 원 장 김 청 택 (인)

부위원장 이 춘 길 (인)

위 원 오 성 주 (인)

위 원 정 상 철 (인)

위 원 이 상 훈 (인)

Abstract

Kim, Kayeon

Psychology in Social Science

The Graduate School

Seoul National University

The primary visual cortex (V1) is a major cortical area for central visual processing. The neural activities of V1 are evoked by the stimulus presented within the receptive field (RF), but various contexts also dynamically modulate its response. Understanding the dynamic modulation and its neural bases in visual processing are important and yet, the precise neural mechanisms within V1 are not completely known.

In this thesis, three studies reveal that primary visual cortex shows dynamic modulations from different levels of contexts involved in perceptual and cognitive processes, which significantly contribute to the activity within V1. I particularly focused on the modulation of V1 activity in relation to the initiation of saccadic eye movement by recording and analyzing single and multiple unit activities and local field potential (LFP) in task-performing macaque monkeys.

In the first study, I examined how the stimulus outside the RF modulates

cell's response to the stimulus within the RF. I analyzed the signal characteristics of spike and LFP evoked by Gabor patches inside and outside the RF. As known previously, when a Gabor stimulus was presented in the RF surround region, it did not evoke spike response, and yet LFP response was robustly induced. This subthreshold (sLFP) induced from surround stimulus alone showed weaker signal power with longer peak latency as the surround stimulus was presented farther away from the RF. It was also found that spike activity in response to the RF center stimulus was modulated by surround stimulus at the stimulus onset asynchrony (SOA) of 0 to 100ms, and this modulation was coupled to the magnitude of LFP change that was simultaneously recorded. The results indicated that the sLFP evoked by the surround stimulus contributed to the modulation of spike activity, and that the contribution varied according to cortical depth.

In the second study, modulation of V1 spike activity was examined during gap saccade task in which a temporal gap from fixation target offset to saccade target onset reduces saccadic latency, so-called gap effect. Modulation of V1 activity accompanying the gap effect may be compatible with the hypothesis that fixation offset represents an event in the RF surround and thus V1 response to appearance of a saccade target inside the RF is modulated by this fixation offset event. As the gap duration increased, saccadic latency and neural latency decreased, and firing rate increased. Also, introducing gap changed the state of V1 cortex by the time of target onset as revealed in LFP signals, implying an important contribution of V1 for saccadic initiation. Additionally, the occurrences of express and regular latency saccades were linked with V1 activity level; the V1 activity during both before and

after saccade target onset time differed between express and regular latency saccade groups.

In the last study, modulation of V1 activity by high-level processes was directly studied by manipulating the level of expectation regarding the timing of saccade target onset. Monkeys were trained to associate the color of fixation target (red or green) with the level of temporal expectation (high or low) regarding upcoming target onset. In high expectation condition in which saccade target was present at a fixed interval into central fixation, spontaneous discharge of V1 prior to target onset was reduced compared to low expectation conditions in which saccade target was presented after a variable duration of central fixation, thus target timing was relatively less predictable. The reduced pre-target spike activity in the high expectation condition correlated with faster reaction times. Also intriguingly, there was a rebound of spike activity after reduction, which is likely to facilitate target detection, enhancing temporal contrast of target information and thereby shortening response latency by downstream stages.

Keywords: visual cortex, local field potential, single-cell recording, saccadic eye movement, response time, spontaneous variability

Student Number: 2009-20135

Contents

Contents of Table

Contents of Figures

Purpose of the study

In central visual system, primary visual cortex (V1) has been widely studied for visual information processes (Nassi & Callaway, 2009). One of the important issues in the processes within V1 is that the neural activities are highly context-dependent. In fact, we perceive and recognize one thing differently depending on the backgrounds of the scene itself or the level of attention on the object (Baluch & Itti, 2011; Todorović, 2010). Upon the issue, one big question remains; how would neurons in V1 deal with context dependency? It sounds simple, but investigating such processes comes along with a complexity and concerns in between internally ongoing states of physical system and externally stimulating assets of information.

In order to answer parts of the big question above, I have done three independent studies with a specific question for each study regarding dynamics of V1 activity starting from low-level to high-level context dependent processes. Those questions include; 1) How V1 activities are modulated between stimuli that are separated in space and time domains and what is the underlying mechanism of the modulation? 2) As being a brain region where given visual information is primarily reached, would the activity modulation in V1 show as much change along the dynamics in behavioral outcome? 3) Although primarily sensory, how would high-level context, especially expecting the time of upcoming stimulus modulate V1

activities?

Throughout the studies in this thesis, it involved intensive analysis and interpretation from the results using two different signals, which are spike activity and local field potential (LFP). The signals may reflect different cortical processes, yet, may compensate to one another and provide essential evidence in information extraction (Quiroga & Panzeri, 2009). Other than those questions literally asked about V1 processes on contextual dependency and dynamic interaction, investigating the relationship between two different neural signals was another issue, which eventually showed complimentary effects of signal prediction from one another and showed some evidence in neural oscillations from LFP may indicate significance of its role in sensory selection (Schroeder & Lakatos, 2009).

Purposely, those pieces of evidence in each study would provide important insights in neural mechanisms for various modulatory effects in visual processing and its relation to behavior as referred by saccadic eye movement.

Chapter 1

Introduction

Visual events are broken down into local signals by retinal cells, and subsequent integration of these signals across visual space constitutes a critical element of central visual processing. Accordingly, the receptive fields (RFs) of cells in the later stages of processing are increasingly large, suitable for integrating signals from wider regions of the visual space. However, numerous studies on surround interaction have shown that even at the very early stages of processing, integration of visual signals across a wide region of visual space can occur for neurons with small RFs. For example, the spike response of cells in the primary visual cortex (V1) is modulated by stimuli presented outside their RFs (Allman, Miezin, & McGuinness, 1985; Angelucci & Bressloff, 2006; Bair, Cavanaugh, & Movshon, 2003; Cavanaugh, Bair, & Movshon, 2002; H. Jones, Grieve, Wang, & Sillito, 2001; Mitesh K Kapadia, Minami Ito, Charles D Gilbert, & Gerald Westheimer, 1995; Series, Lorenceau, & Fregnac, 2003). This surround interaction has important implications for signal integration, because it reflects a refinement of integration process with increased response selectivity (Haider et al., 2010; Kim, Kim, Kim, & Lee, 2012; Vinje &

Gallant, 2002). However, the precise mechanism by which modulation of spike response by surround stimuli leads to increase of response selectivity remains poorly understood.

A stimulus falling outside the RF, by definition, does not evoke a spike response, but it does robustly evoke synaptic potentials as revealed by intracellular (Bringuier, Chavane, Glaeser, & Fregnac, 1999; Fregnac et al., 2009) or optical (Das & Gilbert, 1995; Grinvald, Lieke, Frostig, & Hildesheim, 1994) recording. There is a coupling between intracellular potentials and the local field potential (LFP) (Buzsaki, Anastassiou, & Koch, 2012; Okun, Naim, & Lampl, 2010), and thus the stimulus outside the RF evokes a subthreshold local field potential (sLFP). If a stimulus is presented inside the RF, while the sLFP evoked by the stimulus outside the RF persists, the cortical site representing the RF is expected to undergo response alteration, in a way similar to refinement of response selectivity by spike threshold (Priebe & Ferster, 2008). This is consistent with the idea that spike activity is potentially under the combined influence of on-going network dynamics and the external stimulus (Buzsaki & Draguhn, 2004; Cardin et al., 2009; Haider, Duque, Hasenstaub, Yu, & McCormick, 2007; Hasenstaub, Sachdev, & McCormick, 2007). Thus, it is predicted that sLFP and spike modulation, both produced by a surround stimulus, may be correlated. However, the relationship between sLFP evoked by surround stimuli and spike modulation has not been directly addressed.

In the current study, I focused on the role of sLFP in surround interactions in awake monkey V1. In order to examine the underlying interaction for non-homogeneous modulation depending on the location within the RF (Walker, Ohzawa, & Freeman, 1999), Gabor patches were used to stimulate focal surround regions, rather than annulus stimuli that have been conventionally used to examine surround interaction. Gabor stimuli evoke a smaller LFP response than annulus stimuli (Kim & Freeman, 2014). I sequentially presented two identical Gabor stimuli with variable stimulus onset asynchrony (SOA), the first (S1) outside the RF evoking a sLFP change, and the second (S2) within the RF generating a spiking response. Varying SOA enabled S2-evoked spiking activity to collide with a different phase of S1-evoked sLFP. Previous studies on the relationship between spike activity and spike-triggered LFPs (Nauhaus, Busse, Carandini, & Ringach, 2009; Ray & Maunsell, 2011) or stimulus-triggered LFPs (Katzner et al., 2009; D. Xing, Yeh, & Shapley, 2009) analyzed suprathreshold LFPs, and did not manipulate the temporal relation between spikes and LFP. In contrast, I characterized the sLFP and examined its role in modulation of spike activity, while keeping S1 and S2 constant and only varying SOA. I found that the magnitudes of LFP and spike modulation varied across SOA, and were correlated, and that the time course of covariation between LFP amplitude and spike activity suggested a role of sLFP for spike modulation, especially in the upper cortical layers.

Methods

1. Experimental procedures

1.1 Subject preparation

Two adult monkeys (*Maccaca mulatta, Maccaca fascicularis*) participated (IR, CR) in this experiment and no specific behavior-related task was required except a simple fixation task since the paradigm has been designed to consider data from neural recording. Each animal had two to three recording sessions a week and the study took four or five months for an animal. They completed approximately 800 trials for two hours in a session. All the experimental procedures were under the approval of the Seoul national University Animal Care and Use Committee. Throughout the experiment, the monkeys were housed and stayed in a colony with hepa-filtered air circulation where 50-60% of humidity of 25℃ of temperature was maintained.

IR (*Maccaca fascicularis*), male, 8 years old, 6.77kg.

CR (*Maccaca mulatta*), male, 7.5 years old, 5.36kg.

Dura Cleaning. A day prior to recording session, dura cleaning process was

performed. Brain tissues around the area where a small piece of skull has been removed inside recording chamber grew after some time. Abandoning those tissues would block the electrode penetration and this required cleaning process before a recording session. During this process, the animals underwent a light sedation with ketamine injection and the grown tissues on the dura were removed by using Dumont forcep and this process eased electrode penetration. The animals performed the experiment after full recovery from the sedation.

1.2 Microelectrode loading and data acquisition setup

Multi unit activity. Extracellular single unit recording was conducted in the monkey primary visual cortex (V1). In the experiment, I used two platinum-iridium microelectrodes insulated with quartz (ES12ecpg, Thomas Recording, Germany) with the aid of 5-channel minidrive (MM05, Thomas Recording, Germany) for each of the recording sessions. The lateral distance between the electrodes was 305μm. The diameter of the electrode was 80 or 23μm with or without insulation, 8μm of exposed tip and the width of 4μm. The impedance was 1~4MΩ at 1kHz. During the recording session, the animal was seated on a monkey chair (Primate Products, USA) and its head restrained at the center of the magnetic field. After the animal was seated and positioned properly, the Teflon cap was removed from the recording chamber and the inside the chamber was cleaned with saline. The Microdrive equipped with microelectrodes was mounted on the chamber and the guide tube was

lowered until it touched the surface of the dura. Into the chamber with guidetube attached to it, melted agarose (Agarose LE, SeMatrix, Korea, 1.5% saline) that had been cooled to ~37°C was applied to improve stability and minimize any possible noise production during recording. The juice tube attached to the frame that was equipped around the monkey chair and put in front of the animal's mouth. When rewarded, juice dripped out of the tube and enabled the monkey to lick. The electrodes equipped to the microdrive were set to move independently from one another and during the actual experiment. The neural signals from the electrodes were amplified by preamplifiers (em112/R, Thomas Recording, Germany) with a gain of 20, and amplified further by main amplifiers (MAF-05, gain: 250-1000, bandwidth: 500Hz to 20kHz, single unit activity filter: SUA-01, Thomas Recording, Germany). The amplified signal was digitized at 25kHz sampling rate and had a 16-bit resolution (PCI-6052E, National Instruments). The typical depth of the first cell activity with respect to the place where guide tube was initially placed on the dura was between 400μm~1800μm. A digitizing oscilloscope (Hitachi, VC-6535) and CRT monitor displayed the neural activity. A computer (Intel Pentium IV 3.0GHz, 2GB memory) stored this data with the aid of DAQ Toolbox (The Mathworks, Inc.).

Waveforms from neural activity were extracted and sorted based on spike duration and amplitude. This procedure further helped determining specific properties of receptive field such as position, preferred orientation, size and spatial frequency.

Local field potential. The local field potential (LFP) signal was obtained simultaneously with spike activity (5-channel LFP-filter, Thomas Recording, Germany). The signal was band-pass filtered (0.1~140Hz) during the task performance and digitized at 0.5~1 kHz in further analysis. We attempted to use the raw signal for the analysis in order to avoid any possible artifacts from the filtering processes.

1.3 Calibration of eye position

At the center of the magnetic field, current was induced through the scleral coil that has been implanted around the cornea. When the animal moved its eyes, the magnitude of induced current is proportional to the cosine of the angle between the axes of Helmhotz filed coils and the scleral coil (Robinson, 1963). In order to determine the eye position, calibration of eye position was performed before the main experiment began by converting voltage signals into visual angle in accordance from horizontal to vertical eye position on the origin at the central fixation point (0, 0). This was processed through pursuit and fixation routines, which provided information of gains (a & b) and offsets (b & d). During the pursuit routine, the monkey was guided to pursuit a moving image of either banana or apple (0.38 x 0.38°) to determine the gain of the eye position. When the eyes moved along

horizontal tracking, vertical offset was specified and along the vertical tracking, horizontal offset was specified.

$$H_{degree} = a \times H_{voltage} + b$$

$$V_{degree} = c \times V_{voltage} + d$$

After completing the tracking task, fixation routine was performed where the same image stimulus was presented in a sequence along the horizontal (-10, -5, 0, 5, 19) and vertical (-5, 0, 5) meridians. The monkeys were trained to follow the image presented on the screen to get a juice reward and this occurred when the position of the eye entered within the circular window (0.5~2°) that had been electrically defined around the target position. When the eye entered this window and overlapped the stimulus position, a key was pressed to adjust the offset of the calibration. Since the voltage of the eye signal and angular gaze direction was assumed to be linear, the offset and the gain were determined through linear regression and this step completed the calibration.

$$\text{Eye Position (degree)} = (Signal_{voltage} + \text{offset}) \times \text{gain}$$

1.4 Receptive field mapping

Prior to running the main experimental task, we had to find the stimulus that would evoke the maximal response and characterize the receptive field properties. In this process, cosine moving grating was used to determine a position since the

previous study has recognized that V1 simple cells have Gabor-like receptive field (J. P. Jones & Palmer, 1987). At first, the stimulus induced cell activity at a rough range of the position and the dimensions such as size, position (vertical, horizontal), diameter, spatial frequency, phase, orientation, luminance, contrast, of this Gabor grating were varied. While adjusting the diameter of the stimulus at a certain size, I listened to the sound of the neural activity and made a rough judgment toward the origin of the sound by means of a position, as it was moving in either horizontal or vertical direction.

The electrode was advanced around 2~30μm at a time and it was ascertained that all the recording site had receptive field within lower visual field since the recording chamber was not much below from lunate sulcus. Once the position was approximated, a flickering cosine grating was randomly presented for 200ms while the monkey was fixating at a central red dot. This was repeated 5~6 times for forward correlation method. The mapping process was performed in a sequence of orientation, position spatial frequency and size of the stimulus. Although I had approximated the optimal stimulus position at the beginning of the RF mapping process, this step provided finer approximation. After the flickering, the spike activities in the trials of the same stimulus dimension were compiled and aligned to the stimulus onset time, providing the plots of spike raster and spike density function during the peristimulus time period (-100~400ms). From the complied result, averaging the number of spike counts between 50~200ms after the stimulus onset

time gave mean firing rate as a response magnitude of each stimulus condition. A tuning curve was fitted by DoG (Difference-of-Gaussian), which gave the peak value, thus, the optimal value of the curve.

1 dimension;

$$DoG_1(x) = \mathrm{k}_1 \text{ x } \exp\left(\frac{-(\mathrm{x}-\mathrm{c})^2}{2\sigma_1^2}\right) - \mathrm{k}_2 \text{ x } \exp\left(\frac{-(\mathrm{x}-\mathrm{c})^2}{2\sigma_2^2}\right) + l$$

2 dimension;

$$DoG_2(x,y) = \left\{\mathrm{k}_{x1} \text{ x } \exp\left(\frac{-(\mathrm{x}-\mathrm{c}_x)^2}{2\sigma_x^2}\right) - \mathrm{k}_{x2} \text{ x } \exp\left(\frac{-(\mathrm{x}-\mathrm{c}_x)^2}{2\sigma_{x2}^2}\right)\right\} \text{x} \left\{\mathrm{k}_{y1} \text{ x } \exp\left(\frac{-(\mathrm{x}-\mathrm{c}_y)^2}{2\sigma_{y1}^2}\right) - \mathrm{k}_{y2} \text{ x } \exp\left(\frac{-(\mathrm{x}-\mathrm{c}_y)^2}{2\sigma_{y2}^2}\right)\right\} + l$$

During the stimulus size mapping process, Gabor stimuli ranging in diameter from 0.2 to 2.0° in steps of 0.2° were presented at the center of the RF in randomly interspersed trials. Although the diameter giving the maximum activity was taken as RF size, occasionally, a diameter slightly larger than this was taken to prevent the surround stimulus from encroaching on the RF, because the circular RF stimulus defined the RF boundary. In most experiments, the chosen diameter was 1.6°. When the neural response did not saturate with an increase in stimulus diameter, which was rare, the largest tested stimulus (2.0°) was taken as the diameter of the RF. Once the

optimal Gabor stimulus of a cell was determined from the receptive field mapping, the animal performed the main experimental task.

1.5 Main experiment paradigm

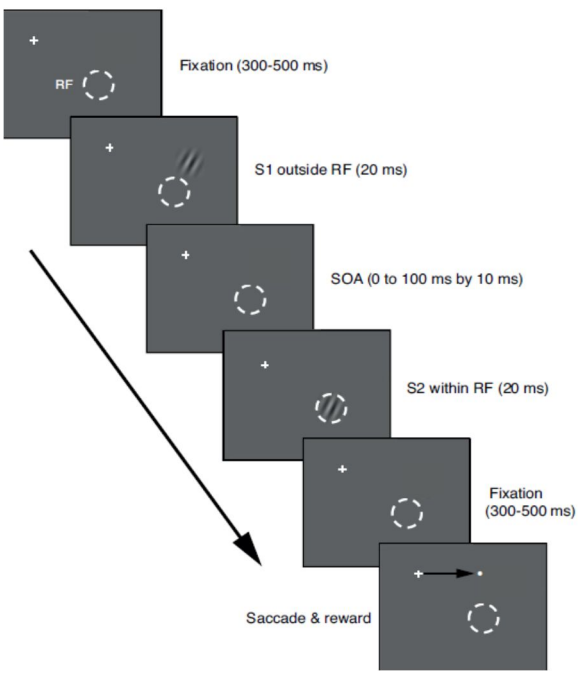

Figure 1. Trial structure of S1-S2 sequence stimuli.

A white cross indicates central fixation and a dashed white circle (invisible to the animal) represents the boundary of the classical receptive field (RF). After fixation duration between 300-500ms, a Gabor stimulus appeared with SOA of 0-100ms with 10ms of step (randomized within a block) on the location of surround (S1) first, and on the center (S2). After stimulus presentation, monkey made a saccade toward one of four locations (left, right, up, down, randomized) in order to get a juice reward.

For the main experiment, the monkeys were trained to perform a simple

fixation task. Each trial began with the onset of a fixation target (0.3°X0.3°, red dot) at the center of a gamma-corrected 25" flat CRT monitor (detailed description in *stimulus generation* part) that was controlled by computer programs written in Matlab (The Mathworks), using the Psychophysics Toolbox(Brainard, 1997; Pelli, 1997). When the eye position entered a circular fixation window of 1.5° in diameter centered on the fixation target, one or two identical Gabor stimuli with the duration of 20ms were presented after a variable delay of 300-500ms. In the trials with two stimuli, the first Gabor stimulus (S1) appeared at a location outside the RF, and then with an SOA ranging from 0 to 100ms in steps of 10ms, the second stimulus (S2), chosen to be optimal for the cell, appeared at the RF (Figure 1). The stimuli were presented on a gray background with a mean luminance of 8.65 cd/m^2. The stimuli presented in peripheral window were also varied in orientation (collinear or parallel to the receptive field preferred orientation) distance (extending up to 1.6~10° away from the RF) and contrast. Those conditions were repeated 15~100 times in one block and when any trials had failed with reasons such as animal failing to enter the eye window (1.5°) of the fixation target, they were discarded and stacked in the end of the trial plan, and repeated. Along a process of completing a trial, monkeys had to make a saccadic eye movement to a saccadic point that was randomly presented from four positions (up, down, left, right) in order to get a juice reward after all.

2. Experimental setup

2.1 Eye movement recording

Coil system. The scleral search coil method (Robinson, 1963) was used during the early phase of the experiment in order to determine horizontal and vertical eye positions. This method is composed of an eye coil implanted around the cornea rotating with the eye at the center of magnetic fields. It is formed by high frequency AC currents that flow through Helmholtz coils, in which the induced current through the scleral coil and the angle between the scleral coil and the axis of magnetic field is related. According to the angle of the eye, the magnitude of induced current changes, where the phase-detection occurs against the field signals (50kHz for horizontal and 75kHz for vertical axes). With the reference to the axis of field coils, the signals related to the horizontal and vertical direction of the coil were attained. The sampling rate was 25 kHz and down-sampled at 500 Hz at later stage. The horizontal and vertical eye position signals were digitized with the aid of DAQ Toolbox (the Mathworks, Inc) and shown in real time through GUI (Graphic user interface) control panel.

Camera system. Other than using scleral search coil, horizontal and vertical eye positions were determined with a video camera (Eye tracking system, ET-49B,

Thomas recording, Germany), during the later phase of the experiment, which was based on optical detection of dark pupil. This method consisted of video camera (USB 2.0 standard), D/A converter insert card and a Microsoft Windows-based software program called “Eyetracer”. The system enabled monitoring the monkey’s eye position without physical surgery, yet with a sufficient resolution.

2.2 Stimulus generation

A 24-inch flat CRT monitor (SONY GDM-FM900, 413X310mm, 800X600 pixel) with a refresh rate at 100Hz was used for presenting a visual stimulus. The distance from the center of the monitor and the monkey eye was 77.6cm where this distance gave ±13.1degrees in horizontal and -11.9~+10.5 degrees in vertical display span. Stimulus generation was controlled with a computer program written in Matlab (The Mathworks) using Psychophysics toolbox. In this process, two computers were used; one (Master) for stimulus presentation (Intel 3.0GHz, memory 2GB, Matrox Parhelia 128MB 400Hz) and the other (Slave) for displaying and storing data. The Slave computer received an order to start A/D signal under the control of Master computer and all the signals were digitized at the rate of 25kHz with the resolution of 16 bits (NI-DAQ PCI 6013, national Instruments) with DAQ Toolbox (the Matworks, Inc). Stimulus onset time was ascertained with the output from a photodiode (GaAsP G1115, 410-690nm, Hamamatsu Photonics, Japan), which was attached at the center part of left margin (50X50 pixels) of the computer screen. This contrivance has also

eliminated the possibility that the temporal gap between the display command time and the actual stimulus onset time might exist.

3. Data analysis

3.1 Spike extraction

The spikes were extracted and sorted off-line from the raw data collected during the neural recording, which involved more thorough procedure than on-line process and the spikes had to satisfy four main criteria in order to be classified as a valid spike activity;

1. Upper threshold, the local maximum within certain interval
2. The lower threshold, the local minimum within certain interval
3. Peak-to-peak height, the peak-to-peak voltage within certain interval
4. Peak-to-peak interval, the peak-to-peak interval within certain interval.

Since a certain pattern of ongoing potential fluctuates even though there is no spike induced, the high and low thresholds were set by the experimenter to extract and save the potential changes that were above the high threshold and below the low

threshold.

The data were collected at a rate of 25 kHz and with this rate, a spike of 1ms takes 25 points. Following this, 13 points before, and 17 points after the high peak were saved as a spike waveform with time marks.

3.2 Spike sorting

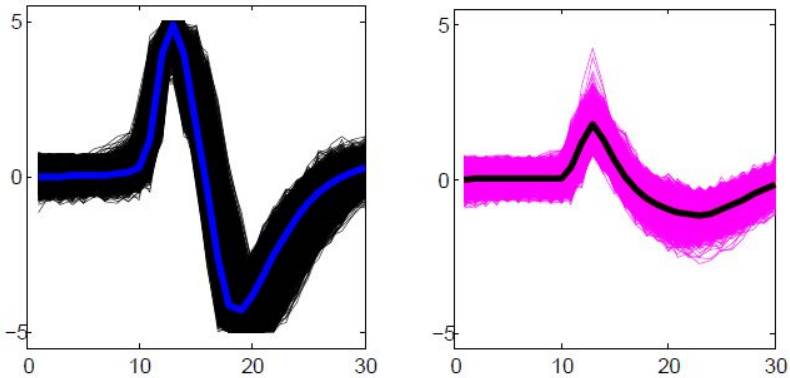

Figure 2. Spike waveform examples after sorting.

Two different waveforms having different peak to peak duration after spike sorting. X-axis indicates 30 points (~=1.2ms) as described in extraction process and y-axis indicates voltage (mV). Left waveform shows narrower peak to peak duration, right shows waveforms having wider peak to peak duration. The bold lines in each panel indicate average of all waveforms.

After the extraction (3.1), the waveforms that had been saved were sorted into spike pattern of 2~4 different cells by a sorting program (wavesorter) developed in our lab. The program was based on principal component analysis and K-mean clustering (Yu, 1999). First, a couple of thousands of waveforms were randomly sampled out of the population data, and a number of axes were extracted most explained by the principal component. When scattergrams were plotted out of the axes, a number of clusters sharing similar characteristics could be determined. Accordingly, a number of waveforms were clustered with its optimal number determined by MLE (Maximum likelihood estimation) that a specific range was

arranged by the experimenter. Then a centroid in each cluster allowed other remaining waveforms being sorted into one of the clusters. Sorting and classifying waveforms also helped eliminating possible noise inclusion in spike data.

3.3 Spike density function

After the completion of sorting process, spike density function was constructed in order to easily notice the initial time of firing and the point where the activity declines. Gaussian-shaped kernel function was traditionally used to replace each spike and construct spike density function (Richmond, Optican, Podell, & Spitzer, 1987). However, symmetric Gaussian filter came out to be underestimating the time information of spike occurrences. For more precise time measurement, asymmetric kernel function of a total length of 150ms was derived.

$$A(t) = (1-\exp(-t/\tau_g)) \times (\exp(-t/\tau_d)) \times k$$

The binary spike train in which 1 was coded as a spike that had been fired, whereas 0 for no spike occurrence was convolved by this kernel with asymmetric kernel function. In this case, the rate as a function of time, $A(t)$, varied with a time constant during the growth (τ_g) or decay (τ_d) phase. Based on the previous physiological data, 1ms and 20ms were good values to represent excitatory synapses for the growth and decay phase, respectively (Sayer, Friedlander, & Redman, 1990),

so was in this study. The present experiment collected data with 25kHz sampling rate, which means that 1ms receives 25 point. Hence, 25(τ_g), 500(τ_d), 25(k) were the values for those parameters.

3.4 Retinotopic map and cortical magnification factor

In order to evaluate the effects of distance between S1 and S2 positions on the LFP change and spike response, the distance on the cortex between the sites of activity evoked by S1 and S2 was estimated as follows. A point on the stimulus monitor, (x, y), was first transformed into polar coordinates, $\varepsilon = \sqrt{x^2 + y^2}$, $a = \arctan(\frac{y}{x})$, where ε is eccentricity and a is inclination, and the position of the activity evoked by the point on the cortex, (X, Y), was estimated with, $X = \lambda \ln(1 + \varepsilon/\varepsilon_0)$ and $Y = -\lambda a \varepsilon/(\varepsilon_0 + \varepsilon)$, where λ = 12 *and* ε_0 = 0.75 (Horton & Hoyt, 1991).

3.5 Data validity evaluation

In this study, temporal interval between S1 (surround) and S2 (receptive field) stimuli were varied from 0 to 100ms by 10ms. The position, distance, and orientation

of S1 were also manipulated, resulting in more than 20 different combinations of stimulus conditions set in one block. Constructing relatively many numbers of conditions in a block that an animal could tolerate in each recording session, around 800 trials were performed at one recording site, allowing 15~20 trials per condition. Not being able to obtain more than 20 trials per stimulus condition, any possible noise or existing outliers, four criterions have invalidated the obtained trials.

1. Trials with eye signal out of fixation window (1.5° in diameter) during stimulus presentation were discarded.
2. Trials with eye velocity greater than 50deg/s during the time period starting from stimulus onset minus 100ms to stimulus onset plus 10ms were discarded.
3. Trials with firing rate within 2 standard deviations were validated.

3.6 LFP classification using support vector machine (SVM)

In the process of classifying different response patterns of LFP to S2 alone stimulus, we first visually discriminated whether the averaged trace from each recording site has the first negative peak or not. Then, with the aid of SVM, we objectively made distinctions for the two different features of LFP (‘no peak’ or ‘peak’). The initial step of analysis involved cross validation process, which randomly partitions the number of observations for making a training set. This

randomly selected training set was used to train a SVM classifier on the data taken (LFP data points staring from stimulus onset to 300ms). Using this trained classifier containing support vectors, we obtained predicted class of test data and used this result for further analysis.

3.7 Quantification of local field potential

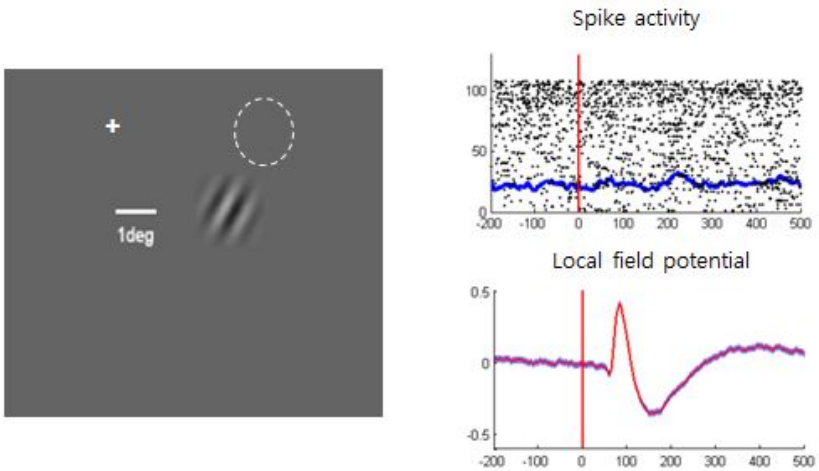

Figure 3. Example of subthreshold local field potential.

When a Gabor stimulus with 64% of contrast was presented at surround region out of the RF (dashed circle in the left panel) while monkey was fixating at the central fixating point (cross), spike activity (band of 300~3kHz, raster plot) did not show a change (right upper panel), whereas in identical trials, LFP (band of 0.1~140Hz) changed robustly (right lower panel). The shade indicates 1SE. X-axis indicates time signal aligned to stimulus onset time (ms). Y-axis indicates spikes/second for spike activity and voltage for LFP.

During the analysis, a strict 'subthreshold' criterion was applied to ensure that the S1 was indeed outside the RF for all results that involved in subthreshold LFP response. For this, if S1 alone evoked a spike response larger than 5% of that evoked by S2 alone in terms of mean spike density during the poststimulus period of 50-150ms, the cells were excluded from further analysis. For the remaining cells, S1-evoked LFPs, that is, sLFP, by averaging LFP traces aligned at S1 onset, were

isolated. Similarly, I also isolated S2-evoked LFPs and S1-S2 sequence-evoked LFPs by aligning and averaging LFP traces at S2 onset. These procedures eliminate non-stimulus related LFPs (Maier, Aura, & Leopold, 2011).

3.7.1 Power spectrum

In order to analyze the spectral component of the LFP activity for each cell, a spectrogram was computed by using the 'Chronux' (see detailed functional descriptions in Chronux.org), which provides spectral analysis toolbox. For this analysis, the multi-taper time-frequency spectrum function for continuous process was used. The sampling frequency of the input data was 1 kHz, and a padding factor of 8 was used. In order to reveal relative power changes from baseline, first, the mean LFP signal was normalized as z-score, then, computed the power for each condition, and divided the power at each frequency band by the mean power from the spontaneous period (-250:0ms) before stimulus onset for the corresponding frequency in steps of 1ms. The results then indicated the magnitude of power increase at a given frequency band following stimulus onset with respect to the level of spontaneous activity in a given condition.

3.7.2 Root mean square (RMS) magnitude

In order to quantify the response magnitude of LFP for each stimulus

condition, root mean square (RMS) magnitude was calculated from the baseline-subtracted stimulus-evoked LFP during the poststimulus period of 0-300ms:

$$RMS = \sqrt{\frac{\sum_{i=n}(x_i - \overline{x_b})^2}{n}} \quad ,$$

where x_i is the LFP at the i^{th} time bin, $\overline{x_b}$ is the baseline LFP during the period from -200 to 0 ms of stimulus onset, and n is the total number of time bins, 300 in this case. Subtraction of the baseline level was to prevent trial-to-trial variability of the overall LFP level from affecting the response magnitude. In order to obtain an estimate of stimulus-evoked LFP magnitude change, the RMS percentage change was calculated as following,

$$RMS\,\%\,change = \frac{RMS_{S1-S2\ Sequence}}{RMS_{S2-alone}} \times 100,$$

where $RMS_{S1-S2\ Sequence}$ is the RMS from the S1-S2 sequence condition, and $RMS_{S2-alone}$ is the RMS from the S2-alone condition. We calculated the RMS percentage change for each trial and derived a geometric mean across trials.

3.7.3 Estimation and division of recording depth

In order to examine the relationship sLFP and spike modulation across cortical depth, estimating the cortical depth of each recording sites was attempted. For this, I used two methods in analysis.

The first one was looking at the pattern of LFP evoked by S2 which showed gradual change with the recording depth, and a negative peak additionally appeared for relatively deeper recording sites. Using this information, the upper and lower depth groups were classified for each recording site, and determined whether the relationship between sLFP and spike modulation is different between the two depth groups. Since the change in the S2-evoked LFP pattern across cortical depth was gradual, and the presence of positive peak was ambiguous at some recording sites, probably at the border transition, SVM classifier for pattern classification was employed. For this, it was first visually judged whether or not the averaged LFP trace of a poststimulus period 300ms from each of the selected recording sites showed a negative peak, and then provided a support vector machine (svmclassify.m of the Matlab) with two patterns of LFP, with and without a peak for training. The classifier returned two groups based on the LFP pattern, Types 1 and 2, corresponding to upper and lower cortical layers, respectively.

The second method was to just use the recording depth for group separation.

The cells in the upper group had the recording depth no greater than 1.2mm, and those in the lower group greater than 1.2mm. Note that the estimates of cortical depth was inevitably inaccurate since a tissue drag during electrode penetration of the dura was unavoidable. The results with these two methods, one based on machine learning classification, and the other on the anatomical depth were compared.

3.7.4 Signal latency

The S1-evoked sLFPs showed distinct peaks whose latency varied depending on the S1 position. In order to estimate the latency, the positive and negative peaks were localized at zero-crossing points of the time-differentiated LFP signal after smoothing with a 50-ms moving average. The amplitude of the sLFP was taken from the change in potential between positive and negative peaks.

In order to determine the latency of S2-evoked LFP change that was initially downward, first, the mean LFP of each type was smoothed with a 20-ms moving average and differentiated. In order to localize the start for the downward change in raw LFP, the time after stimulus onset was taken when the first time-derivative of the mean LFP cross a threshold (1.75 μV/s) away from the baseline level (0.04 μV/s).

3.7.5 Correlation between spike and LFP modulation

In order to determine the time course by which SOA-dependency of spike activity matches SOA-dependency of the LFP, the instantaneous Pearson product-moment correlation coefficient, *c(t)* in 1-ms steps as following:

$$c(t) = \frac{\sum_{i=1}^{11}[r_i - \bar{r}][v_i(t) - \overline{v_i(t)}]}{\sqrt{\sum_{i=1}^{11}[r_i - \bar{r}]^2}\sqrt{\sum_{i=1}^{11}[v_i(t) - \overline{v_i(t)}]^2}},$$

where r_i is the average firing rate during the poststimulus time period of 50-150 ms obtained for the i^{th} of 11 SOA conditions, and $v_i(t)$ is the instantaneous LFP at time t for the corresponding i^{th} SOA condition. This procedure is basically to temporally localize the pattern of SOA-dependent spike activity in LFP data, and enabled to determine the temporal precedence between the SOA-dependent spike activity and the LFP change, and, thus, to determine a modulatory role of sLFP. The significance of correlation was statistically tested every 1ms with a bootstrap method, in which the obtained correlation was tested against the probability distribution of the correlation coefficient for corresponding time derived from 1000 repetitions of randomized shuffling across SOA conditions.

Results

1. Data summary

The complete spike and LFP data described in the study 1 are based on 62 single cells that were recorded from 62 sites in the dorsal operculum of V1 during 62 recording sessions in two monkeys performing a simple fixation task. During the analysis, it was found that in 22 of these sites, S1 encroached upon the RF that had been defined with the spatial summation test, so that the 'subthreshold' criterion was violated (section 3.7). Accordingly, the data from these 22 sites were excluded (CR=11, IR=11 sites) for analyses that required strict surround criteria. The average diameter of the RF (size of S2) of the remaining 40 sites was 1.61±0.03°. The mean eccentricities of the RFs for these sites, 25 from monkey CR and 15 from monkey IR, were 4.69±1.03° and 4.04±0.34°, and the mean recording depths from the surface of the dura were 1.39±0.34mm and 0.91±0.32mm, respectively.

2. Properties of subthreshold local field potential

One of the distinctive features from the local field potential signal is that surround stimulus induced large amplitude whereas there is no spike response. The response amplitude induced by surround stimulus was even larger than center stimulus-induced LFP. In order to characterize sLFP, spike responses evoked by S1 were paid with particular attention. Although non-responsive spike activity to surrounding stimulus, the dependency of sLFP on the spatial distance between the center of the Gabor stimulus in the RF surround and the center of RF was observed (Figure 4). As the distance between the two in the cortical dimension increased, the power of sLFP and the positive-to-negative peak amplitude of sLFP decreased. The sLFP change was evoked by the surround stimuli that were represented at cortical distances up to 10mm away. These patterns of LFP change were similar between both monkeys.

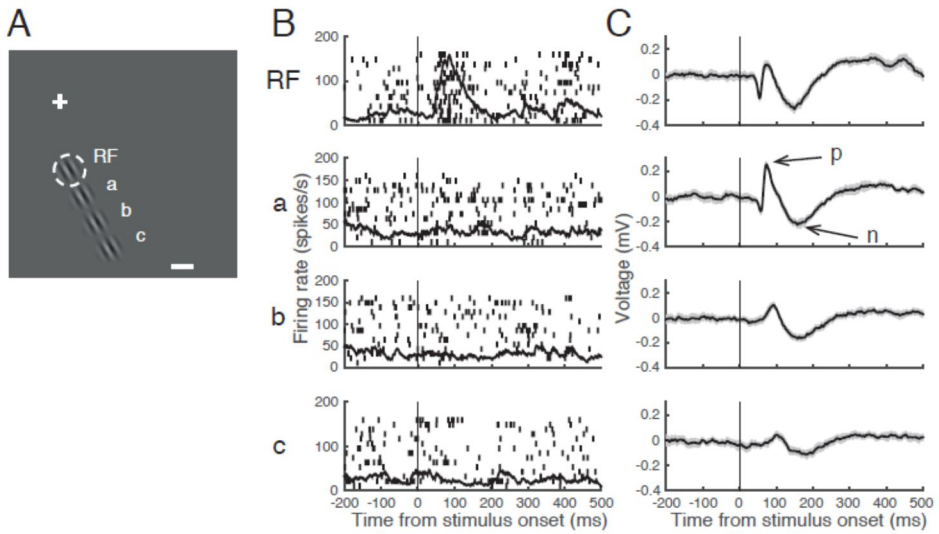

Figure 4. Properties of subthreshold (sLFP)

A.Spatial layout of stimulus configuration: the cross marks the central fixation target; dashed white circle represents the RF (1.6° in diameter, centered at 0.6° right and 4.1° down); a Gabor stimulus at the RF and three identical stimuli positioned outside the RF spaced at intervals of one RF diameter away from the RF along the direction collinear to preferred orientation (a,b, and c); the calibration bar indicates 1°. The distance of stimuli at a,b, and c from the RF center in cortical dimension was estimated to be 3.28, 5.89, and 8.06mm, respectively. **B, C**. raster and spike density plots (B) and mean LFP traces (C). From top to bottom, responses to the Gabor stimulus at the RF alone, and those at a,b, and c alone are shown, aligned at the stimulus onset times (vertical lines). Note that a robust LFp change was evoked by the stimuli at a,b, and c, while spike activity remained unchanged. The dominant positive and negative peaks of this sLFP are indicated as 'p' and 'n', respectively.

From the latency-distance relationship of Figure 5, the propagation speed of sLFP can be estimated. The inverse of the slope of the regression line, an estimate of propagation speed, was 0.36 and 0.39 m/s for positive and negative peaks, respectively (monkey CR, 0.31m/s, 0.37m/s; monkey IR, 0.21m/s, 0.25m/s, positive and negative peaks respectively). These estimates agree well with previous estimates of propagation speed through horizontal connections, which range between 0.05 and 0.5m/s (Bringuier, 1999; Gilbert & Wiesel, 1989; Grinvald et al., 1994; Katzner et al., 2009; Nauhaus et al., 2009; Nauhaus, Busse, Ringach, & Carandini, 2012). Note that for an angular distance of 1.6° between the Gabor stimuli in the RF center and the most adjacent surround (a typical RF diameter in this study) or for its corresponding distance of 2.58 to 4.87mm (mean=3.63±0.58mm) in cortical dimension depending on eccentricities examined in the current study, the transmission speed between the sequential stimulus sites corresponds to 16-160°/s for SOAs of 10-100ms. It can be verified that this speed induced a perception of apparent motion, consistent with previous report (Burt & Sperling, 1981). This speed is comparable to the velocity tuning of MT neurons (Maunsell & Van Essen, 1983; Rodman & Albright, 1987) and to the motion velocity eliciting propagating waves in V1 (Dirk Jancke, Frédéric Chavane, Shmuel Naaman, & Amiram Grinvald, 2004), suggesting a role of sLFP for processing of global motion that extends both inside and outside the RF.

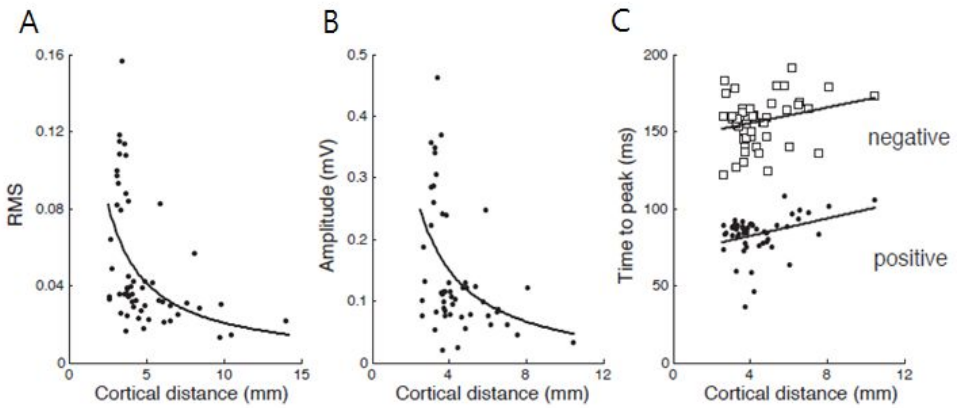

Figure 5. Distance-latency relationship of sLFP

A.Power (RMS) of sLFP as a function of cortical distance between the center of Gabor stimulus in the RF surround and the center of RF, extracted from data on 56 surround stimuli tested at 40 cortical sites. The curve is a fitted function in the form of $y = A\frac{1}{x} + B$, following the inverse distance law of sound pressure, where x is cortical distance in mm between the center of Gabor stimulus in the RF surround and the center of RT. Parameter A was estimated to be 0.21, and its 95% confidence limits were 0.10 and 0.31; B was estimated to be 0.00. **B**. The amplitude of the sLFP, as measured from positive to negative peaks as a function of cortical distance between the center of Gabor stimulus in the RF surround and the center of RF for 52 conditions. Four of the 56 conditions in A, for which the peaks could not be determined, were excluded. The curve is a fitted function in the same form as in A. Parameter A was estimated to be 0.67, its 95% confidence limits were 0.27 and 1.07; B was estimated to be 0.02. **C.** Latency to positive (dots) and negative (open squares) peaks of sLFP as functions of cortical distance between the center of Gabor stimulus in the RF surround and the center of RF for the 52 conditions shown in B. The data were separately fitted with linear regression equations: y=2.82x+70.86 for latency to the positive peak, and y=2.54x+145.1 for latency to the negative peak, where x is cortical distance between the two stimuli (r=0.38 and 0.31, respectively, $p<0.05$ for both).

3. Signal characteristic

3.1 Classification of LFP

It is known that the stimulus-evoked LFP change varies across cortical depth (U Mitzdorf, 1987; Dajun Xing, Yeh, Burns, & Shapley, 2012), and that the pattern of surround interaction differs across cortical layers (Ichida, Schwabe, Bressloff, & Angelucci, 2007). Interestingly, the LFP change evoked by focal Gabor stimuli also appeared to vary with cortical depth in the current experimental conditions, and thus, for quantifying the relationship between LFP and spike modulation, the recording sites were divided according to cortical depth based on the negative peak at deeper recording sites (Figure 6, presence of negative peak when cortical depth is >1.2mm). In this analysis two methods were used and compared; one was classification based on the presence of negative peak with SVM classifier, and the other was based on the cortical depth of recording site for separating upper and lower layers (described in *Methods*). The results from both methods did not differ significantly.

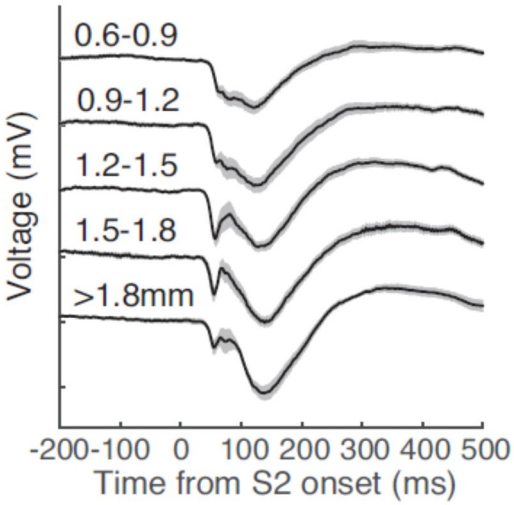

Figure 6. Patterns of evoked-LFP for single stimulus.

LFP traces from all 62 sites in which S2 alone was tested, averaged for five depth groups divided into depth segments of 300μm, measured from the surface of the dura. The deepest trace (bottom) includes all recording sites below 1800μm from the dura. The shading represents ±1 SE.

Based on the classification depending on the presence of negative peak/cortical depth, the upper layer cells were called as Type 1, and the lower layers cells were called Type2.

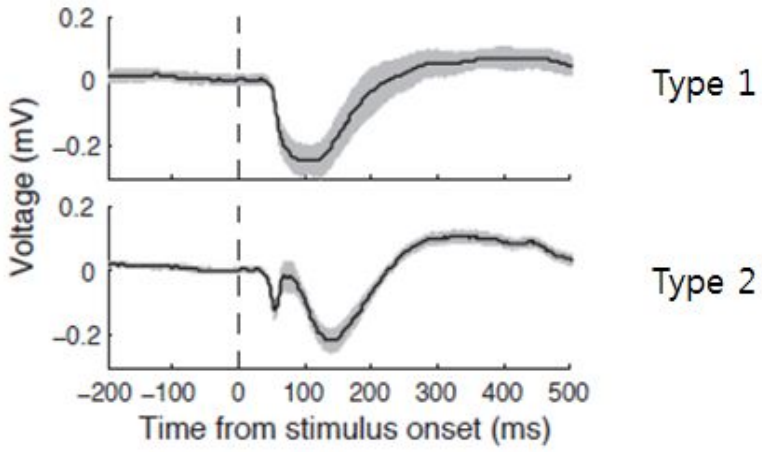

Figure 7. Types of S2-alone evoked potential

Mean LFP traces evoked by S2 alone, separated into two types by a support vector machine based on the presence of a negative peak; Type1 (peak absent) and Type2 (peak present). Shown are the mean LFP traces (shading indicates ±2 SE) from 13 sites for Type1 and 27 sites for Type2. Note that separation by recording depth gave similar results.

4. Subthreshold LFP and modulation of spike response

In this result section, two example cells represent subthreshold LFP response and modulation of spike response depending on the temporal interval between S1 and S2. Figure 8 illustrates the results from an example cell for which S1 was presented 1.5 RF diameters away from the RF (Figure 8A). The stimulus at the RF (S2) evoked a burst of spike activity (Figure 8B, upper) accompanied by a simultaneous change in LFP (Figure 8C, upper). In contrast, S1 did not evoke a spike

response (Figure 8B, lower) but it robustly evoked a LFP change with a distinct positive peak followed by a negative peak (Figure 8C, lower). When S1-S2 sequence stimuli were presented, modulation of spike activity was apparent depending on SOA (Figure 8D). For example, compared to the reference activity in response to S2 alone (Figure 8D, bottom; black trace of Figure 8E), the spike response increased for an SOA of 70ms (blue traces in Figure 8D, E). For an SOA of 70ms, S1 induced a positive change in the LFP before the start of a negative response, resulting in a pronounced negative peak (Figure 8E, lower panel). Changes in spike and LFP responses induced by S1 at 70-ms SOA (blue traces) occurred at specific times (Figure 8E, F, lower panels).

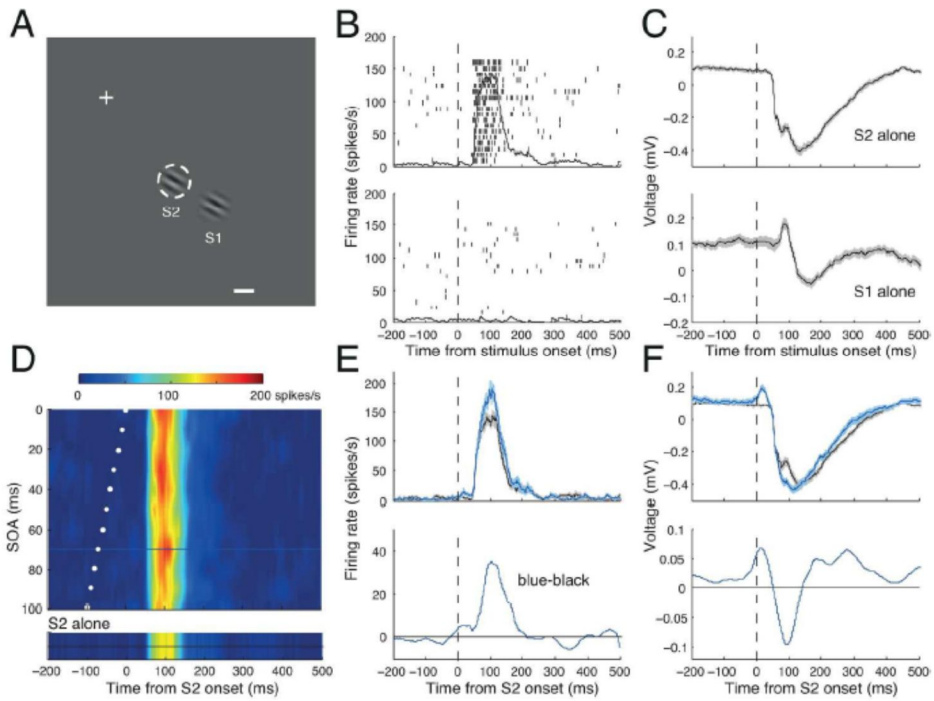

Figure 8. Spike and LFP activity example cell 1

A. Spatial layout of stimulus configuration. The RF was centered at 3.3° right and 4.2° down. Two Gabor stimuli, one at the RF (S2), and the other in the RF surround are shown. **B, C**. Raster and spike density plots (B) and mean LFP traces (C) in response to S2 alone (upper) and S1 alone (lower), aligned at their onset times (dashed vertical line). Shading indicates ±2 SE. Y-axis indicates spike density in spikes/s in B, and LFP amplitude in mV in C. **D**. SOA time plot for response modulation during trials with S1-S2 sequence stimuli, showing spike activity as a function of SOA and time, aligned at S2 onset. Activity is coded by color, as indicated by the calibration bar at top. White dots indicate the time of S1 onset for each SOA condition. The spike activity for the S2-alone condition is given in a separate colormap at bottom for comparison. Note that depending on SOA, spike density varied considerably in terms of magnitude and time course. Spike density for an SOA of 70ms is indicated by the blue horizontal line, while the reference density for S2 alone (at bottom) is indicated by the horizontal black

line; the time courses of both are shown in the upper panel of E with the same color coding. **E.F**. Upper: Spike (E) and LFP activity (F) in response to a S1-S2 sequence with a 70ms SOA (blue), aligned at the time of S1 onset (dashed vertical lines). In each panel, a black trace indicates the reference from the S2-alone condition. Shading indicates ±2 SE. Lower: The magnitude of modulation (S1-S2 sequence minus S2-alone) in firing rate (E) or LFP (F) is plotted for a 70ms SOA.

Figure 9 illustrates another example cell for which S1 was tested at one RF diameter away from the RF (Figure 9A). Again, S2 evoked a burst of spike activity (Figure 9B, upper) and a simultaneous change in LFP (Figure 9C, upper). The S1 stimulus did not evoke a spike response (Figure 9B, lower) but it robustly evoked sLFP (Figure 9C, lower). Modulation of spike activity by S1 was apparent depending on SOA and time (Figure 9D). For example, the spike response decreased for the SOA of 10ms (red traces in Figure 9D, E) and increased for the SOA of 40ms (blue traces in Figure 9D, E). Note again that spike modulation did not occur for the entire spike response, but rather was confined within fixed temporal windows. For the SOA of 10ms, the spike response decreased only during an interval about 100ms after target onset, but the spike response outside this interval remained unchanged (Figure 9E, up and bottom panels), and for the SOA of 40ms, the change occurred in two intervals for this cell (Figure 9E, middle and bottom). Corresponding mean LFP traces are shown in matching colors in Figure 4F. For the SOA of 10ms, the LFP change caused by S1 was subtle, only slightly modifying the later phase of the LFP

response (Figure 9F, up and bottom), whereas for the SOA of 40ms, S1 added an LFP change at a very early phase, nullifying the negative and subsequent positive peaks of the S2-alone condition (Figure 4F, middle and bottom). The SOA-time plot from Figure 8D and Figure 9D was drawn with the analysis method that had been previous developed (Kim et al., 2012).

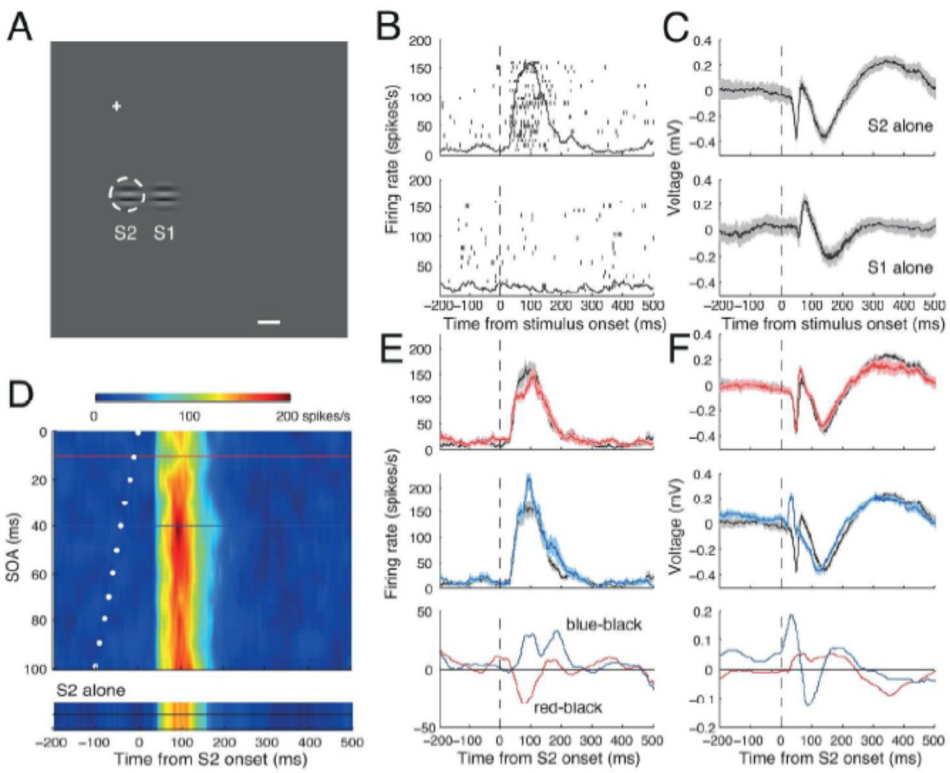

Figure 9. Spike and LFP activity example cell 2

A. The RF was centered 0.6° right and 4.0° down. **B.C**. Raster and spike density plots (B) and mean LFP traces (C) in response to S2 alone (upper) and S1 alone (lower) aligned at their onset times. Shading indicates ±2 SE. **D**. SOA time plot. Representative spike densities for SOA of 10 and 40ms are indicated by red and blue horizontal lines, respectively. **E.F**. Upper and middle panels: Spike (E) and

LFP activity (F) in response to a S1-S2 sequence with SOAs of 10 (red) and 40ms (blue); black traces indicate references taken from the S2-alone condition. Bottom panels: the magnitude of modulation (S1-S2 sequence minus S2-alone condition) in spike (E) and LFP (F) are plotted for SOAs of 10ms (red) and 40ms (blue). Note that for the 10ms SOA, the magnitude of modulation in spike activity was negative (suppressed) and the modulation of LFP was relatively weak, whereas for the 40ms SOA, the magnitude of modulation in spike activity was positive (facilitated) and the modulation of LFP was relatively strong.

5. Correlation between LFP and spike activity

5.1 Correlation of spike and LFP modulation magnitude

In order to reveal the roles of sLFP for spike modulation, it was first determined whether the modulation of spike activity by S1 was quantitatively related to that of LFP. The magnitude of spike modulation was taken from the percentage change in spike density in the 50-150ms following S2 onset during S1-S2 sequence conditions relative to that during S2-alone condition, and the magnitude of LFP modulation was similarly quantified by the percentage change in RMS power on a trial-by-trial basis. In 9 of the 40 valid cells, only S1-alone and S2-alone conditions were tested. From 30 of the remaining 31 cells, the S1-S2 sequence stimuli for the S1 closest to the RF (for one site, the closest S1 was not tested, and for some sites, multiple S1 positions were tested) were selected, and calculated the magnitude of

spike and LFP modulation for each SOA condition from these sequence conditions.

5.1.1 Classification using support vector machine (SVM)

It is known that the stimulus-evoked LFP change varies across cortical depth (U Mitzdorf, 1987; Dajun Xing et al., 2012), and that the pattern of surround interaction differs across cortical layers (Ichida et al., 2007). In the data of the current study, the pattern of LFP evoked by S2 changed gradually with the recording depth, and a negative peak additionally appeared for relatively deeper recording sites (Figure 6). Although the recordings in this study were made with a single electrode, it appeared to be consistent with additional stimulus-locked negative potentials recorded from lower layers in monkey V1 (Kraut, Arezzo, & Vaughan, 1985; C. Schroeder, Tenke, Givre, Arezzo, & Vaughan, 1991) and A1 (Kajikawa & Schroeder, 2011). Thus, two methods were applied to separate the types of S2 LFP it was further examined with its role in correlation between SOA-dependent spike and LFP modulation magnitude. The first one is the division made using SVM based on the presence of additional negative peak and the result in difference between Type1 and Type2 LFP on the correlation of spike and LFP modulation magnitude is presented below.

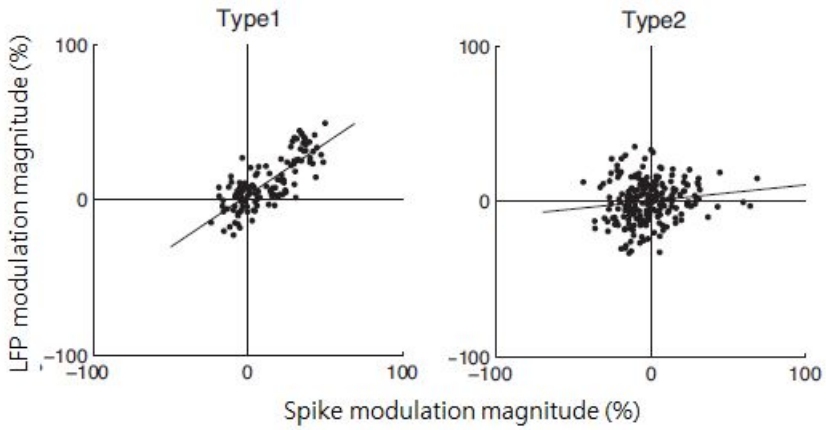

Figure 10. Relationship between spike LFP modulation (Type separation using SVM classifier).

Scatter plot between the percentage changes in spike activity and RMS LFP power in the S1-S2 sequence with respect to the S2-alone condition for Type1 sites (Left). Only the data from the closest S1 for 11 sites (1-1.5 diameters away from the RF) were included. Each dot represents one SOA condition. The mean spike and LFP modulations are 13.69 and 16.59%, respectively (one sample t-test, both $p<10\text{-}^{10}$). The line is a linear regression (r. =0.81, $p<10^{-4}$). Similar data from the closest S1 for 19 Type 2 sites (r. =0.05, p=0.37, left). The mean spike modulation was 6.04% ($p<10^{-7}$). One point with spike modulation of 130.39% and LFP modulation of 5.83% is beyond the axis range and not shown, but included for statistical calculation.

First, facilitative spike modulation (>0%) occurred more frequently in Type1 (71.07%) than in Type2 (43.0%), whereas suppressive spike modulation (<0%) occurred more frequently in Type2 than in Type1 (Figure 10). Additionally, the difference in mean spike modulation between two types was statistically significant

(-1% (Type1) vs. 9% (Type2), two-sample t-test, $p<10^{-4}$). Second, the proportion of RMS increase with respect to decrease was greater in Type1 than in Type2, and the difference in mean LFP modulation between the two types was statistically significant (two-sample t-test, $p<10^{-6}$). Finally, the degree of correlation coefficient between spike and LFP modulation for Type 1 sites was 0.81 and significant ($p<10^{-4}$), whereas that for Type 2 sites was 0.05 and non-significant (p=0.37).

5.1.2 Classification using depth division of recording sites

The same analysis was performed as shown in Figure10, but in this case, the LFP types were subdivided into two depth groups not based on the presence of the negative peak but based on the recording depth; upper (<1.2mm) and lower (>1.2mm) (refer to Figure6). Note that the recording depth was taken as the distance the electrode was advanced at right angles from its touchdown on the surface of the dura, and this was subject to considerable error due to uncontrolled tissue drag during penetration of the dura, despite routine thinning. A few relatively large depths of about 3mm are undoubtedly due to such errors. Nevertheless, it was observed that the correlation between the percentage changes in spike activity and LFP RMS power relative to the S2-alone condition was statistically significant in 17 upper groups cells (Figure 11, left panel), but not in 13 lower groups cells (Figure 11, right panel) (r=0.64 vs 0.03). This was consistent in both animals; in monkey CR, the correlation between spike and LFP modulation was 0.64 for 4 upper groups cells, and 0.05 for

13 lower group cells, and in monkey IR, it was 0.78 for 7 upper groups cells, and 0.40 for 6 lower groups cells.

There are also additional differences between these two depth groups. First the magnitude of spike modulation differed; facilitative spike modulation (>0%) occurred more frequently in the upper group (62.81%, 76 out of 121 conditions) than in the lower (42.23%, 87 out of 206 SOA conditions), and conversely suppressive spike modulation (<0%) occurred relatively more frequently in the lower than in the upper groups. The difference in mean spike modulation between the two groups was statistically significant (11.49% for the upper vs -0.93% for the lower, two-sample t-test, $p<10^{-4}$). Second, the frequency of RMS increase following S1-S2 sequence was greater in the upper (76.03%, 92 of 121 SOA conditions) than in the lower group (51.46%, 106 of 206 SOA conditions), and the mean LFP modulation differed significantly between the two groups (10.79 vs 0.27%, two-sample t-test, $p<10^{-6}$). Thus, facilitation of spike and LFP response was dominant for the upper group, resulting in a stronger and more positive correlation between the two responses (r=0.64), whereas both suppression and facilitation of spike and LFP response were equally observed for the lower groups and the correlation between the magnitudes of spike and LFP responses was virtually absent (r=0.03). To summarize, in the upper group, surround stimuli tended to increase RMS power and facilitate the spike response, and these changes were coupled to each other. In contrast, in lower layers, the spike response tended to be relatively equally modulated by surround stimuli, and

this change was variably coupled to the magnitude of LFP change.

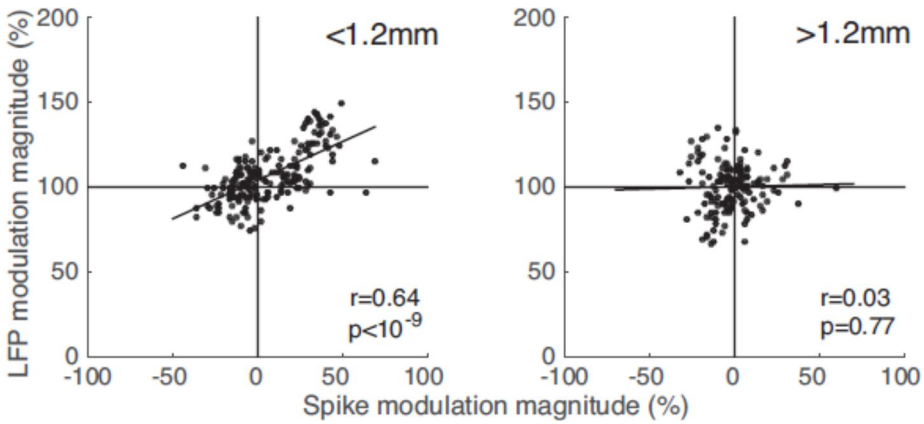

Figure 11. Relationship between spike and LFP modulation (Type separation using recording depth).

A. Scatter plot showing the percentage changes in spike activity and RMS LFP power in the S1-S2 sequence relative to the S2-alone condition for upper layer sites. They are positively related as indicated by the Pearson correlation coefficient and its p-value inside the panel. **B**. Same convention as A, but the conditions with lower layer sites, showing virtually no correlation.

For the overall population, disregarding type designations, the correlation coefficient for percentage modulation of spike and LFP was examined. The correlation coefficient was 0.47 ($p<10^{-3}$) for the total of 517 stimulus conditions (11 SOAs X 47 S1-S2 sequences). For this particular analysis, the RMS values of the LFP during the period of 0-300ms after S2 onset were calculated. However, such

interval may truncate the sLFP evoked by S1, especially in those trials with relatively long SOA. For this reason, the same analysis was repeated using a wider window for the LFP signal, spanning from 100ms before to 300ms after S2 onset, and found similar results; the mean correlation between percentage modulation was 0.37 ($p<10^{-4}$).

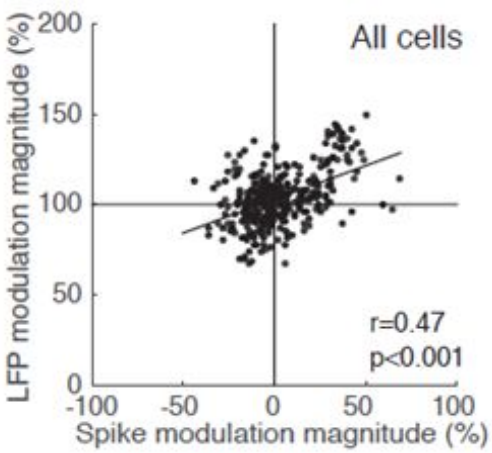

Figure 12. Relationship between spike and LFP modulation (All types combined).

Scatter plot showing the percentage changes in spike activity and RMS LFP power in the S1-S2 sequence relative to the S2-alone condition for all conditions and sites (517 stimulus conditions, 11SOA X 47 S1-S2 sequences). They are positively related as indicated by the Pearson correlation coefficient and its p-value inside the panel.

5.1.3 Spike and LFP modulation of different SOA conditions

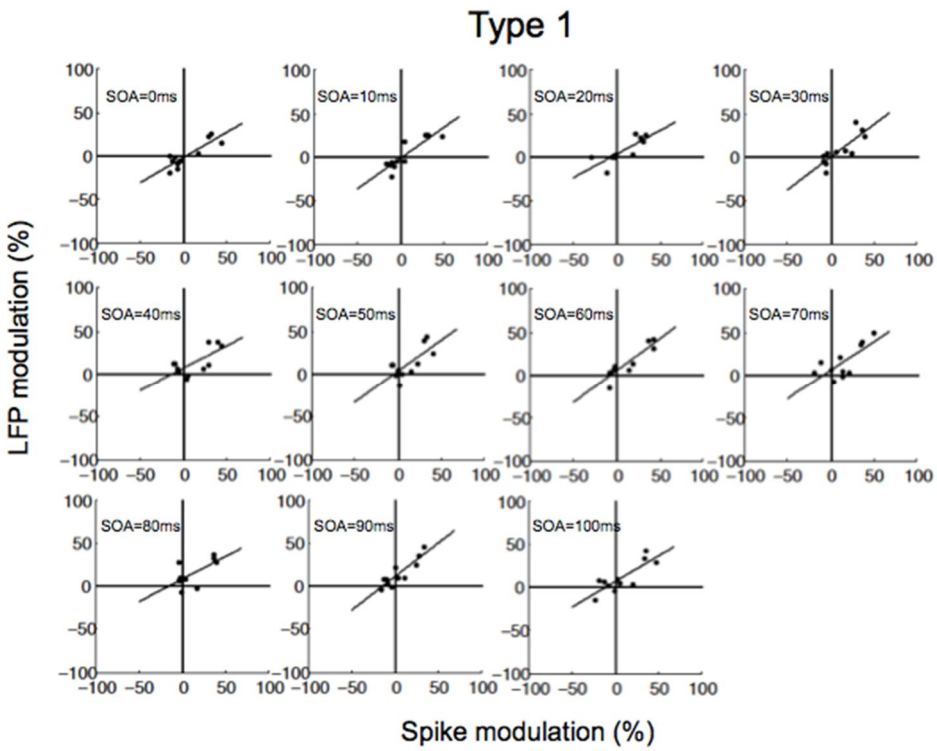

Figure 13. Relationship between spike and LFP modulation; Type 1 across SOA conditions

Scatter plots showing the percentage changes in spike activity and RMS LFP power in the S1-S2 sequence relative to the S2-alone condition for all 11 SOA conditions separately for Type 1. Each panel contains 11 dots from 11 sites. All conditions are positively related as indicated by the Pearson correlation coefficient but only significant p-values were observed from SOA 10, 30, 50, 60, 70ms ($p<0.05$).

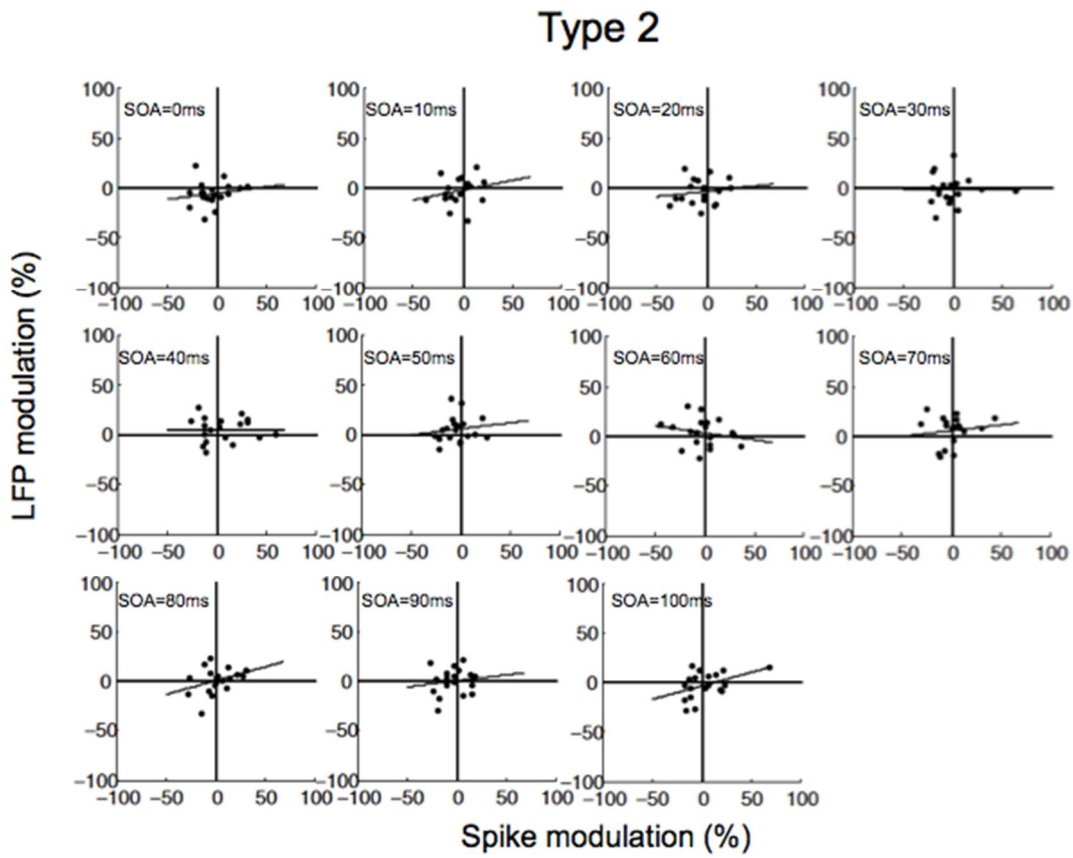

Figure 14. Relationship between spike and LFP modulation; Type 2 across SOA conditions

Scatter plots showing the percentage changes in spike activity and RMS LFP power in the S1-S2 sequence relative to the S2-alone condition for all 11 SOA conditions separately for Type 2. Each panel contains 11 dots from 11 sites. They are not as positively related as in Type 1 indicated by the Pearson correlation coefficient but the significant p-values were observed from SOA 50, 80, 90, 100ms ($p<0.05$)

The figures 10, 11, 12 illustrate relationship between SOA-dependent modulation of spike and LFP for all SOA conditions combined. In figures 13 and 14, all the 11 conditions were separated and plotted. Highly significant correlation still

exists in Type 1 across SOAs (Figure 13), and relatively weaker relationship between spike and LFP modulation in Type 2 (Figure 14) compared to Type 1 across 11 SOA conditions.

5.1.4 Spike and LFP modulation of each subject

S2 Classified	Subjects (n=30)					
	CR			IR		
	Coefficient	P-value	cells	Coefficient	P-value	cells
Type 1	0.64	10^{-4}	4	0.78	10^{-4}	7
Type 2	0.047	0.57	13	0.40	10^{-3}	6

Table 1. S2 Types classification and animal difference in relationship between spike and LFP modulation

The relationship between spike and LFP modulation was compared between subjects. Monkey CR showed significant correlation between spike and LFP modulation depending on the SOA for Type 1 and non-significance for Type 2. Monkey IR showed significant relationship for both Type1 and Type2 (Table 1).

5.2 Time course of correlation coefficient

During S1-S2 sequence presentation, the S1-evoked sLFP is likely to mediate LFP modulation. However, its role in modulation of spike activity cannot be determined by the correlation shown in Figures 10, 11, and 12. For that, we examined the precise time course of correlation between the magnitude of SOA-dependent LFP and that of spike activity. The goal of this analysis was to temporally localize the pattern of SOA-dependency of spike activity on the trace of LFP signal. Figure 15 graphically illustrates how this analysis was done. First, the SOA-dependent spike activity (Figure 15A) was drawn from mean spike density during 50 to 150ms after S2 onset. This example cell is the same cell shown in Figure 8, showing facilitative response for most SOAs with respect to response magnitude of the S2-alone condition (Figure 15A, dashed line). For the time course of correlation between the magnitude of SOA-dependent spike and corresponding LFP activity, the Pearson product-moment correlation coefficient was calculated based on 11 SOA conditions for each S1-S2 sequence condition, and averaged over all 47 sequence conditions tested at 31 recording sites. Overall, the correlation was initially positively peaking, but decreased until it reached a negative peak at around 100ms after S2 onset (Figure 15C), a phenomenon that was mainly due to the upper group cells (Table 2). The initial positive correlation occurred before the onset of spike activity in response to S2; the peak of correlation occurred at 33ms after S2 onset (Figure 15C, arrow), and at 26ms after S2 onset for upper group cells. These results indicate

that the raw LFP amplitude before onset of spike activity can predict the pattern of SOA-selectivity of spike activity that was calculated over the period of 50-150ms after S2 onset.

We localized the first and second peaks of correlation (Figure 15D), and calculated the correlation coefficients at these peaks (Figure 15E) for each stimulus condition. For all 47 S1-S2 sequence conditions tested at 31 sites, the first and second peaks were found at 45.15±36.0ms and 119.32±38.3ms (dashed line in Figure 15D). The mean correlation coefficients at these peaks were 0.32±0.24 and -0.42±0.33, respectively (Figure 15E). Again, the timing of the first peak correlation occurred before the peak spike activity, and even before the start of spike activity in some sequence conditions (Figure 15D, upper histogram). In other words, for these conditions, the pattern of SOA-dependency of LFP change predicted the SOA-dependency of spike modulation, even before the onset of spike activity, suggesting that the sLFP evoked by S1 influenced the spike modulation in response to S1-S2 sequence, consistent with Figure 15C. The timing of the second peak and its negative correlation suggest that this resulted from the peak spike activity being coupled to negative LFP (Gray & Singer, 1989) and a sharp negativity of the LFP at the time of the spike (Rasch, Gretton, Murayama, Maass, & Logothetis, 2008).

Since surround interaction involved suppression with varying temporal dynamics (Henry, Joshi, Xing, Shapley, & Hawken, 2013a), we repeated the above

analysis using different analysis windows for calculating SOA-dependency of spike activity: 50-200ms and 50-300ms after S2 onset. The results revealed similar locations and magnitudes of peak correlation, and the number of conditions with significant correlation, 10 of 47 conditions for a positive first peak and 21 of 47 conditions for a negative second peak were significant with both analysis windows.

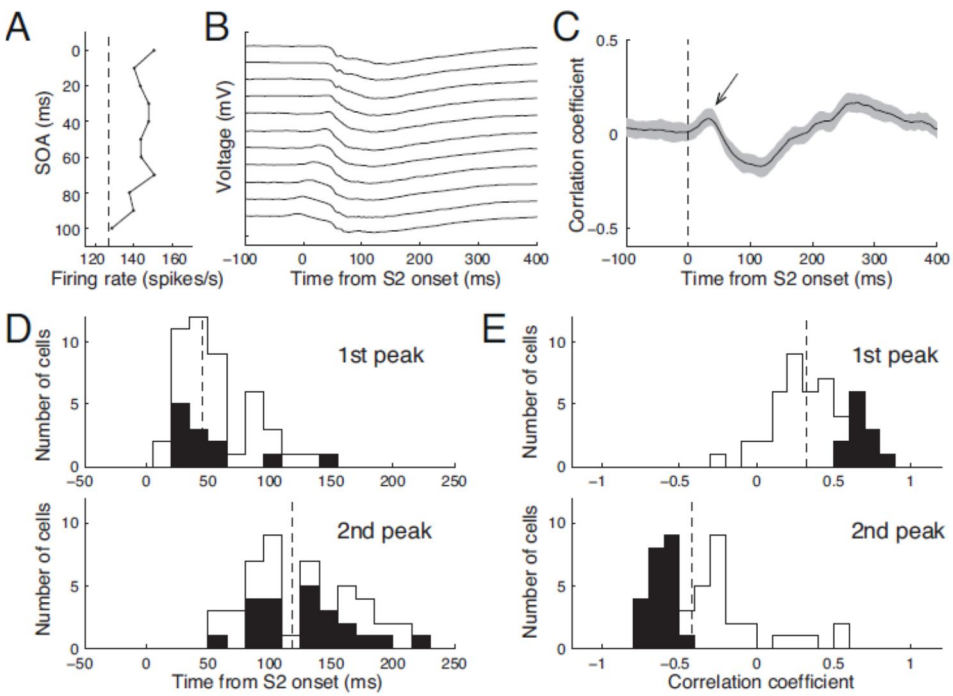

Figure 15. Correlation between spike activity and LFP.

A.SOA-dependent spike modulation for the cell shown in Figure 8. The mean firing rates during the post-stimulus period of 50-150ms of S2 are plotted as a function of SOA. Vertical dashed lines are the reference response levels evoked by S2 alone. **B**. Simultaneously recorded mean LFP traces for corresponding SOAs, ranging from 0 to 100ms in steps of 10ms (from top to bottom), are aligned at S2 onset for the cell shown in A. Traces are vertically shifted for visibility. **C**. Time

course of mean correlation between spike and LFP modulation. The correlation coefficient between the SOA-dependent firing rate (as shown in A) and the instantaneous amplitude of LFP (as shown in B) was first calculated every 1ms for each condition. Shown is the mean correlation coefficient time course averaged over all 517 stimulus conditions (11 SOAs X 47 S1-S2 sequences) from 31 cells including cases in which S1 was tested at more than one RF diameter away. The shading represents ±1 SE. Note a positive correlation immediately after S2 onset (arrow) and a subsequent negative correlation. **D.E**. Frequency histograms of the time from S2 onset 13D) and the correlation coefficient (E) for the 1st (upper panel) and 2nd (lower panel) peaks in the time course of correlation. Dashed vertical lines indicate distribution means. For the 1st peak correlation, the mean location was 45.25± 36.0ms and the mean correlation coefficient was 0.32 ±0.24. For the 2nd peak, the mean location was 119±38.3ms, and the mean correlation coefficient was -0.42±0.33. Black bars indicate significant cases, as determined with a bootstrap statistical test ($p<0.05$).

S2 Classified	Subjects							
	CR				IR			
	Positive Peak		Negative Peak		Positive Peak		Negative Peak	
	Coef (r)	Latency (ms)	Coef (r)	Latency (ms)	Coef (r)	Latency (ms)	Coef (r)	Latency (ms)
Type 1	0.27	33	-0.35	103	0.23	22	-0.39	93
Type 2	0.11	-7	-0.225	75	0.26	47	-0.33	129

Table 2. Peak correlation location of correlation timecourse between SOA-dependent spike and LFP modulation.

As mentioned above, the positively peaking phenomenon is largely contributed by the upper group cells especially for monkey CR having relatively higher correlation

coefficients for Type1 (=upper group) than Type 2 (=lower group) (Table2).

6. Control of eye position

A critical issue for comparing the response magnitude across SOA conditions is the stability of eye position, because trained monkeys can make short-latency saccades to visual targets, and the latency can be close to 100ms (Rohrer & Sparks, 1993) or even less (Boch, Fischer, & Ramsperger, 1984). For this reason, the eye stability was examined in two ways. First, for each SOA conditions, I checked whether the mean horizontal and vertical eye positions during the 20-ms presentation S2 were within 2 or 3SD of the mean of the site. Second, we determined if the presentation of S1 resulted in a change in eye position by the time S2 was presented by examining the statistical difference in the mean vectorial eye positions, $\sqrt{h^2+v^2}$, where h and v are horizontal and vertical eye positions, respectively, between the S2-alone condition and the S1-S2 sequence condition with an SOA of 100ms. The reason for using the SOA of 100ms for this comparison was that if there had been any change in eye position, it could have most likely occurred following the preceding S1. For the example cell of Figure 8, all the mean eye positions for each SOA conditions were within 2SDs of the mean eye position of the site, the vectorial eye position for the S2-alone condition was 0.26±0.14° and the vectorial eye position for the S1-S2 sequence condition with an SOA of 100ms was 0.23±0.14°. This was examined for 595 stimulus conditions tested at 31 cortical sites: 31 S2-alone, 47 S1-

alone (30 near and 17 farther S1), and 517 S1-S2 sequence (47X11 SOA). In 581 of 595 conditions, the mean horizontal and vertical eye positions were within 2SD of the mean of the site, and in the remaining 13 conditions, the eye position (either horizontal or vertical) was within 3SD of the mean, indicating that stable eye position was maintained during S2 presentation. The mean vectorial eye position during the S2-alone conditions and the S1-S2 sequence condition with an SOA of 100ms (31 S2-alone and 47 S1-S2 conditions) did not differ significantly ($p=0.12$, two sample t-test). Thus, it can be concluded that the eye position was not influenced by S1, and was stable across SOA conditions.

Conclusion & Discussion

1. Propagation of subthreshold LFP (sLFP)

Cortical cells express fast spiking activity in the midst of slow LFP changes. The spike-LFP relation has been intensively examined (Berens, Keliris, Ecker, Logothetis, & Tolias, 2008; Burns, Xing, & Shapley, 2010; Buzsaki et al., 2012; Galindo-Leon & Liu, 2010; Gaucher, Edeline, & Gourevitch, 2012; Goense & Logothetis, 2008; Jia, Xing, & Kohn, 2013; Lashgari et al., 2012; Okun et al., 2010; Rasch et al., 2008; Rutishauser, Ross, Mamelak, & Schuman, 2010). The electric field in the brain is generated exogenously by electromagnetic stimulation or endogenously by neural activity of the brain itself. Small electric fields, not strong enough to trigger action potentials by themselves, may have physiological effects by affecting spike timing and rate in response to concurrent supra-threshold synaptic inputs (Anastassiou, Perin, Markram, & Koch, 2011; Frohlich & McCormick, 2010; Ozen et al., 2010; Radman, Su, An, Parra, & Bikson, 2007). In general, the electrical activity at one site in the brain can propagate to other sites in the form of action potentials along axonal arbors and across synapses, or in the form of electromagnetic energy via volume conduction. The propagation speed of the former is constrained by myelination, diameter of conducting axons, and synaptic delays, and follows a distance-latency relationship, whereas the latter shows no such relationship because

volume conduction occurs non-synaptically with virtually no delay. In ephaptic coupling in which an electric field associated with activity occurring in a population of neurons transmits non-synaptically to neighboring neurons, even small extracellular potential changes under 0.2 mV lead to modulation of spiking time, suggesting a high sensitivity of spiking activity to extracellular potential change (Anastassiou et al., 2011; Weiss & Faber, 2010). The distance-dependency of sLFP latency (Figure 5C) indicates that sLFP is mediated via synaptic coupling. Nevertheless, the amplitude of sLFP evoked by S1 (Figure 5B) was comparable to that of ephaptic coupling, and it appears that S1-evoked sLFP similarly led to modulation of spiking activity. It is thought that long distance propagation reflects a mixture of volume conduction from distal location and local potentials (Kajikawa & Schroeder, 2011). This may help explain surround interaction with the SOA of zero.

A focal visual stimulation triggers a wave of activity propagation on the surface of visual cortex (Benucci, Frazor, & Carandini, 2007; Bringuier et al., 1999; Grinvald et al., 1994; D. Jancke, F. Chavane, S. Naaman, & A. Grinvald, 2004; Nauhaus, Busse, Ringach, & Carandini, 2012). The current study was not designed to reveal the anatomical substrates of sLFP propagation. However, the dependency of sLFP on the spatial distance between S1 and S2 (Figure 5) is consistent with the observation of Nauhaus et al. (2009) that the amplitude of spike-triggered LFPs decreases as the position of the electrode (in a 10x10 electrode array) becomes more distant from sites where spike activity is recorded in response to full-field visual

stimulation. The pattern of non-linear decay of amplitude and linear increase in latency with distance in Figure 7 is also found with the slow component of spike-triggered LFPs (Nauhaus et al., 2009; Nauhaus et al., 2012; Ray & Maunsell, 2011). The propagation speed estimated from the results shown in Figure 5C suggests that the sLFP is a result of slow propagation through horizontal connections, rather than through volume conduction from the cortical site representing the S1, consistent with the conclusions of a previous study (Benucci et al., 2007; Bringuier et al., 1999; Nauhaus et al., 2012). In the study of Bair et al. (2003), who employed large grating stimuli surrounding the RF at different distances from the RF, the latency of spike suppression did not increase with distance, but depended on the strength of suppression, and suppression sometimes arrived faster than the excitatory CRF response. However, a direct comparison with our results is difficult due to several differences in experimental protocol. First, latency was determined for the sLFP in our study, whereas they measured the latency of spike suppression. Second, in our study, S1s were identical in size and orientation, regardless of distance from the RF, whereas Bair et al. (2003) manipulated center-surround distance by varying the inner diameter of full-field surround stimuli. Consequently, a nearer annulus occupied a larger visual space than a farther one in their study. We also note that for SOA of 0 and 10ms, S1 and S2 temporally overlap, and we only speculate the effect of this overlap. Since off-response is faster than on-response (Bair, Cavanaugh, Smith, & Movshon, 2002), interaction between sLFP and spike activity may involve complex processes especially for sequences with short SOAs. However, we noticed no

apparent difference in correlation coefficients across SOA conditions in correlation coefficients between geometric means of percentage changes of LFP and spike across trials calculated separately for each SOA condition (otherwise same as Figure 10) for both cell types (Table 1) or types separated based on cortical depth as shown in Figure 11.

I found that the sLFP was reliably evoked by stimuli falling as far as 10mm away from the RF in cortical distance. This extent is much greater than the estimates based on spike/stimulus-triggered LFPs (Katzner et al., 2009; Nauhaus et al., 2009; Nauhaus et al., 2012; Ray & Maunsell, 2011; D. Xing et al., 2009), but comparable to previous subthreshold intracellular responses evoked by peripheral stimuli as distant as 10-15° (Series et al., 2003), and consistent with a passive spread of LFPs over 10mm (Kajikawa & Schroeder, 2011). In some cases, I could even detect an sLFP induced by a Gabor stimulus that was confined within the contralateral hemisphere. The sLFP showed decreased magnitude and increased latency as the cortical distance between S1 and S2 increased, consistent with previous studies on spike-triggered average of LFP signals (Nauhaus et al., 2009; Ray & Maunsell, 2011), suggesting that both these potentials arise through the same mechanism.

2. Interaction between sLFP and response to RF stimulus

Previous studies examined the cortical spread of the LFP and its relationship to spike activity (Katzner et al., 2009; J. Liu & Newsome, 2006; Logothetis, Kayser, & Oeltermann, 2007; U Mitzdorf, 1987; Nauhaus et al., 2012; D. Xing et al., 2009). These studies, which were mostly based on the spike-triggered LFP, revealed a decrease in correlation between spike activity and LFP response as stimulus size extends beyond the classical discharge field, and suggest a local nature of LFP in relation to multiple unit activity (Katzner et al., 2009; D. Xing et al., 2009). In contrast, we specifically isolated a stimulus-locked LFP in the V1 that was subthreshold for evoking a spike response, and examined its role in surround interaction. To meet the criteria of 'subthreshold', one-third of the data were excluded following off-line analysis. This procedure enabled us to evaluate the roles of LFP for spike responses, as otherwise, the LFP contributed by spiking itself confounds the analysis.

A major goal of the current study was to examine the influence of the sLFP on neural response by analyzing the interaction between the sLFP induced by a surround stimulus and the spike or LFP response to an RF stimulus. It is known that the LFP and membrane potential of the cortical neurons in awake animals are correlated (Okun et al., 2010). Also, particularly in awake animals, responses to visual stimulation are dominated by synaptic inhibition (Haider, Hausser, &

Carandini, 2013), and spike initiation is correlated with a decrease of inhibition (Rudolph, Pospischil, Timofeev, & Destexhe, 2007). We found that facilitation of spike response was associated with the increase in the RMS power of LFP, whereas the link between spike suppression and LFP change was not as evident as with spike facilitation (Figure 12). This apparent asymmetry in linking LFP and spike activity is interesting. The LFP originates from extracellular currents of multiple sources including action potentials, excitatory currents, and inhibitory currents that may contribute differently to the induction of a LFP change. For example, inhibitory currents mediated by $GABA_A$ are assumed to contribute little to field potentials (Buzsaki et al., 2012).

Introducing a variable SOA enabled us to examine covariation between SOA-dependent modulation of LFP and spike activity. Under the assumptions that the S1-induced sLFP collides with neural activity evoked by S2 with a timing relation dictated by the SOA, and that this collision modulates spike activity, SOA-dependency of spike activity (variable magnitude of spike response as a function of SOA) should mimic the SOA-dependency of LFP modulation. The analysis of correlation between the magnitudes of LFP and spike modulation revealed a significant correlation for some neurons, substantiating this assumption and revealing the temporal relation between the two. In particular, the first positive correlation of Figure 15C-D suggests that modulation of LFP by S1 precedes spike modulation. The magnitude of the positive correlation was comparable to the ensuing negative

correlation (Figure 15E). Therefore, we conclude that the sLFP evoked by S1 participates in modulation of spike activity in response to S2.

One interesting finding from the current study is that the pattern of interaction between the LFP and spike activity appears to differ across cortical depth. In the current study, we used the suprathreshold LFP as a guide to divide recording sites into two depth groups in a situation where anatomical verification of recording sites was hard to obtain because the subjects are now participating in other studies. Note that these LFP responses were evoked by the optimal stimulus tailored to the individual recording site for orientation, size, and spatial frequency, as well as retinal position. This is important because the optimal spatial frequency and the size of the receptive field vary depending on laminar position of recording sites (Wang et al., 2013), and a common visual stimulus used with array electrodes, diffuse light stimulation (C. E. Schroeder, Mehta, & Givre, 1998), or electrical stimulation of afferent fibers (U. Mitzdorf & Singer, 1978) may not be optimal for cells at some recording sites due to the variable contribution of phase-sensitivity, spatial summation, or surround interactions. The additional negative peak has been noted to start at the border between supragranular and granular layers (Kajikawa & Schroeder, 2011), and the relatively short LFP latency of lower sites that was associated with the negative peak strongly suggests that the border between upper (=Type1) and lower (=Type2) is near layer 4C (Maier, Aura, & Leopold, 2011). We conclude that the upper sites were mostly in the supragranular layers, and the lower sites included the

granular and infragranular layers. Regardless of the match between our depth division and anatomical laminar border, the roles of sLFP was depth-specific; surround stimuli evoked an sLFP in the upper cortical layers with large RMS power and facilitated the spike response in a manner suggesting systematic coupling to the LFP change, whereas at lower cortical depths, sLFP power was relatively lower, and spike response tended to be suppressed. The layer-specific surround interaction has been studied in terms of feedforward versus feedback pathways (Ichida et al., 2007), but direct comparison is difficult due to different stimulus configuration.

One possibility that correlation was high in upper sites compared to lower sites is that the distance between the recording site and the guide tube that was used for signal ground was relatively close in upper sites compared to lower sites, thus sLFP recorded from the upper sites was more local than that from lower sites. This may explain a higher correlation in the upper than the lower sites. However, the differential proportion of facilitative effects of spike activity by S2 (Figures 10~12) discounts this possibility.

Previous studies reported various effects of surround stimuli, both suppressive and facilitative (Cavanaugh et al., 2002; M. K. Kapadia, M. Ito, C. D. Gilbert, & G. Westheimer, 1995; Y. J. Liu, Hashemi-Nezhad, & Lyon, 2011; Polat, Mizobe, Pettet, Kasamatsu, & Norcia, 1998; Sceniak, Ringach, Hawken, & Shapley, 1999), and conflicting results on the laminar effects of surround interactions, ranging

from no significant laminar difference in surround suppression (H. Jones et al., 2001; Levitt & Lund, 2002) to laminar-specific surround suppression (Sceniak, Hawken, & Shapley, 2001). These inconsistent results may have been due to differences in the stimuli tested. Some studies used grating patches (Levitt & Lund, 2002; Sceniak et al., 2001), and others used grating annuli (Ichida et al., 2007; H. Jones et al., 2001) of varying contrast. Since we additionally introduced temporal aspects in the stimulus condition, it is difficult to directly compare ours with previous studies. Nevertheless, dominant facilitation in upper group and suppression in lower depth group observed in the current study are consistent with previous reports (Ichida et al., 2007; Sceniak et al., 2001), and different surround interactions for Types 1 and 2 are at least consistent with a recent report that cells of layers 2/3 show a greater contrast sensitivity to surround stimuli than to RF stimuli (Henry, Joshi, Xing, Shapley, & Hawken, 2013b).

Spike modulation by surround stimulation is thought to enhance response selectivity (Haider et al., 2010; Kim et al., 2012; Vinje & Gallant, 2002) and integration of context information (Haslinger et al., 2012; Smith & Muckli, 2010). Signals evoked by S1 and S2 follow their own fixed time courses, and then disappear. Therefore, these signals can interact with each other only during a limited temporal window that is determined by the SOA between S1 and S2. However, as we pointed out in a previous study, this temporal window only partially explains the SOA-dependency of spike activity; spike modulation occurs within that temporal window,

but even within the window, the magnitude of spike modulation varies with SOA (Kim et al., 2012). Since surround interactions are mediated by multiple pathways, feedforward, lateral, and feedback connections (Angelucci & Bressloff, 2006), one possibility is that S1 mediates LFP modulation via pathways that interact with each other even before modulating spike activity. Thus, the process determining LFP-dependency and SOA-dependency of spike modulation is intricate, and the precise relation between these components and sLFP in surround modulation awaits future studies.

Study 2

Introduction

The spike activity in primary visual cortex shows variability across trials, and that the activity is likely to mediate visually-guided behavioral responses. Electrophysiological studies on the V1 of monkeys performing visuo-motor tasks have shown that the V1 activity extends beyond pure sensory processing (Nienborg & Cumming, 2014; Palmer, Cheng, & Seidemann, 2007; Super, 2006). Furthermore, when the animal makes a saccadic eye movement toward a visual stimulus that suddenly appears in periphery, the time of first spike, or neural latency of V1 activity elicited in response to the visual stimulus is correlated with saccade latency on a trial-to-trial basis (J. Lee, Kim, & Lee, 2010). The nature of the link can be further evaluated by varying spike timing, but it is difficult to do so in awake monkeys. On the other hand, experimental manipulations are available that are known to influence saccade latency, such as the gap saccade paradigm. In the current study, we examined whether and how the V1 activity changes with the gap effect.

In the gap effect, saccade latency is reduced when a fixation point is extinguished prior to saccadic target onset, and express saccades, saccadic eye

movements of extremely short latency, occur more frequently (Dick, Kathmann, Ostendorf, & Ploner, 2005; M. C. Dorris & Munoz, 1995; B. Fischer & R. Boch, 1983; Fischer & Ramsperger, 1984; Jin & Reeves, 2009; Kingstone & Klein, 1993a, 1993b; Pratt, Bekkering, Abrams, & Adam, 1999; Pratt, Lajonchere, & Abrams, 2006; Reuter-Lorenz, Hughes, & Fendrich, 1991; Saslow, 1967; D. Sparks, W. Rohrer, & Y. Zhang, 2000). Such occurrence of RT reduction known as gap effect is already well known and has been replicated by many studies. A number of attributors for this reduction of RT include facilitated sensory processing (Reulen, 1984), oculomotor readiness (Rolfs & Vitu, 2007), attentional processes (Fischer & Breitmeyer, 1987), and its neural correlate of superior colliculus with fixation cell (M. C. Dorris & Munoz, 1995). However, those attributors were found to be unlikely to generate such effects.

In gap paradigm, the offset of fixation target before appearance of saccade target is a critical element for gap effects, may represent a surround interaction in which V1 response to appearance of a saccade target inside the receptive field (RF) is modulated by offset of fixation target outside the RF, thereby influencing saccadic response time. Such hypothesis (Figure 16) can be drawn from the results of Study 1 that showed quite strong effect of LFP signal propagation, having the extent up to 10mm of cortical distance. Even some of our results showed low frequency signal propagated across the other visual field of the recording cell.

The main goal of the current study was to determine whether changes in V1 activity accompany the gap effect, specifically, whether first spike of V1 occurs earlier in the gap condition and whether first spike occurs earlier with a larger gap duration in parallel with a greater reduction of saccade latency. We also determined whether presenting gap changes the state of V1 cortex by the time of target onset, and whether changes in V1 activity accompany before express latency saccades are made as well. In doing so, we examined the local field potential (LFP) that was simultaneously recorded along spike signal, since the cortical activity during pre-target period is related to generation of human express saccades (Hamm, Dyckman, Ethridge, McDowell, & Clementz, 2010).

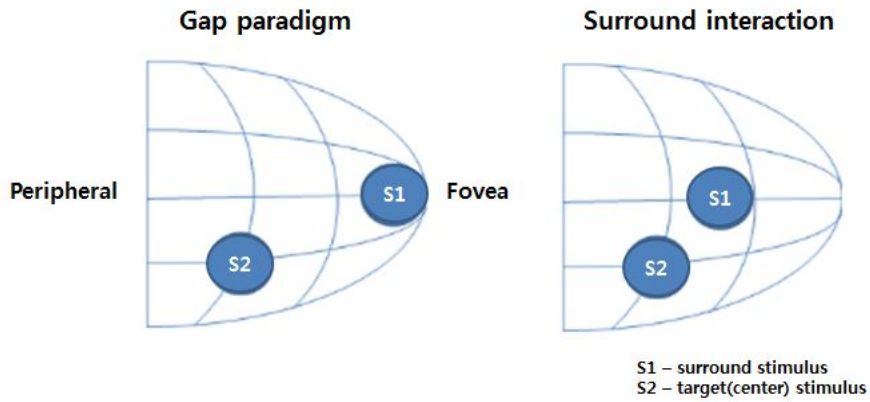

Figure 16. Topographic representation of gap paradigm and surround interaction.

The contours illustrate topographic map of V1 (left is peripheral right is foveal location). S1 indicates surround stimulus, S2, target (center) stimulus. The topographic map and the location of S1 and S2 graphically show the anatomical distance between fixation (S1) and saccadic target (S2) locations during gap paradigm. Similarly the right panel represent the distance between S1 (surround) and S2 (RF) stimulus from study1. Note that S1 location (fovea) is farther away from S2 location in gap paradigm compared to surround interaction scheme.

Methods

Methods in this study have the same processes as described in study 1 including daily recording session, device setup as well as post-processing of spike activity (e.g. spike extraction, spike sorting), unless stated otherwise below.

Subject

Two adult monkeys (DC, NB, *Macaca mulatta*, 8-9 years old) were used in the current study. Both monkeys had been trained extensively for visual discrimination tasks involving visually guided saccades prior to the current study, and readily performed gap saccade task.

1. Gap paradigm

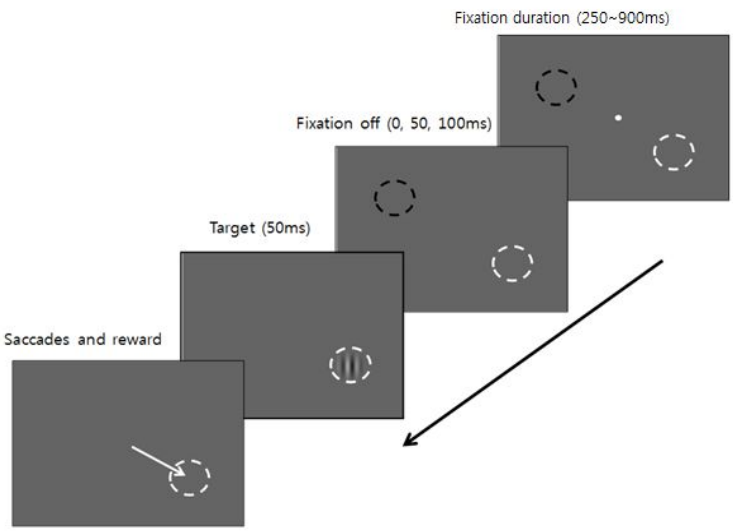

Figure 17. Trial sequence during gap paradigm

White dashed circle indicates a saccadic target location, where receptive field of recording cell is located as well. Black dashed circle indicates the saccadic target location symmetrically presented to the other hemifield. While monkey was fixating at the central fixation target (white circle), a Gabor target appeared (50ms

duration) after fixation duration randomized between 250-900ms, and monkey had to make a saccadic eye movement to the target location. A number of conditions with/without gap between fixation offset and target onset time were randomly presented within a block.

In the current study, the trial conditions included Gap0 (fixation offset and target onset occur at the same time), Gap50 and Gap100 (a temporal gap of 50ms and 100ms between fixation offset and saccade target onset, respectively) for both RF and RF-opposite sides. All the trial conditions were pseudo-randomized within a block. Due to RF mapping that lasted more than half an hour, for any recording session, only one cell was recorded. Once the animal learned to not leave the fixation point until its offset, the gap saccade task was easy and the animal was successfully rewarded more than 95% trials. If the animal failed the task, which was mostly due to the animal's distraction, the failed trial condition was supplemented at the end of each block.

2. Data analysis

Note that the off-line procedures for determining saccade latency, neural latency and firing rate were identical to those employed in the previous study (J. Lee et al., 2010).

2.1 Saccade latency analysis

In order to analyze saccadic latency, a number of steps were performed. First, the initial horizontal and vertical eye signals of 25 kHz from the experiment were down sampled to 1 kHz signal for this analysis. Then, the signals were separately smoothed with 20ms window, which brought noise elimination effect. Using 50ms or larger smoothing window slightly delayed the latency, thus, 20ms window was used to avoid overestimation of saccadic latency. The eye signals then differentiated and the saccade latency was defined with a velocity criterion of 15°/s, where the latency was drawn from backward sliding from its maximum velocity.

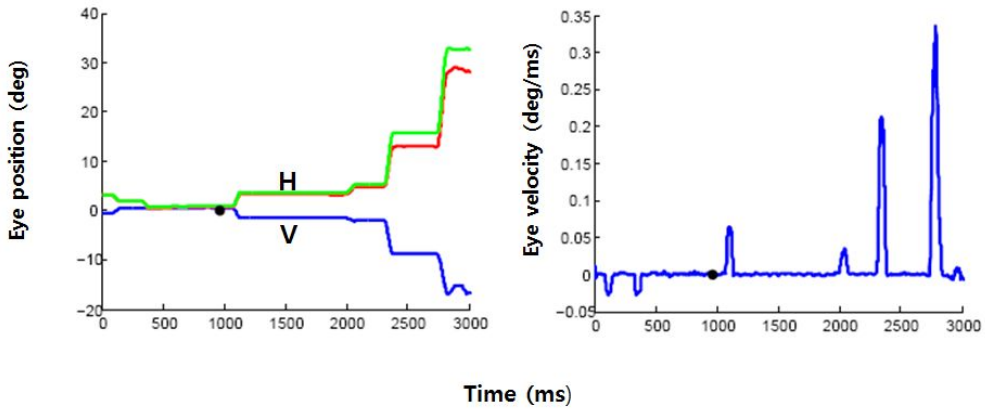

Figure 18. An example trial of eye signal

Horizontal (H) and vertical (V) eye positions are shown in the left panel. Black dot indicates target onset time. The eye position signals in the left were converted into eye velocity is shown in the right panel with the black dot indicating target onset time.

2.2 Neural latency analysis

In order to define neural latency from each trial, first, spike density was derived by convolving the spike sequence with a kernel function with asymmetric time constants for growth (1m) and decay (20ms) phases. Neural latency was defined as the time of first spike after spike density crossed one SD above the mean density of the pre-target period of 200ms and remained above the crossing level for at least 5ms. The crossing point was searched backward from the peak density to avoid false discovery. The spike timing and LFP signals were downsampled to 1 kHz for

subsequent analyses.

2.3 Invalid trials

Invalid trials were discarded during off-line analysis. These included the trials in which the eye position overstepped the circular window of 1.5° in diameter about the fixation point, the eye velocity exceeded 50°/s during presentation of saccade target for 50ms, and firing rate during the post-target period of 50-150ms, or neural latency deviated more than 3SDs from the mean of each trial condition. The trials of saccade latency less than 50ms or larger than 500ms were also excluded. The excluded trials were around 5% of total trials. For the later spectral analysis, the fixation duration shorter than 400ms were eliminated such particular results in order to avoid possible effect from fixation attainment to the neural activity for shorter fixation duration trials. Those were around 8 % of total trials used for main analysis results.

2.4 Separation of express and regular latency saccades

2.4.1 Least square using two-termed Gaussian model

One of the distinctive behavioral results was bimodality of saccadic latency distribution. In order to examine the bimodality of saccadic latency, the distribution

had to be properly separated into two populations; express (faster saccade) and regular (slower saccade) groups. In order to do this, the frequency distribution of saccade latency was fitted with a 6-parameter Gaussian model; $F(x)=A \bullet G(\mu_1,\sigma_1)+B \bullet G(\mu_2,\sigma_2)$, where $F(x)$ is frequency distribution of latency, x, in millisecond, and A and B are the amplitude parameters of two Gaussians with position and shape parameters, μ, and σ, respectively.

2.4.2 Population distribution based separation

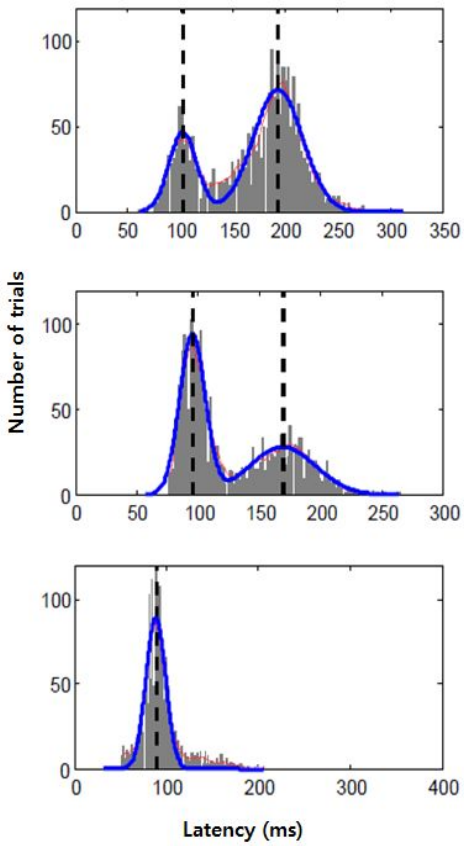

Figure 19. Example of two-termed Gaussian model fitting on population distribution

Population saccade latency distribution from all trials is plotted as histogram format. Step condition is shown in the upper, Gap50 condition in the middle and Gap100 in the lower. Step and Gap50 conditions show clear bimodality, whereas Gap100 condition show increased number of faster saccades. The blue lines in all three panels indicate fitted result drawn to the distribution. The dashed lines show mean of distribution peak for each separated groups. Note that the above distributions are from only subject DC, and the saccades were made toward contralateral side.

From the fitting result, the minimum value between first and second latency group was used as the dip separating express and regular saccade groups in population level.

2.4.3 Individual session based separation

The same fitting process was performed for individual site and some of the fitting results (from two sites) are shown in Figure 20. The arrow in the left panel of Figure 20 indicates the minimum point that was used as the dip for separation of express and regular saccade groups. The same convention was applied to others throughout experimental conditions.

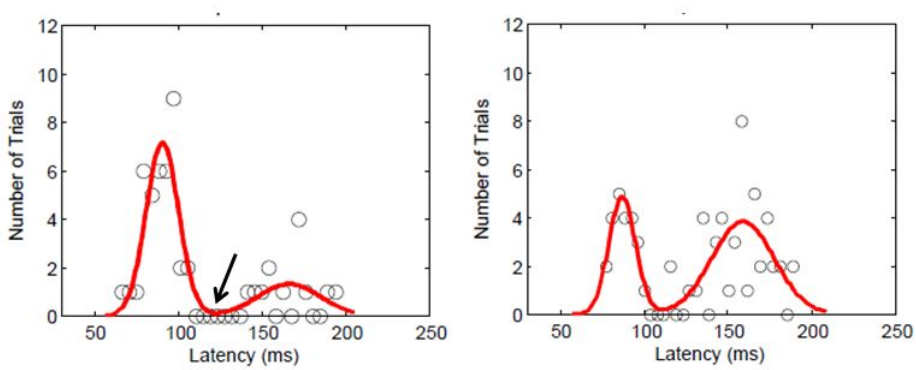

Figure 20. Examples of two-termed Gaussian model fitting on individual sites
Frequency of population saccade latency distribution is plotted as circles in each panel. The minimum point from the fitted result was determined to be the dip separating express and regular trials (left, arrow, same convention for the right panel example). Each panel show fitted result from different recording sessions.

Fitting the latency distribution with the least square using two-termed Gaussian model allowed us to identify a dip separating the two groups on a session basis as explained above (Figure 20). However, when the bimodality was not apparent, the division latency was taken from the population distribution summed over all sessions for each gap duration condition for each animal (Figure19). The session-based division latency varied across sessions, and its mean for Gap0 and Gap50 conditions was later than that based on the population distribution, by 9.53 and 5.31ms, respectively, and that for Gap100 condition was earlier by 2.62ms.

2.5 Statistical test of difference in spike density

We statistically evaluated the difference in spike density between express and regular latency saccade groups with a bootstrap test. The difference in spike density calculated over a moving window of 10ms was evaluated against the probability distribution derived from 1000 simulations under the hypothesis of no difference between the two latency groups. The test was performed for each time bin (1ms). In order to correct for multiple comparison, we controlled false discovery rate (FDR) according to Benjamini & Hochberg (1995). This controlled type I error with adjusted p-values.

2.6 LFP power analysis

In order to examine the correlation between oscillatory power of LFP and saccade latency, and the difference in LFP power between express and regular latency saccade groups, first, 60Hz line noise was removed from LFP signal using rmlinesc.m provided by Chronux.org. The sampling frequency of the input data was 1kHz, and 3 tapers were used with frequency range between 0.1-140Hz for computation. Then, spectral power was estimated with the noise-removed LFP using mtspectrumc.m. The same number of tapers, sampling frequency and frequency range (0.1-140Hz) was used as above using Chronux Matlab toolbox (Bokil, Andrews, Kulkarni, Mehta, & Mitra, 2010).

2.7 Evaulation of eye stability

The eye stability is obviously a concern in comparison of neural activity across different conditions. The eye movement during fixation includes microsaccade, drift, and tremor (R. H. Carpenter, 1988). We derived an estimate of eye stability based on a metric, $CV(t)=\sum_{i=0}^{t}\left|EV(i)\right|$, where $CV(t)$ is a cumulative velocity of the eye from the start to time *t*, and $\left|EV(i)\right|$ is the absolute value of instantaneous vectorial velocity at i_{th} bin of 1ms .We evaluated the eye stability in the behavioral data

obtained from 20 sessions in the early phase of study in which various gap durations were employed (Figure 21). For this, we calculated $CV(t)$ starting from 300ms before saccade target onset for each gap duration condition. It monotonically increased until about 150ms after fixation target offset, then, it started to increase rapidly. Thus, with the gap duration of 200ms, the eye fixation was already unstable at the time of saccade target presentation (Figure 21, black trace). This is not necessarily related to occurrence of microsaccades since the rate of monkey microsaccade decreases as a trial progresses (Hafed, Lovejoy, & Krauzlis, 2011). Also, longer gap duration caused weak visual response due to shift of receptive field location with significantly unstable eye position. In any case, based on these results, we limited the range of gap duration within 100ms in the current study.

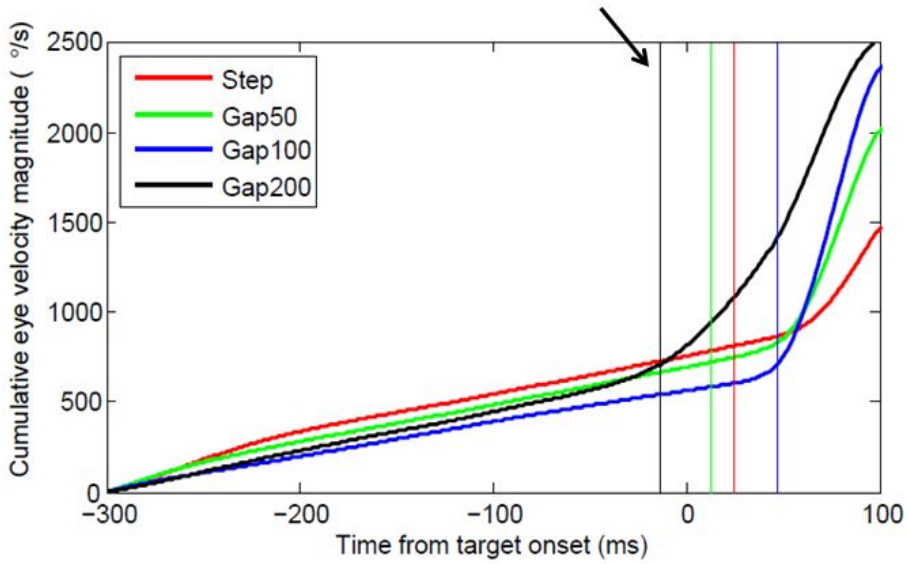

Figure 21. Cumulative eye velocity

Mean trace of cumulated eye velocity from 20 sessions having Gap200. X-axis is the trace aligned to the target onset. Each condition has 1000 trials; Gap0 (Red), Gap50 (Green), Gap100 (Blue), Gap200 (Black). The vertical lines (arrow) indicate the point crossing 1SD from cumulated eye velocity of mean baseline (-300ms) periods.

Results

1. Data summary

The results are based on 74 single cells recorded from 74 sites in the operculum V1 of two monkeys (monkey DC: 45 cells, monkey NB: 29 cells) during 74 recording sessions. The mean recording depth from the dura surface was 1.33±0.44mm for DC and 1.77±0.44mm for NB. Although the dura was thinned every week, the tissue drag during penetration was inevitable, and accordingly these numbers are rough estimates of true cortical depth of recording sites, potentially containing considerable errors. The mean eccentricities of the RFs were 3.59°±0.29° for monkey DC and 4.17°±1.55° for monkey NB.

2. The effect of gap on behavior

Figure 22 illustrates the overall gap effect on behavior combined from the data for all 74 recordings. Confirming previous studies (M. C. Dorris & Munoz, 1995; B Fischer & R Boch, 1983; David Sparks et al., 2000), the mean saccade latency decreased as the gap duration increased over the range of the current study in both monkeys; the mean saccade latencies combined from two monkeys were 165.37,

122.87, and 100.12ms for Gap0, Gap50 and Gap100 conditions, respectively.

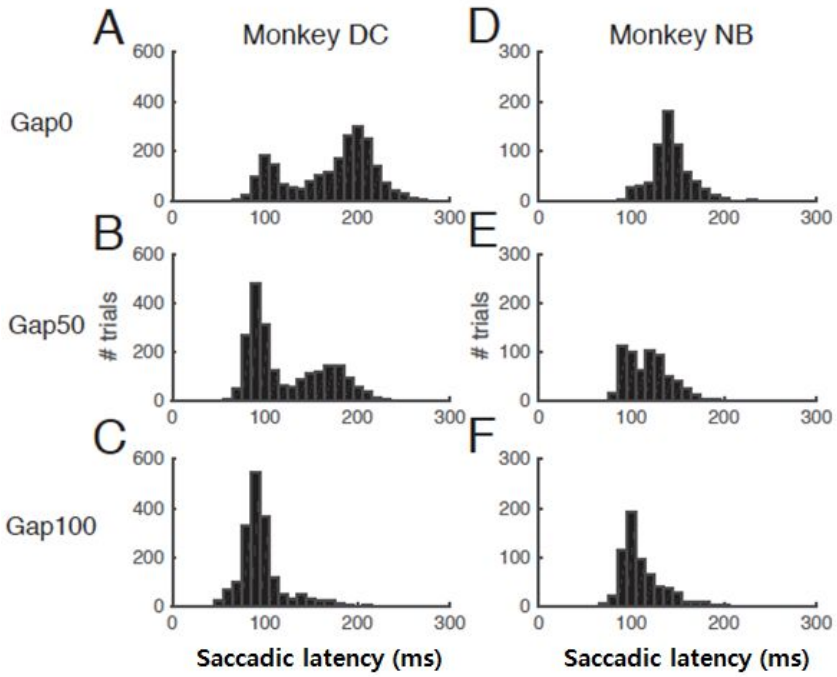

Figure 22. Saccadic distribution of gap effect

Summary of the gap effects on saccade latency (A-F) for each monkey. As gap duration increased from 0 (A, D), to 50 (B, E), to 100ms (C, F), the mean latency decreased. Mean latency is 172.03, 124.06, 96.19ms (one-way ANOVA, $p<0.05$) for A,B, and C, respectively, and 142.66, 118.70, and 111.20ms (one-way ANOVA, $p<0.05$) for D,E, and F, respectively. Also note that the distribution of saccade latency is bimodal in some conditions (A, B, E).

3. The effect of gap on physiology

Figure 23 illustrates the effect of gap on physiology, showing a representative cell activity from monkey DC while he performed the task. With the gap duration of 0ms ('Gap0'), most saccade latencies were around 200ms (Figure 23A, blue symbols), whereas with the gap duration of 100ms ('Gap100'), most saccade latencies were around 100ms (Figure 21C). With the gap duration of 50ms ('Gap50'), two latency groups of saccades, express and regular, were observed. Accompanying this decrease in overall saccade latency with an increase in gap duration, the spike activity of the cell changed. The spike activity of initial visual response differed depending on gap duration (Figure 23D). Quantitative aspect of this change is given in Figure 23E; the firing rate during the post-stimulus period of 50-150ms increased, and the time of first spike of visual response, or neural latency, decreased with the increase in gap duration. The difference between Gap0 and Gap100 was statistically significant for both firing rate and neural latency (two-sample t-test, $p<0.05$). The spike activity was similarly contrasted between saccades of express and regular latencies (Figure 23F, G); neural latency was shorter (two-sample t-test, $p=0.01$) and firing rate tended to be higher for express compared to regular saccades, but the difference was not statistically significant (two-sample t-test, $p=0.10$).

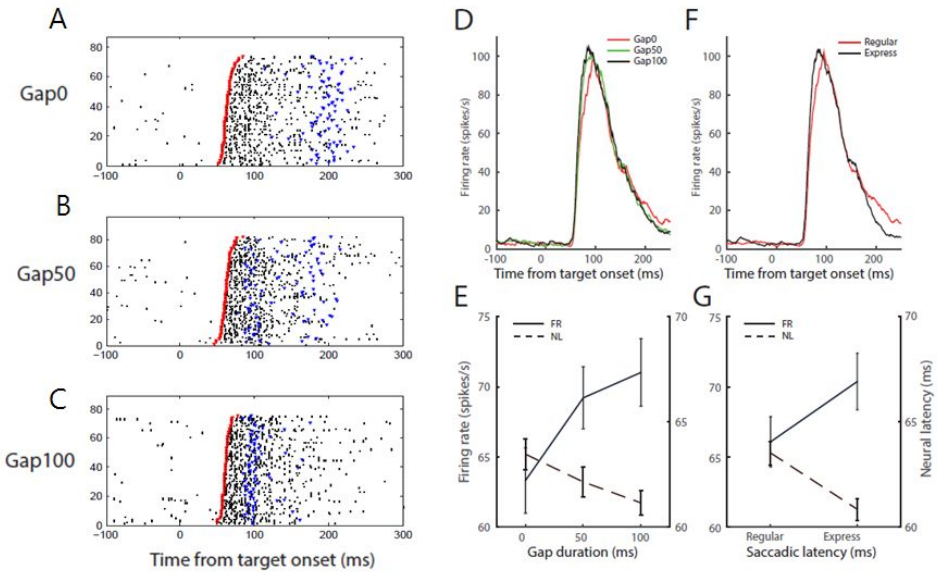

Figure 23. Raster plot of a representative cell during the gap saccade task. Raster plots for each gap condition, Gap0 (A), Gap50 (B), Gap100 (C) are shown in A. The raster plots are sorted according to neural latency, the first spike, as indicated with red symbols. Saccade latencies are marked with blue symbols. **D**. Spike density plots of the same data. **E**. Mean firing rate (FR) during the post-stimulus period of 50-150ms and neural latency (NL) and their standard error as a function of gap duration. **F**. Spike density plots for express and regular saccades. **G**. Same as E, but for express and regular saccade groups.

Figure 24 illustrates the overall gap effect on physiology as mentioned in Figure 22. Accompanying gap effect on behavior (Figure 22), the mean neural latency was shorter for shorter gap duration in both monkeys (Figure 24A, B, one-way ANOVA F-test, $p<10^{-17}$ (DC); $p<10^{-3}$(NB)). The effect of gap duration on firing rate was variable between two monkeys; in monkey DC, the firing rate increased

with gap duration and the difference was significant (Figure 24A, one-way ANOVA F-test, $p<10^{-11}$), but in monkey NB, the effect of gap duration on firing rate tended to be higher with than without the gap and the difference was marginally significant (Figure 24B, two-sample t-test, $p<0.05$).

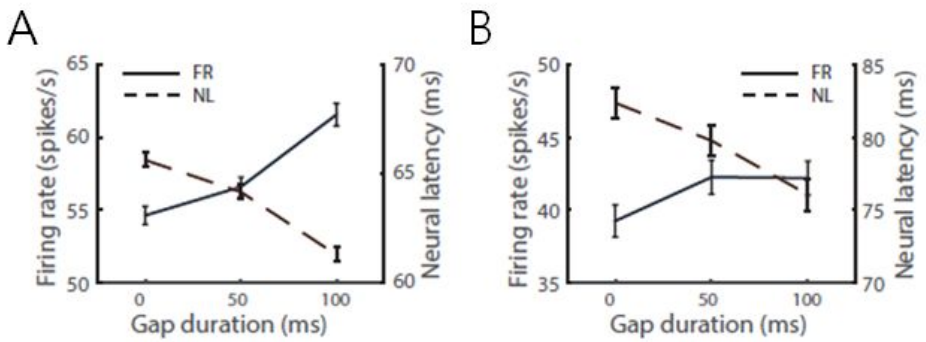

Figure 24. Gap effect in FR(firing rate) and NL (neural latency)

A, B. Mean firing rate (real) and neural latency (dashed) against gap duration for monkey DC (A) and monkey NB (B).

Note that the idiosyncratic spike activity that in Figure 24A and B, monkey NB showed a lower firing rate and lengthened neural latency compared with monkey DC. However, the overall impression of the results is consistent across subjects that the gap effect is reflected in V1 activity.

4. Trial-to-trial correlation

4.1 Reaction time and NL vs. FR

Figure 25 shows the histograms of correlation coefficient between neural latency and saccade latency for all 74 cells from two monkeys. Overall, the mean correlation between neural latency and saccade latency (Figure 25A was 0.10 (±0.12), and significantly different from zero (t-test, $p<10^{-10}$). In 15 out of 74 cells (20.3%), the correlation was significant ($p<0.05$, black bars in Figure 25A), and the mean coefficient of these cells was 0.24 (±0.08). The mean correlation between firing rate and saccade latency (Figure 25B) for all 74 cells was -0.06 (±0.12, t-test, $p<10^{-4}$). In 12 out of 74 cells (16.2%), the correlation was significant ($p<0.05$, black bars in Figure 25B), and the mean coefficient of these cells was -0.22 (±0.06). Thus, earlier neural latency and higher firing rate were associated with shorter saccade latency.

The mean value of partial correlation coefficient between neural latency and saccade latency controlling the gap duration for 74 cells was 0.05 (±0.13, p=0.001), and that between firing rate and saccade latency was -0.04 (±0.13, p=0.02). The mean partial correlation calculated between the firing rate for the interval of 100ms starting from neural latency and saccade latency was -0.01 (±0.13, p=0.64). Thus, the activity of V1 single cells correlates with saccade latency on a trial-to-trial basis, and neural latency is more reliable predictor than firing rate, confirming the previous

study (J. Lee et al., 2010).

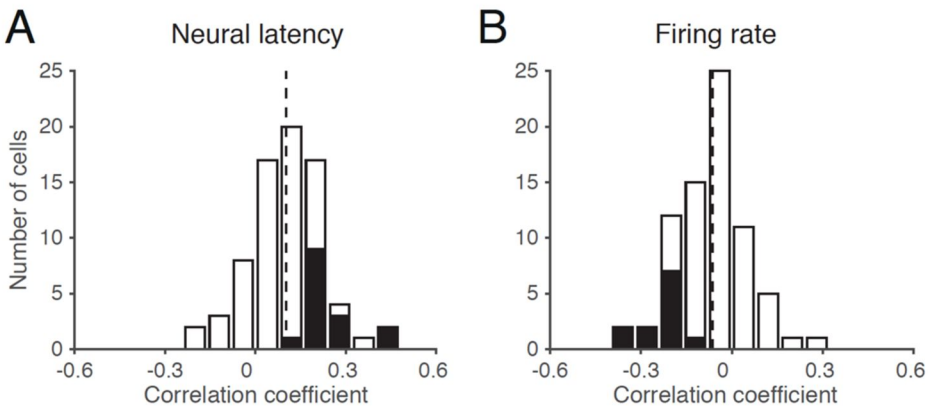

Figure 25. Correlation coefficient histograms of RT vs NL and FR.

Histogram of correlation coefficient between neural latency and saccade latency (A) and between firing rate during the post-stimulus period of 50-150ms and saccade latency (B). The dashed vertical lines are the means of distribution. Black bars indicate cells with significant correlation ($p<0.05$).

4.2 Comparison between subjects

Figure 26 illustrates the results of the same analysis method that was performed in Figure 25. But results are shown for separate monkeys. The two panels in the first row show results from monkey DC. The correlation coefficient between saccadic latency and neural latency was 0.10 (±0.13, t-test, $p<10^{-6}$), and between saccadic latency and mean firing rate of post stimulus period 50-150ms was -0.05 (±0.09, t-test, $p<10^{-3}$). The two panels in the second row of Figure 26 are the results from monkey NB. The correlation coefficient between saccadic latency and neural latency was 0.10 (±0.13, t-test, $p<0.001$), and between saccadic latency and mean firing rate of post stimulus period 50-150ms was -0.078 (±0.15, t-test, $p=0.0095$). To summarize, the results of combined subjects shown in Figure 25 is consistent through subjects.

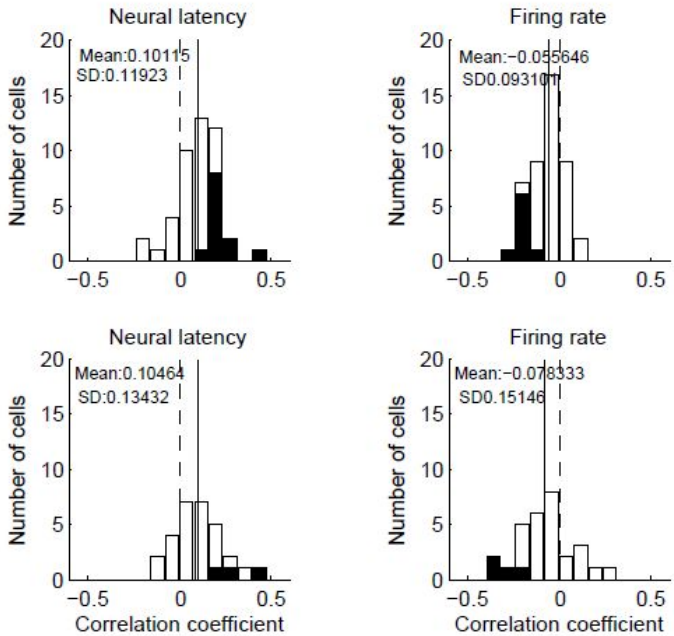

Figure 26. Correlation coefficient histograms of RT vs NL and FR of each subject. Histogram of correlation coefficient between neural latency and saccade latency (upper, left) and between firing rate during the post-stimulus period of 50-150ms and saccade latency (upper, right) for monkey DC. The same convention for monkey NB is shown in bottom two panels.

4.3 Comparison between express and regular trials

The positive correlation between saccadic latency and neural latency has been consistent from previous study (J. Lee et al., 2010) as well as current study, indicating that neural latency is a valid predictor of saccadic latency, even across subjects (Figure 26). Since it is one of the interesting results that we observed some

conditions having distinctively different modes of saccadic latency distribution, the correlation between RT and NL, and RT and FR was also compared within each saccade group (within express and within regular). However, the result showed no significant correlation for any of the saccade groups (either express or regular) or subjects (Figure 27).

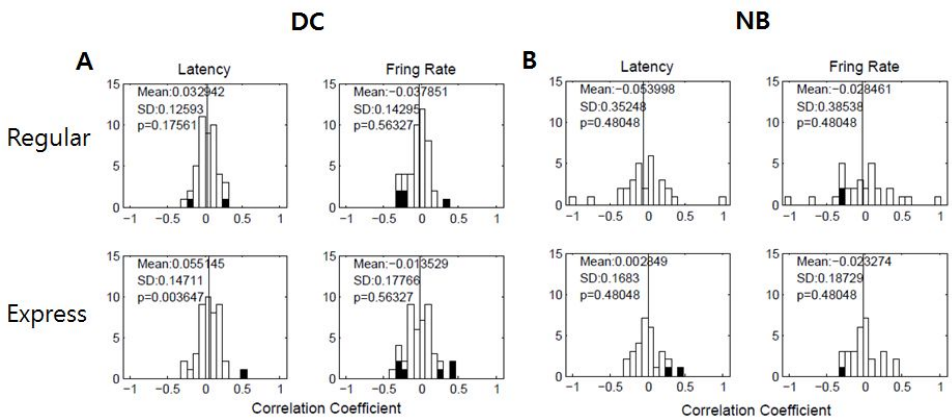

Figure 27. Correlation coefficient histograms of RT vs NL and FR of each subject within express and regular saccade groups. Histograms of correlation coefficient between neural latency and saccade latency (A, upper and lower, left, for monkey DC, B, upper and lower, left, for monkey NB) and between firing rate during the post-stimulus period of 50-150ms and saccade latency (A, upper and lower, right, for monkey DC, B, upper and lower, right for monkey NB). The first row shows comparison within regular saccades, and second row shows within express saccades. The same convention as Figures 25 and 26, but showing no significant correlation.

5. V1 activity difference between express and regular saccades

A peculiar feature in the latency distribution during the gap saccade task is its occasional bimodality. The latency of the earlier mode, typically around 100ms, characterizes express, and that of the later mode characterizes regular latency saccades. Figure 28 illustrates the differences in neural latency (A) and firing rate (B) between express and regular latency saccades, averaged over all trials collected for 74 cells from two monkeys. The neural latency was shorter before express with respect to regular latency saccades (Figure 28A), by 4.31ms (±5.04) on average (t-test, $p<10^{-11}$). The firing rate was higher before express with respect to regular latency saccades (Figure 28B), by 2.81 spikes/s (±5.23) on average (t-test, $p<10^{-6}$).

Note that the division of express and regular saccades shown in Figure 28 was made within individual sessions (refer to Figure 20). When the division was made based on the population distribution of saccade latency for each animal, the differences in neural latency and firing rate between express and regular saccades were similarly significant (neural latency, $p<10^{-7}$, firing rate, p<0,01).

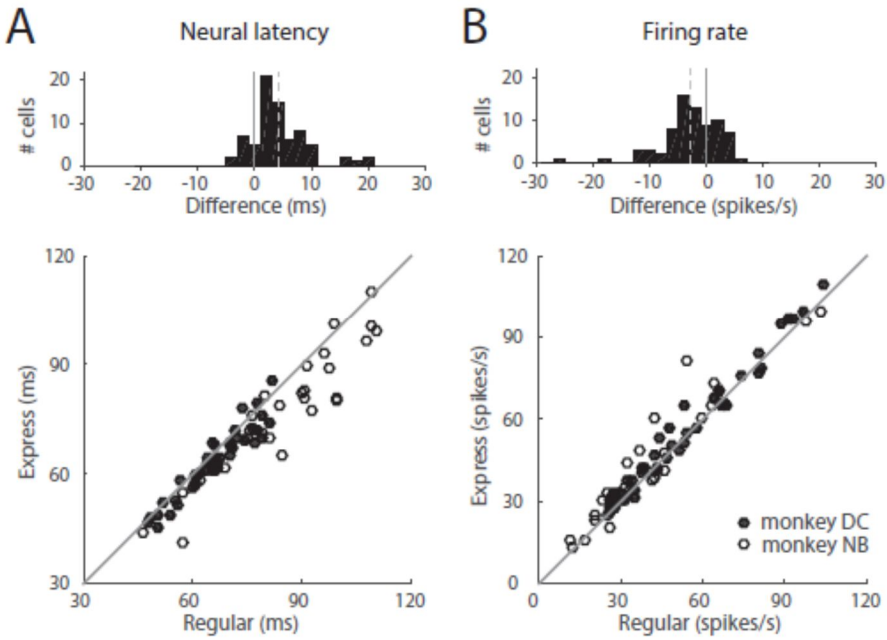

Figure 28. NL and FR comparison between express and regular saccade groups. Comparison of neural latency (A) and firing rate (B) between express and regular saccades. Difference (regular minus express) histograms (upper) and scatter plots between express and regular saccade trials averaged for each cell (lower), for neural latency (A) and firing rate during the post-stimulus period of 50-150ms (B). Dashed vertical lines in histograms indicate the mean values. Filled and open symbols in the scatter plots indicate monkeys DC and NB, respectively.

Figure 28 represents population sessions combined of all conditions. However, in order to confirm the results within condition, the neural latency and firing rate between express and regular trials in only Gap50 condition over all 74 cells was also analyzed. Figure 28 illustrates the result showing a similar pattern of

the differences in neural latency (A) and firing rate (B) between express and regular latency saccades, averaged over all trials of only Gap50 condition. The neural latency was also shorter before express with respect to regular latency saccades (Figure 29A), by 3.03ms (±6.89) on average (t-test, $p<10^{-3}$). The firing rate was higher before express with respect to regular latency saccades (Figure 29B), by 2.59 spikes/s (±7.25) on average (t-test, p=0.0025). Overall, the results indicate that express and regular saccade groups have differences in neural latency and firing rate for all combined conditions (Gap0, Gap50, Gap100) as well as within Gap50 condition.

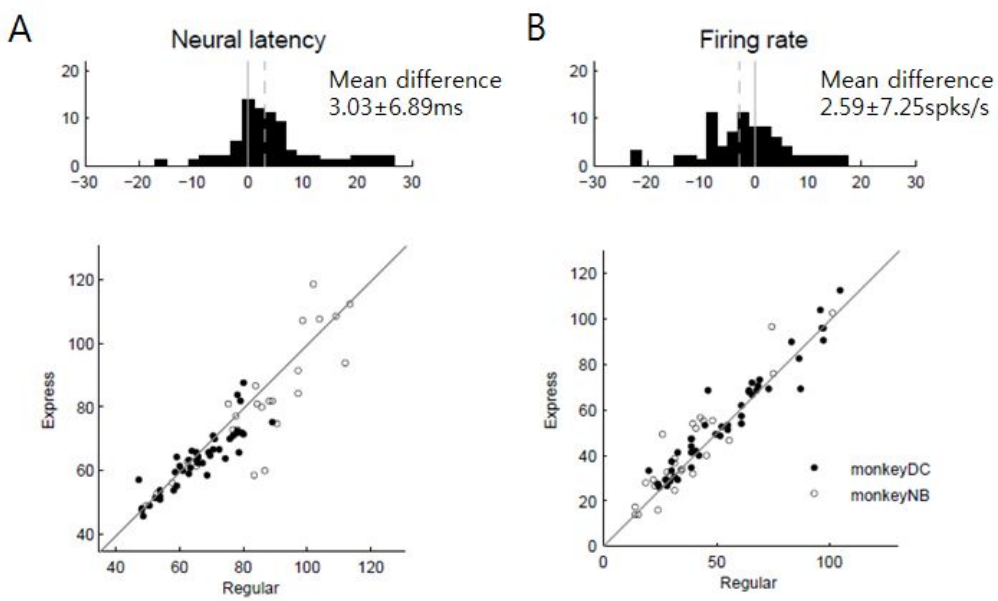

Figure 29. NL and FR comparison between express and regular saccade groups in

only Gap50 condition. Comparison of neural latency (A) and firing rate (B) between express and regular saccades. Difference (regular minus express) histograms (upper) and scatter plots between express and regular saccade trials averaged for each cell (lower), for neural latency (A) and firing rate during the post-stimulus period of 50-150ms (B). Dashed vertical lines in histograms indicate the mean values. Filled and open symbols in the scatter plots indicate monkeys DC and NB, respectively. The same convention as Figure 28.

6. V1 activity during pre-stimulus period

6.1 Oscillatory cortical potential during pre-stimulus period

The oscillatory cortical potential during the period immediately before target onset has been shown to be correlated with saccadic latency (Bompas, Sumner, Muthumumaraswamy, Singh, & Gilchrist, 2015; Drewes & VanRullen, 2011; Everling, Krappmann, Spantekow, & Flohr, 1997) and generation of express saccades (Hamm et al., 2010) in human. This led us to examine the local field

potential signal during the period immediately before target onset. First, we examined the event-related mean LFP for each gap duration condition (Figure 30). During the task, the event-related mean LFP could be dissociated by the gap duration condition during pre-target period for both saccade directions, toward the RF or its opposite side. This was likely to be due to the different timing of the offset of fixation target, such that the potential negativity was associated with fixation offset and thus, at the time of target onset, the LFP amplitude was different depending on the gap duration. This may modulate spike timing and rate in response to the appearance of saccadic target.

In contrast, the black trace in Figure 30 represents the event-related mean LFP from simple fixation task experiment (n=62). The task of the experiment was as monkey fixating at the central fixation point and the stimulus was presented at the location of receptive field (refer to the paradigm in study1). Interestingly, the trace shows no indication of oscillatory potential change prior to presentation of stimulus onset in this task.

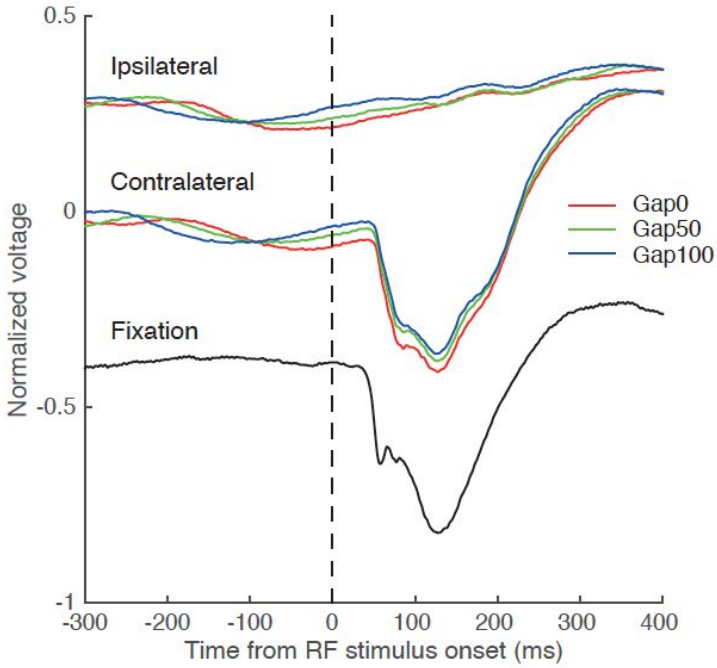

Figure 30. Event-related raw LFP activity. Shown are raw LFP traces for trials in which a Gabor stimulus was presented as a saccadic target in the hemifield opposite to the RF ('Ipsilateral') or at the RF ('Contralateral'), averaged for each of Gap0, Gap50, and Gap100 conditions from 74 cells of the current study. For clarity, the traces for 'Contralateral' shifted downward by 0.3. The black trace is from 62 cells of monkeys performing simple fixation task (study 1) aligned to the stimulus onset time.

6.2 Spike density difference during pre-target period

In order to further investigate difference in pre-target activity of V1 and its effect on saccadic latency, the spike density trials were divided into express and regular saccade groups. Figure 31 illustrates the population spike density averaged

over all trials collected from 74 cells from two monkeys for both latency groups. It can be seen that the mean spike density trace is lower before express compared with regular latency saccades. Note in Figure 31 that the mean spike density is significantly different before target onset and the difference lasts until 33ms after target onset, as indicated by black marks above x-axis. The mean difference during the pre-target period of 200ms corresponds to 2.38 spikes/s (±3.73) and significantly different from zero (t-test, $p<10^{-11}$). The firing rate during the initial visual response from 55-123ms after target onset was significantly higher for express than for regular saccades (gray marks above x-axis), consistent with shorter neural latency and higher firing rate shown in Figures 26 and 27.

Since Figure 31 includes all three gap duration conditions, we additionally compared the spike density between express and regular saccade trials within the identical stimulus condition. The trials of 1607 express and 1221 regular latency saccades from the Gap50 condition of all cells were compared. For this comparison, we measured the firing rate from -200 to -100ms of target onset to exclude the potential effect of target offset at -50ms on spike activity. The mean firing rate of this period was similarly lower before express compared with regular latency saccades by 1.61 spikes/s (±0.56, t-test, $p<0.001$).

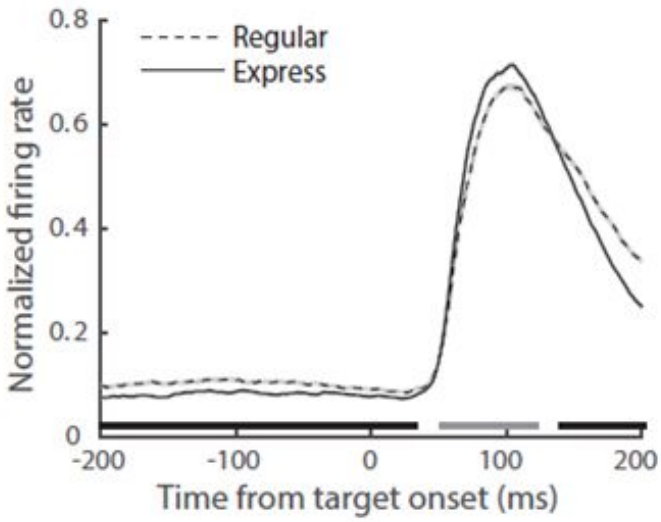

Figure 31. Mean spike density of express and regular trials.

Mean spike density of 4240 express (real) and 3842 regular (dashed) saccade trails combined from all cells. The spike density of each trial was first normalized to the maximum of each cell, and then averaged for express and regular saccades across all cells. One SE for the mean trace is indicated by shade. Thick horizontal line segments above x-axis consist of filled square marks that represent the times of significant difference during a period of 10ms centered about corresponding marks, based on a bootstrap test performed every 1ms ($p<0.05$, black; express < regular; gray: express>regular).

6.3 LFP power difference during pre-target period

Next, we compared the power of LFP during the pre-target period of 500ms between express and regular saccade trials of Figure 31. The spectral power was lower before express than regular latency saccades, and the frequency bands of significant difference were 22-24, 55-84, and 90-94Hz (Figure 32).

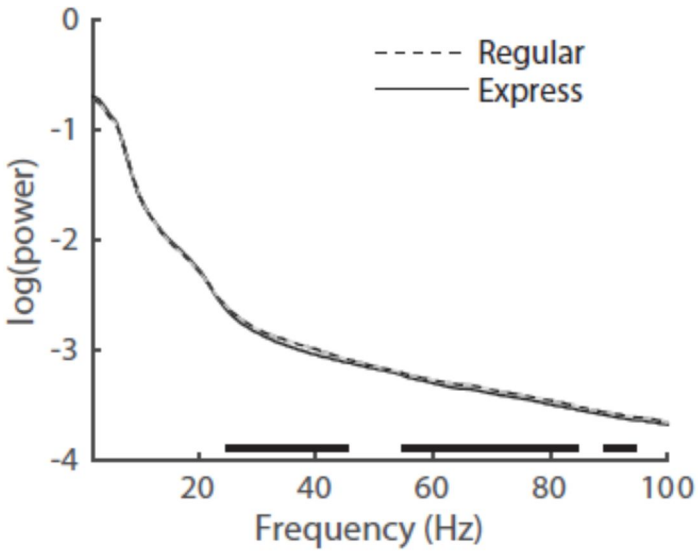

Figure 32. Mean LFP power spectrum of baseline periods (-500:0).
Mean LFP power during the pre-target period of 500ms in $\log_{10}$(power). The LFP power was first computed for each trial, and averaged for the same trials shown in Figure 31 for express and regular saccade conditions. Black symbols above x-axis indicate the frequency points (0.98 Hz/point) of significant difference between regular and express saccade conditions based on a bootstrap test ($p<0.05$). The data points of a significant difference, but continuous for less than 5 frequency points are considered false discovery and are not marked.

6.4 Possible effect from fixation attainment

The fixation durations of this study was between 250~900ms that were randomized for each stimulus trial. Upon the analysis of pre-target activity which accounts V1 activity during 500ms of pre-stimulus periods (Figures 31, 32), it is possible that the effect from fixation attainment for trials having shorter fixation

durations around 250~400ms might have contaminated the results. In order to avoid such concern, we have further analyzed the pre-target activity including V1 spike density level and power spectrum of LFP (same analysis method used in Figures 31, 30) excluding trials of fixation duration less than 400ms. Also, with the concern of Gap100ms that may have affected the results as well, we used 300ms of baseline period starting from -400 to -100ms prior to target onset time. As results, 8% of total trials were excluded for this analysis and compared with the previous results, which had used 500ms of baseline period.

Figure 33 illustrates the results of the same analysis but using trials with >400ms of fixation duration and baseline period of 300ms. The mean difference of spike density during -200 to -100ms was 2.63 spikes/s (Figure 33A, two sample t-test, $p<10^{-9}$) and the significant power difference frequencies were 1~4Hz, and all those ranges larger than 24Hz (Figure 33B), having broader frequency ranges compared to the results using longer baseline window. Note that the significant tests were corrected for multiple comparison with false discovery rate. Overall, the results confirm that pre-stimulus spike density and power difference between express and regular trials consist with the results using larger baseline period analysis window and shorter fixation trials.

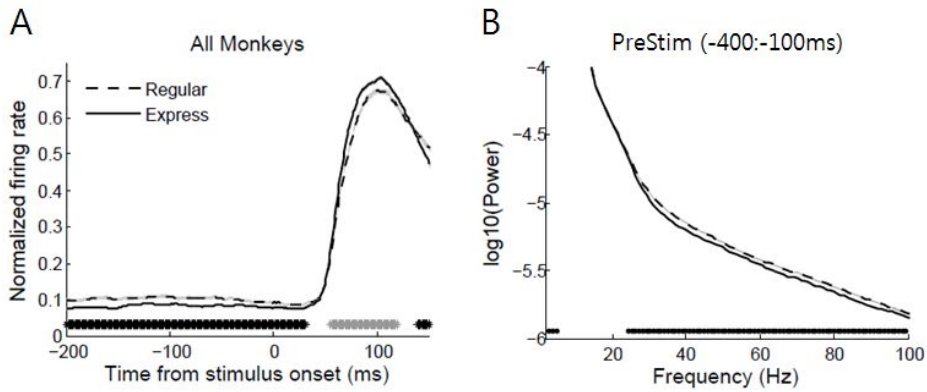

Figure 33. Spike density and LFP power difference using baseline periods (-400:-100).

A.Mean spike density of express (real) and regular (dashed) saccade trials combined from all cells but excluding trials having less than 400ms of fixation duration. Same convention as Figure 31. **B**. The LFP power during the pre-target period of 300ms in $\log_{10}$(power). Same convention as Figure 32

6.5 LFP power difference during pre-target period between subjects

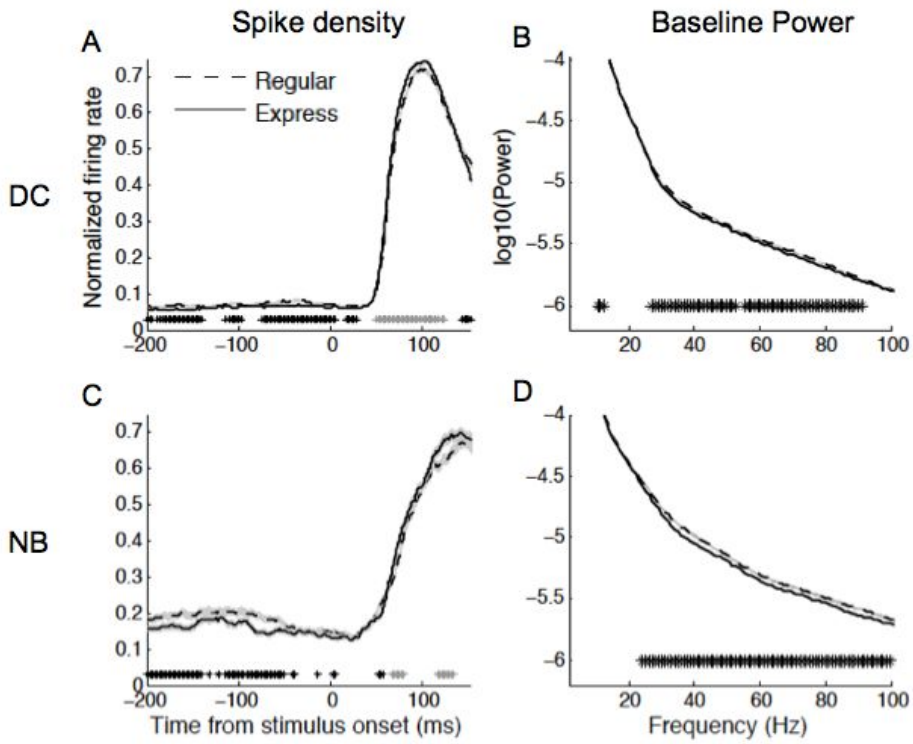

Figure 34. Mean spike density and LFP power spectrum of baseline periods (-500:0ms); separate subjects.

The same convention as figure 31 for mean spike density (A, C) and mean LFP power during the pre-target period of 300ms in $\log_{10}$(power) (B, D). A, B are Monkey DC; C, D are monkey NB. Black symbols above x-axis indicate the frequency points (0.98 Hz/point) of significant difference between regular and express saccade conditions based on a bootstrap test ($p<0.05$) with the correction for multiple comparisons.

Both subjects (DC, NB) showed suppressed mean spike density during pre-target

period for express saccades than regular saccades. Accordingly, mean LFP power difference was significantly lower for express (20Hz<) for both monkeys, consistent with the result of the two subjects combined.

7. Base LFP power vs. saccadic latency correlation

7.1 Correlation of LFP power and all saccadic latency conditions

The correlation analysis between the trial-to-trial variability in the oscillatory power calculated over the pre-target period of 300ms and saccade latency for each frequency point (0.98Hz) revealed that the range of 10~17Hz, 20, 21, 26~44, and 82Hz< was associated with significant correlations ($p<0.05$) (Figure 32). Some of these ranges, particularly frequency ranges larger than 26Hz overlap with the results shown in power relation of differentiation between express and regular latency saccades (Figures 32, 33B).

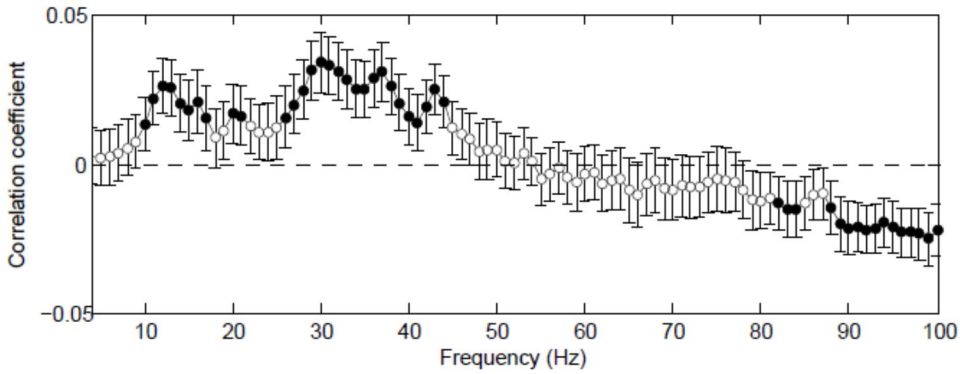

Figure 35. Correlation between baseline LFP power and RT

Correlation coefficients between each frequency point (0.98Hz/point) and saccade latency for all conditions including saccades made toward either ipsilateral or contralateral side, and their one SEs. Correlation was calculated for each cell and then averaged over 74 cells. Black symbols are statistically significant points based on a bootstrap test derived with 1000 simulations ($p<0.05$), 10~17Hz, 20, 21, 26~44, 82Hz<.

7.2 RF site vs. RF opposite site

The previous result in Figure 35 was performed between baseline LFP power and saccadic latencies of all conditions including all saccadic directions, meaning the activity of V1 from left and right hemispheres were also parts of the results. However, it is certainly an interest whether such significant correlation comes from particular hemisphere or all left and right brains are associated as an indication of global regime of baseline cortical activity affecting latency variability. In order to test this idea, the same correlation analysis was performed as Figure 35, but the trials were

divided into saccadic directions; RF (Contralateral, Figure 35A) vs. RF opposite (Ipsilateral, Figure 35B). As results, significant correlations were observed in frequency ranges of 10~12, 31~44Hz for contralateral saccade direction, and 11~20, 27~44Hz were for ipsilateral saccade direction. The patterns of correlations of two hemispheres were little different, showing higher correlation coefficient was observed from ipsilateral side. Nevertheless, some significant frequency ranges such as 10~20Hz, or low gamma range (30~40Hz) still survived from all hemispheres.

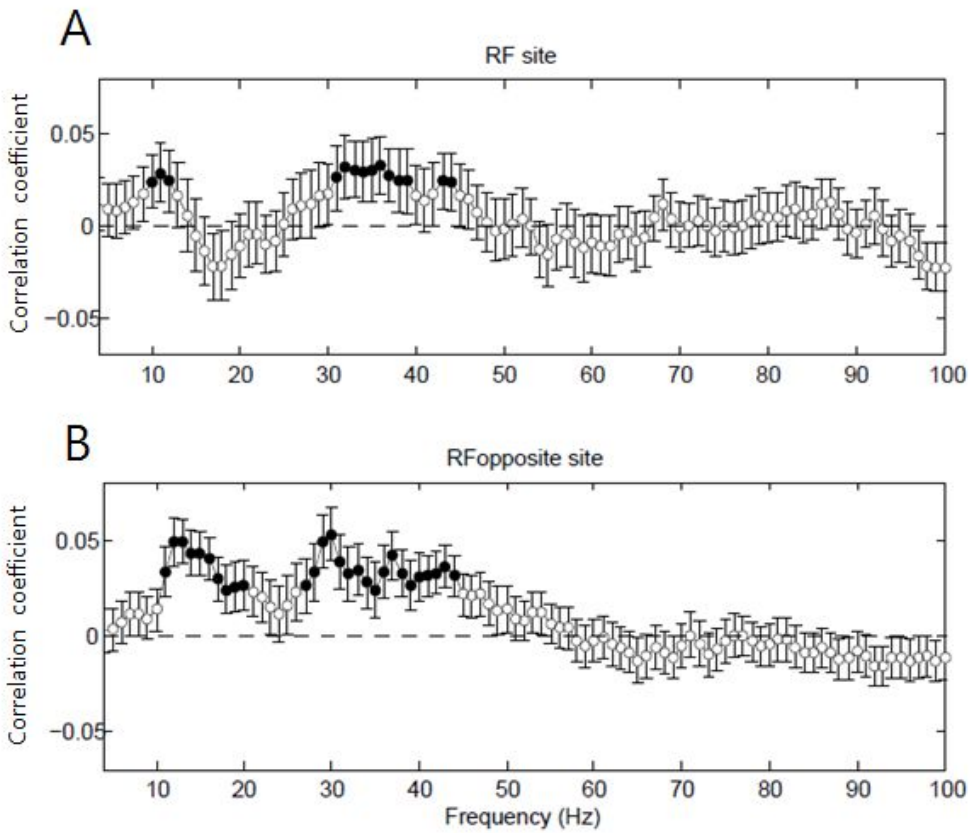

Figure 36. Correlation between baseline LFP power and RT; RF vs. RF opposite

site

Correlation coefficients between each frequency point (0.98Hz/point) and saccade latency for all conditions. **A**. Correlation coefficient of RF site (Contralateral saccade direction) and their one SEs. Significant frequency ranges: 10~12, 31~44Hz. **B**. Correlation coefficient of RF opposite site (Ipsilateral saccade direction) and their one SEs. Significant frequency ranges: 11~20, 27~44Hz.

The same convention as explained in Figure 35; Correlation was calculated for each cell and then averaged over 74 cells. Black symbols are statistically significant points based on a bootstrap test derived with 1000 simulations ($p<0.05$).

8. Effect of trial history

Previous studies reported that monkey saccade latency (Michael C Dorris, Pare, & Munoz, 2000) and the occurrence of human express (R. Carpenter, 2001) are influenced by the preceding saccade direction (but see Bompass and Summer, 2008). We examined whether the differential pre-target activity between express and regular saccade trials was related to the saccade order effect. When the saccade had been made in the preceding trial in the direction same as the current trial, the saccade latency was non-significantly shorter by 1.51ms on average (Figure 37A, I and C, t-test, $p=0.14$) with respect to the opposite direction. The difference between express and regular saccade conditions in firing rate (Figure 37B, I and C, 0.08spikes/s) and neural latency (Figure 37C, I and C, 0.11ms) were not significantly different ($p=0.08$, and 0.90, respectively). When two preceding saccade directions had been made in the

direction same as the current trial with respect to the opposite direction, the difference in saccade latency to 2.09ms (Figures 37A, II and CC), consistent with previous report (Munoz, Dorris, Pare, & Everling, 2000), but this difference was still non-significant (t-test, p=0.14). In this comparison, the difference in neural latency was 0.08ms (Figure 37C, CC, II, t-test, p=0.90), that for firing rate was 0.48 spikes/s (Figure 37B, CC, II, t-test, p=0.63), and that for spike density during the pre-target period of 200ms was 0.29 spikes/s (t-test, p=0.55). We conclude that the preceding saccade direction did not influence V1 activity during both pre-target and post-target periods in our experimental paradigm. Note that the two potential saccade targets were diagonally symmetric across fixation in our experiment, so that the return saccade from the target in the opposite hemifield in the previous trial is the same vector as the required if the target appears that the RF in the current trials, preserving the order effects, if any.

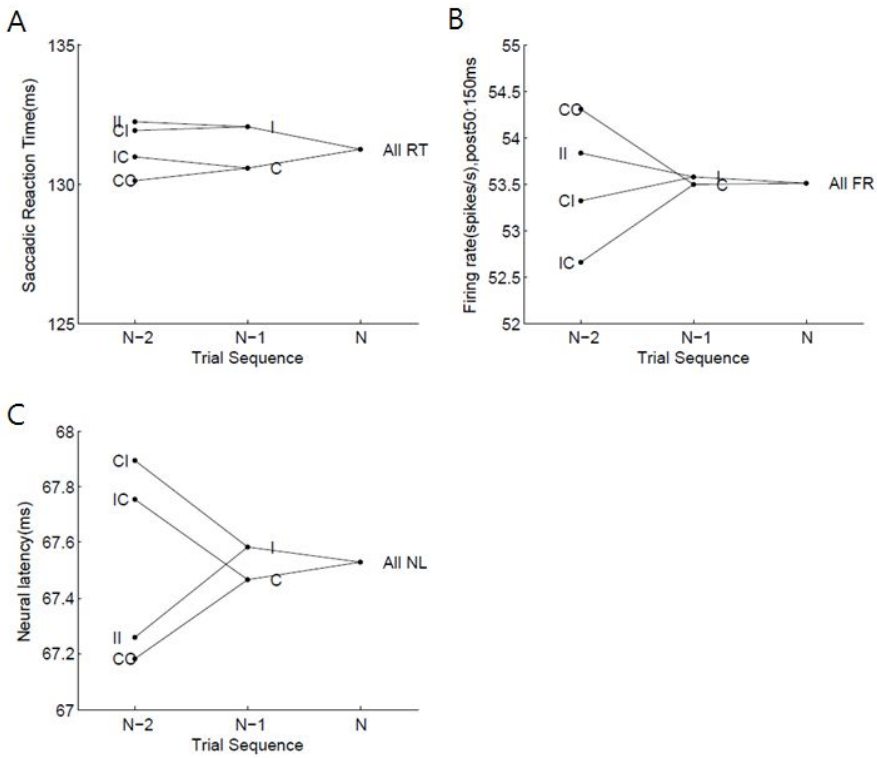

Figure 37. Trial sequence history. A. Saccade reaction time of current trial (N), one trial before (N-1) and two trials before (N-2), marked in the x-axis. I indicates 'ipsilateral' saccade direction and C means 'contralateral' saccade direction. **B**. Same convention as A, but y-axis is firing rate (spikes/s) during post stimulus time between 50:150ms. **C**. Y-axis is plotted with neural latency (ms).

9. Trial auto-covariation

One of the general concerns of gap effect on V1 activity was whether the correlations between saccadic latency and V1 activity (Figures 25, 26) are caused by

a causal link or by a common variable such as variations in behavioral state that impact on V1 activity and also on saccadic latency, in other words, whether the saccadic latency and V1 activity varied accordingly as a result of gradual progress of sessions. In order to check this, we sorted the saccadic latency with trial sequence and calculated linear regression coefficient with least squares of saccadic latency as a function of trial number (example site, Figure 38A, p=0.012) and mean spike density (50:150ms after stimulus onset) as a function of trial number (example site, Figure 38 B, p=0.006) for each cell.

As a summary, the polynomial coefficients for each monkey (monkey DC=45, NB=29 cells) were plotted as histograms in Figure 39. The mean p-value for the linear regression coefficient between saccadic latency and trial sequence for monkey DC was 0.0138 (±0.036), and monkey NB was -0.018 (±0.039); and spike density and trial sequence for monkey DC was -0.0006 (±0.039) and monkey NB was -0.01 (±0.063), indicating that the neither saccadic latency nor spike density level is related to the progress of trial numbers within sessions.

From the results, we confirm that the trials of slower and faster saccades were uniformly distributed across the sessions, without overrepresentation of fast or slow saccades in the beginning or towards the end of the sessions.

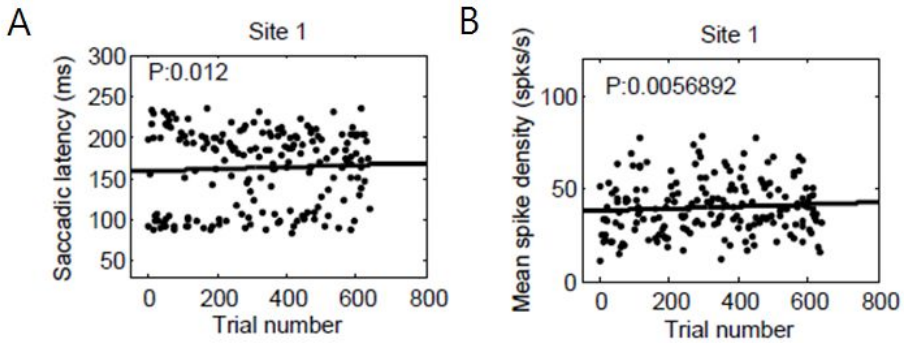

Figure 38. Trial sequence vs. saccadic latency/ V1 activity. A. Saccadic latency (ms) was plotted against trial sequence within a session. The polynomial coefficient (p=0.012) for this site. Solid line indicates fitted result with the least square using polynomial coefficient. **B**. Mean spike density (50:150ms after stimulus onset) was plotted against trial sequence, same convention as A. The polynomial coefficient is 0.006.

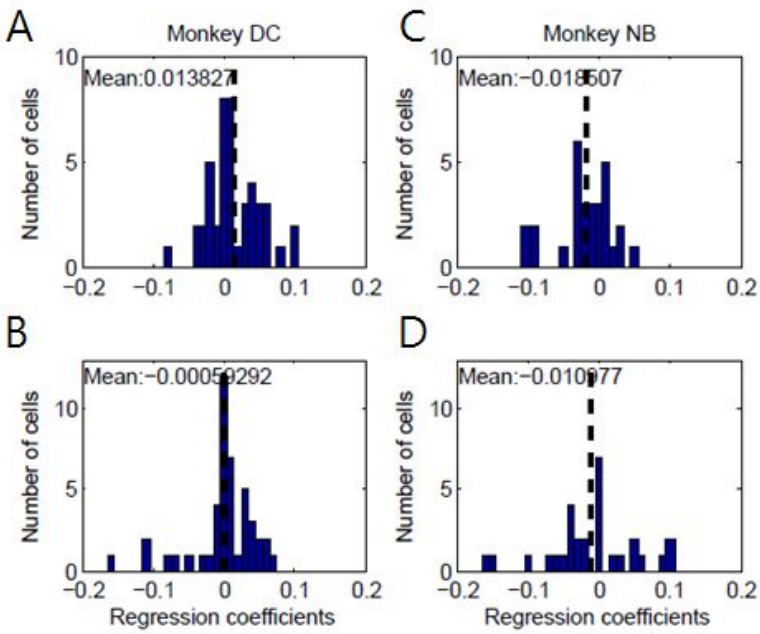

Figure 39. Summary Trial sequence vs. saccadic latency and V1 activity. A-B. Histograms of regression coefficients between trial sequence and saccadic latency (ms) (A) and trial sequence and spike density level (mean spike density between 50 to 150ms after stimulus onset) (B) for monkey DC. Dashed lines indicate mean coefficients over all tested cells (N=45). **C-D**. Same convention as A-B; Histograms of regression coefficients between trial sequence and saccadic latency (C) and trial sequence and spike density level (D) for monkey NB. Dashed lines indicate mean coefficients over all tested cells (N=29).

10. Eye stability during express vs. regular saccades

There was no significant difference in eye stability between express and regular latency saccade trials during the pre-target period of 200ms. We compared

the estimates of eye stability between express and regular saccades with a metric, *CV*(t), a cumulative absolute vectorial velocity of the eye. When the overall cumulative velocity averaged over all 74 cells, the cumulative functions starting from 200ms prior to target onset for express and regular latency saccade trials closely overlapped within their one SEs until about 50ms after target onset around which saccades started (Figure 40). Quantitatively, the mean of absolute eye velocity over the pre-target period of 200ms was not significantly different between express and regular latency saccade conditions (t-test, p=0.53). Note that the metric is a gross estimate of fixational stability and its accuracy is limited by our recording system that only monitors one eye, which is inevitably insufficient for disconjugate fixational movements, such as drifts, leaving refined studies in this regard open. During central fixation there was no visual contrast within the receptive field. Thus, microsaccade-induced neural activity (Bosman, Womelsdorf, Desimone, & Fries, 2009; Martinez-Conde, Macknik, & Hubel, 2000) is not likely to explain the difference between express and regular saccades. We conclude that the spike and LFP power during pre-target period was not related to differential stability of eye fixation.

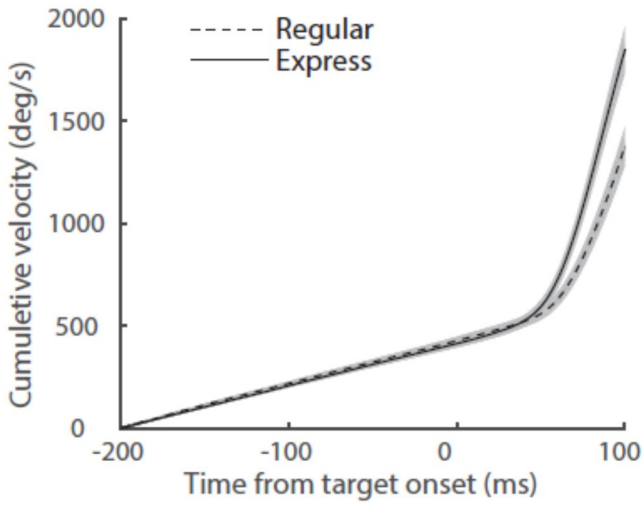

Figure 40. **Eye stability**. Shown are the mean *CV*(t), absolute eye velocity functions for express (real) and regular (dashed) latency saccade conditions with 1SE (shade).

Conclusion & Discussion

1. Gap effects in V1

In the current study, we found that the changes in spike activity of V1 neurons accompanied the gap effect. Saccade latency decreased with an increase in gap duration, and accompanying this change, the neural latency of V1 neurons

decreased and firing rate increased. We confirm the gap effects in V1, in addition to previously studied structures including superior colliculus (M. C. Dorris & Munoz, 1995; Edelman & Keller, 1998; D. Sparks, W. H. Rohrer, & Y. Zhang, 2000) and various cortical regions, such as lateral intraparietal area (Chen, Liu, Wei, & Zhang, 2013) and prefrontal cortex (Tinsley & Everling, 2002).

Are the changes in V1 activity during gap saccades compatible with the possibility that the superior colliculus confer their gap-related effects? For example, the build-up activity of superior colliculus changes about 100ms after fixation offset in the gap saccade tasks, so that in Gap100 conditions, the times of first V1 spikes are within the window of the potential influence from the collicular build-up activity. In Gap50 trials, however, first V1 spikes occur prior to the start of build-up activity, and yet revealed consistent gap effects on V1 activity (Figures 23 and 24), suggesting the possibility of superior colliculus conferring the gap effects to V1 unlikely.

For the V1 neurons that respond to the visual saccadic target, fixation offset is an event in the receptive field surround. Thus, the stimulus condition of gap saccade task is similar to surround interaction in which neural response to RF stimulus is modulated by a focal stimulus in RF surround, and gap paradigm introduces a temporal gap between offset of a surround stimulus and onset of an RF stimulus. A focal stimulus presented in the distant surround zone of the RF, even in

the hemifield opposite to the RF, can modulate spike activity of V1 neurons evoked by a subsequently presented RF stimulus in a manner that depends on temporal interval (Kim et al., 2012). Thus, the fixation target offset, a critical visual event of the gap effect, possibly interacts with ensuing spike generation evoked by the saccadic target.

The variation of V1 spike activity is not directly related to saccade latency variation. For example, the neural latency is 4.3ms earlier on average for express than for regular latency saccades (Figure 28A), too small to account for the latency difference between express and regular saccades. This is comparable to the superior colliculus; earlier onset time of visual activity before express with respect to regular latency saccades for buildup and burst neurons is reported to be 3.1 and 2.4ms, respectively (M. C. Dorris, Pare, & Munoz, 1997).

2. Pre-target spike activity

It is thought that the cortical activity during pre-target period is related to saccade latency (Bompas et al., 2015; Drewes & VanRullen, 2011; Everling et al., 1997), and generation of express saccades (Hamm et al., 2010) in human. The pre-target state of V1 was related to occurrence of express saccades; during the pre-target period, even before the fixation target went off, the level of spike activity was lower

(Figure 31), and the spectral power of LFP was lower before express compared to regular saccades (Figure 32). These results on the relationship between the spontaneous variability before target onset, or before fixation offset, and generation of express saccades are the first evidence found in monkey, to our knowledge, and support the previous findings in human, specifically, that the oscillatory EEG potential during pre-target period is correlated with generation of human express saccades (Hamm et al., 2010), and that the spectral power of magnetoencephalography during pre-target period from wide cortical areas including V1 was lower for fast with respect to slow saccades (Bompas et al., 2015).

A central issue about the generation of express saccade is more of why the latency distribution is often not unimodal, as in Gap50 of Figure 20, than of shortening of latency. In other words, it is about, if indeed different routes mediate different groups of saccade latency (Guan, Liu, Xia, & Zhang, 2012; Isa, 2002; Schiller, Sandell, & Maunsell, 1987), what makes visuo-saccadic processing routed via one as opposed to other pathways, even with identical stimulus condition and task requirements. The bimodality in saccade latency suggests that the mechanism generating express saccades is different from the mechanism determining saccade latency, and is supported by our results that a lower LFP power in the gamma frequency range is involved in occurrence of express saccades (Figures 32, 33), whereas a lower LFP power in the low frequency range is related to saccade latency (Figures 35, 36). The variability in pre-target spike and LFP power may reflect a

spontaneous change in global cortical state (Goris, Movshon, & Simoncelli, 2014; Schölvinck, Saleem, Benucci, Harris, & Carandini, 2015), and thus, the lower pre-target spectral power and lower spike activity in V1 before express compared to regular saccades may be a local manifestation of a more global regime for modulating visuo-saccadic signal processing.

Study 3

Introduction

Temporal expectation of upcoming events is known to shorten detection latency (Coull & Nobre, 1998) and enhance sensitivity of stimulus discrimination (Cravo, Rohenkohl, Wyart, & Nobre, 2013; Rohenkohl, Cravo, Wyart, & Nobre, 2012). The expectation is also beneficial for improvement of detection accuracy and response timing, which would eventually be used in optimizing behavioral outcomes (Nobre, 2001; Oswal, Ogden, & Carpenter, 2007). However, cellular mechanisms mediating temporal expectation and its influence in early visual processing remain largely unknown.

In the previous study, the spike activity of the primate V1 is suppressed before a burst of discharge in response to a visual stimulus used as a saccade target. The initial suppression occurred before the onset of target presented either in the receptive field (RF) or even in the hemifield opposite to RF, suggesting that the suppression of spike activity at the time of target onset may reflect temporal expectation of target onset (J Lee, Kim, Chung, & Lee, 2013).

In the current study, we attempted to investigate whether the level of

spontaneous discharge is modulated in a behavioral paradigm in which the level of expectation of the timing of target was directly controlled.

Monkeys were trained to fixate at a central target and then to make a saccadic eye movement toward an eccentric Gabor stimulus. When the fixation target was a square in green, the saccade target appeared after a fixed central fixation of 800ms. When it was a circle in red, the target appeared after a variable duration of central fixation (400-1300ms). These two trial types, 'high' and 'low' expectation conditions, were randomized within a block.

Our results show that the saccade latency was significantly reduced in the 'high' with respect to 'low' expectation condition, indicating that the level of expectation was controlled. The V1 activity was simultaneously recorded while the subject performed the task. The size and orientation of the Gabor stimulus matched to the RF of a cell under study, and it was presented at the RF or in the hemifield opposite to the RF. The spontaneous discharge of V1 neurons was suppressed during fixation period in the 'high' expectation condition, whereas it was not in the 'low' expectation condition. This was true for both saccade targets at the RF and contralateral to the RF. Thus, temporal expectation made the state of V1 different at the time of saccade target onset. These results are consistent with the previous studies that the level of spontaneous activity of V1 plays roles in modulating perceptual processing of visual information by downstream neurons (J Lee et al., 2013; Supèr, van der Togt, Spekreijse, & Lamme, 2003).

Methods

1. Behavioral paradigm

In this study, monkeys had to make a saccadic eye movement after detecting the stimulus either to the direction receptive field (Figure 41, Gabor patch) or to the asymmetric hemispheric direction (Figure 41, opposite to the Gabor patch where the white circle alone is located). Along this simple dictation task, we controlled the expectation level toward upcoming target by varying the fixation duration. Note that the white dashed circles are invisible to the monkey in Figure 41; they are just used for schematic illustration in this figure. The key to this paradigm is the fixation target configuration; when green square (0.3°X0.3°) fixation target appears, it means the fixation duration fixed (400ms or 800ms, HIGH expectation condition). When red circle fixation target appears it means the fixation duration is variable (200~1300ms, LOW expectation condition). Approximately 100~150 trials composed of HIGH and LOW experimental conditions were randomized within a block. If animals failed to perform a trial, it was stacked at the end of the block and was repeated for completion of the block. Monkeys got juice reward at the end of each trial.

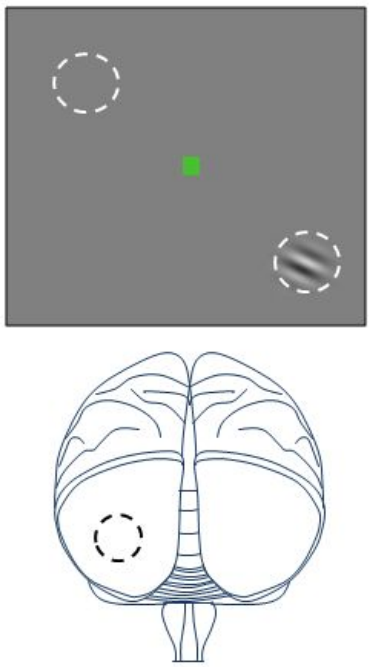

Figure 41. **Expectation paradigm**. Illustration of the relation between the stimulus screen and the brain of monkey facing it during experiment session. The black circle on the left of the brain indicates where the electrode is penetrated as of the receptive field is located (the location of the RF was varied to either left or right brain). The white circles in the screen are potential locations of the target that randomly appeared either on the RF side or opposite to the RF side. Monkey had to make a saccadic eye movement toward the target location after a certain fixation period. When green square appears, the fixation duration is fixed (HIGH expectation condition) and when red circle appears, the fixation duration is variable (LOW expectation condition)

1.1 Generation of low expectation condition trials

Throughout the experimental sessions, we developed and tested using two

types of low expectation trials being generated. During the first phase of the experiments, we used LOW expectation durations among 400 to 1300ms with a step of 300ms (=400, 700, 1000, 1300ms fixation durations). The fixation duration for HIGH expectation condition was fixed to 400ms for that time. Second, during the later phase of the experiments, LOW expectation fixation durations were generated by using uniform distribution among 200 to 1200ms with a step of 1ms, and HIGH expectation condition had fixed fixation duration at 700ms (just in between 200 and 1200ms), which was purposed to confirm that the fixation duration for HIGH expectation condition set at the right middle of the fixation duration among more variable fixation durations of LOW expectation condition would show the same effect as using fixed fixation durations in the earlier phase of the experiment.

2. Data analysis

Along the data analysis methods in study1 and study2, this current study also follows the same methods for off-line analysis including procedures determining saccade latency, neural latency and firing rate, unless stated otherwise below.

2.1 Definition of temporal contrast

In order to examine the development of activity rising from spontaneous discharge, temporal contrast has been defined (J Lee et al., 2013). Implying from the definition of SNR, this analysis has been attempting to detect the contrast between spike activity (signal) from spontaneous spikes (noise);

$$c(t) = [\int_{t-\tau}^{t} r(t)\,dt - \int_{t-2\tau}^{t-\tau} r(t)\,dt] / \tau$$

where *r(t)* is a linear sum of spike density with τ, a precision of temporal contrast. In this analysis, the detection occurred when temporal contrast reached a threshold contrast based on 3SDs above the mean baseline contrast of LOW expectation condition during 300ms prior to target onset. Detection gain was derived by subtracting the detection time of HIGH condition from the detection time of LOW condition for further analysis.

Results

1. Data summary

In this study, 45 and 27 single cells were recorded from two adult monkeys: DC (*Macaca mulatta*, 8-9 years old) and NB *(Maccaca fascicularis,* 8-9 years old). The temporal expectation paradigm was new to both monkeys and each monkey took several months to be acquainted for the current paradigm. The mean recording depth from the dura surface was 1.725±0.496mm for monkey DC, 1.1784±0.314mm for monkey NB. The mean eccentricities of the RFs were 3.832°±0.735° for monkey DC and 2.75°±0.23° for monkey NB.

2. Temporal expectation effect on behavior

2.1 Example of a training session

Figure 42 illustrates the training effect of HIGH expectation condition (Figure 42A) and LOW expectation condition (Figure 42B), showing as an example session result. The results show significantly reduced saccadic latency for HIGH condition than LOW, and the latency difference between two conditions 20ms

(p=0.0025, two-sample t-test). Such effect was consistent through stimulus intensity (contrasts), as well as saccadic directions (refer to Figure 43). These behavioral results confirm that the monkeys were well trained with the task.

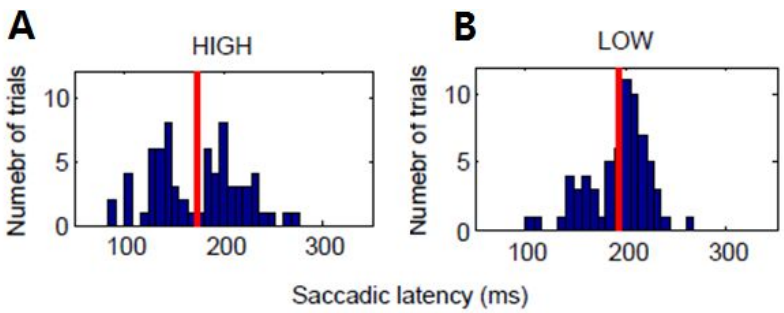

Figure 42. **Example of a training session result**. Saccadic latency (ms) from a session showing HIGH expectation (A) and LOW expectation (B) condition. The mean latency for HIGH is 173±43.99ms and LOW is 193±30.54ms (two-sample t-test, p= 0.0025). Note that the stimulus contrast was 32%, and contralateral saccade direction trials for this session. Other (16% or 8%) contrasts and ipsilateral/contralateral saccade directions showed the same behavioral effect (refer to Figure 43).

2.2 Expectation effect on behavior

Figure 43 illustrates expectation effect on behavior for all sessions. Figure 43A shows results with saccadic direction made to contralateral side. The latency difference between HIGH (160.23±43.9ms) and LOW (180.55±29.17ms) expectation condition was 20.32ms ($p<0.00$) with 32% stimulus contrast. For the stimulus contrasts of 16% and 8%, the difference was also significantly different (difference, 9.05ms ($p<10^{-10}$), 10.8ms ($p<0.00$, two-sample t-test), respectively). Figure 43B shows expectation effect when the saccadic was made toward ipsilateral side. The difference of the latency between HIGH and LOW condition was 24.31ms, 3.57ms, 22.40ms for stimulus contrasts of 32%, 16%, and 8%, respectively (all conditions were statistically significant with two-sample t-test). The difference was little smaller for 16% contrast (=3.57ms) but the p-value for this condition was still significant ($p<0.001$). Overall, the expectation effect was shown from behavior of all subjects, all stimulus contrasts and both of saccade directions (contralateral vs. ipsilateral); saccadic latency was significantly reduced in the HIGH with respect to LOW conditions (refer to Table 3 for each subject results).

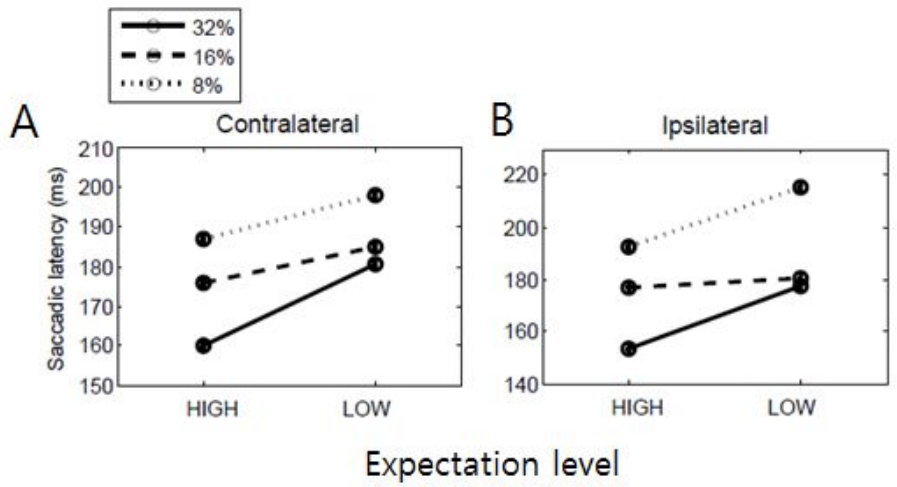

Figure 43. **Population summary of temporal expectation effect on behavior**. **A**. Mean saccadic latency (ms) toward contralateral side plotted on the y-axis; HIGH and LOW expectation conditions on the x-axis. Different contrasts were marked (refer to the asterisk at the top). **B**. Same convention as A, but the saccadic was made toward ipsilateral direction.

Subject	DC							
Number of cells	45							
Stimulus contrasts tested	32%				8%			
Expectation Level	HIGH		LOW		HIGH		LOW	
Saccadic direction*	C**	I**	C	I	C**	I**	C	I
Saccadic latency (ms)	160.23 (±43.9)	153.45 (±38.6)	180.56 (±29.2)	177.76 (±42.2)	187.06 (±37.79)	192.76 (±43.4)	197.86 (±28.9)	215.25 (±42.1)

Subject	IR			
Number of cells	27			
Stimulus contrasts tested	16%			
Expectation Level	HIGH		LOW	
Saccadic direction*	C**	I**	C	I
Saccadic latency (ms)	175.97 (±36.4)	176.68 (±31.57)	185.02 (±45.3)	180.25 (±31.09)

*Saccadic direction:
C, Contralateral, I, Ipsilateral
** Two-sample t-test between HIGH vs. LOW $p<0.05$

Table 3. **Summary for temporal expectation effect on behavior**.

Note that only 32% and 8% stimulus contrasts were used for monkey DC, and 16% for monkey IR (Table 3).

3. Temporal expectation effect on physiology

3.1 Representative cell activity

3.1.1 Representative cell activity- contralateral to the target

Figure 44 illustrates mean spike density difference between HIGH and LOW expectation conditions with contralateral to the target. Interestingly, stimulus contrasts of both 32% (Figure 44A) and 8 % (Figure 44B) showed spontaneous levels significantly suppressed prior to the target onset time. The mean density difference between HIGH and LOW was 7.4spikes/s during -400 to -100ms prior to target onset ($p=0.0091$) for 32% stimulus condition. For 8% contrast condition, the difference between HIGH and LOW was 8.99spikes/s during -250 to 0ms prior to target onset ($p=0.0087$). Although the significant time window differs between stimulus contrasts, the mean spike density difference between HIGH and LOW condition is strikingly high. Accordingly, the saccade latency difference was also significantly faster for HIGH than LOW condition (difference, 13.94ms, $p=0.002$) for stimulus contrast of 32% (Figure 44A) and 14.7ms ($p=0.0031$) for stimulus contrast of 8% (Figure 44B).

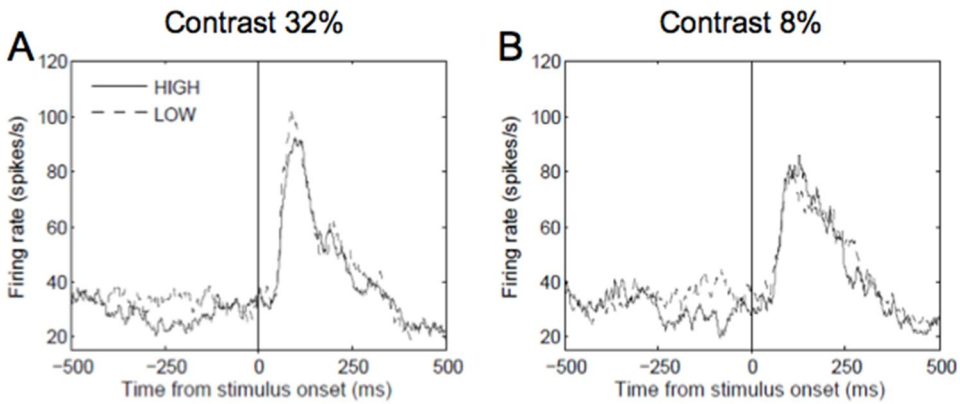

Figure 44. **Representative cell activity**; contralateral to the target **A**. Mean spike density aligned to the time from target onset, contralateral to the target for stimulus contrast of 32%. The mean density between HIGH (solid line) and LOW (dashed line) expectation condition was significantly different (-400:-100ms prior to target onset, p=0.0091, two-sample t-test). Mean spike density aligned as same convention as A for stimulus contrast 8%. The mean density between HIGH and LOW expectation conditions for this stimulus condition was also significant (-250:0ms prior to target onset, p=0.0087, two-sample t-test). Note that the above example cell is from monkey DC and only stimulus contrasts of 32% and 8% were performed for this subject.

3.1.2 Representative cell activity- ipsilateral to the target

Figure 45 illustrates the same cell as shown in Figure 44, but the mean spike density for the ipsilateral target. Figure 45A indicates stimulus contrast of 32%, showing marginal difference in spike density between HIGH and LOW condition prior to the target onset (p=0.22). Also, the time course of significant window

between the two conditions is shorter than that was shown in Figure 44A (refer to the black horizontal bar). When the stimulus contrast was 8%, the mean spike density was larger between HIGH and LOW (Figure 45B, -250 to 0ms prior to target onset, $p<0.05$). Along the suppression of spontaneous discharge prior to target onset, saccadic latency reduction occurred for the ipsilateral to the target as well. For the stimulus contrast of 32%, and 8%, the saccadic latency difference was 14.84ms, and 26.81ms, respectively, $p<0.05$).

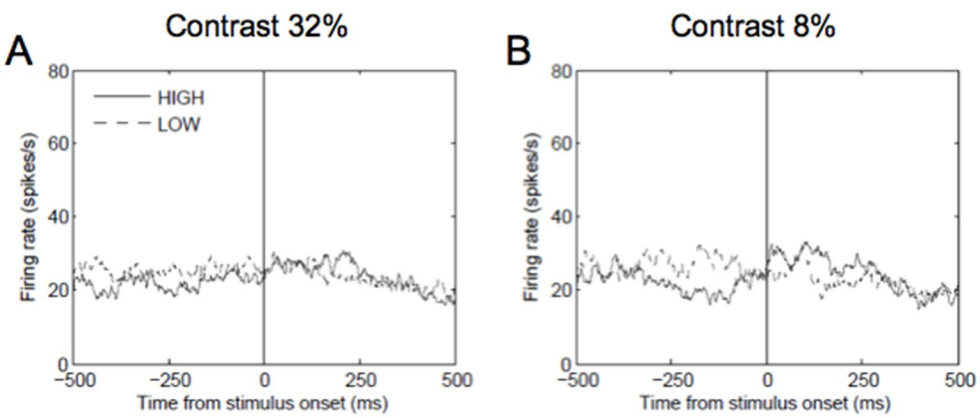

Figure 45. **Representative cell activity**; ipsilateral to the target. **A-B**. Mean spike density aligned to the time from target onset, contralateral to the target for stimulus contrast of 32% (A) and 8% (B). The same convention as Figure 44.

3.2 Population Summary

Figure 46 illustrates the spike density averaged over all 74 single cells. Spike density of each trial was normalized to the maximum firing rate within a cell. Since the suppressive response in HIGH condition during spontaneous discharge prior to the target onset time shown in Figure 46 seems invariant to stimulus contrast, in the Figure 46, all the stimulus contrasts were normalized within a cell with the maximum firing rate during 50 to 150ms after stimulus onset. Figure 46 represents mean spike density when the target was presented on the ipsilateral side (46A) and contralateral side (46B). The averaged density level between HIGH (black line) and LOW (red line) was significantly different (two-sample t-test for every 1ms with correction for multiple comparison with false discovery rate, marked with magenta symbols, Figure 46A, B). Overall, in HIGH condition, spontaneous discharge of V1 activity was suppressed compared to LOW conditions prior to target onset along the significant reduction of saccade latency.

Subject	DC				IR	
Stimulus contrast	32%		8%		16%	
Saccadic direction	C*	I*	C*	I*	C*	I*
% Suppressed (HIGH-LOW)	-19.1± 3.4	-13.4± 4.05	-15.6± 3.18	-14.2± 2.62	-6.4± 3.8	-4.4± 2.94

*paired-sample t-test, $p<0.05$

Table 4. **Summary for suppression % change during pre-stimulus period (HIGH-LOW)**

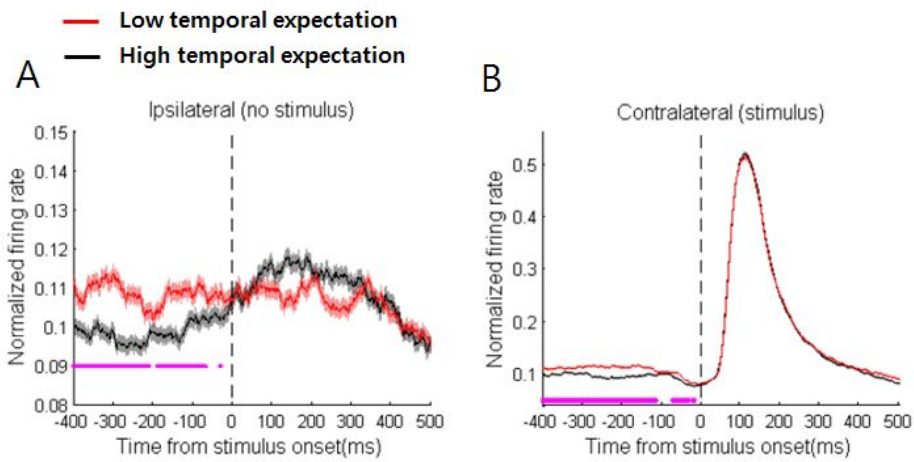

Figure 46. Summary of 72 single cells, (DC=45, IR=27) averaged trials. All density trials were normalized to the maximum firing rate within a cell. **A**. Mean spike density ipsilateral to the target, aligned to the time from target onset (ms). Black trace is HIGH, and red trace is LOW condition. Shades indicate 1SE. Statistically significant time course between HIGH and LOW density were marked with the magenta color dot. **B**. Mean spike density aligned to the time from target onset, contralateral to the target. The same convention as A. The significance tests were corrected for multiple comparisons. Dashed black lines in A and B indicate

the time of target onset.

4. Detection facilitation in temporal expectation

The distinctive result of temporal expectation effect on V1 activity is suppressive response during spontaneous period prior to target onset (Figure 46 A, B) on both ipsilateral and contralateral side. In order to check the role of such large suppression during HIGH expectation condition, analysis on detection contrast was derived (see *Methods*) onto the spike activity in response to contralateral target side. Figure 47 (upper) shows averaged spike density of HIGH (black) and LOW (red) condition of all 74 cells. After computing temporal contrast with 100ms of tau (analysis width) using the averaged densities, the detection gain (difference in detection time between LOW and HIGH) came out to be 5ms (Figure 47, lower), which looks little marginal in the plot, and yet, positive number indicates HIGH condition density level rose 5ms faster than LOW condition density level from spontaneous discharge.

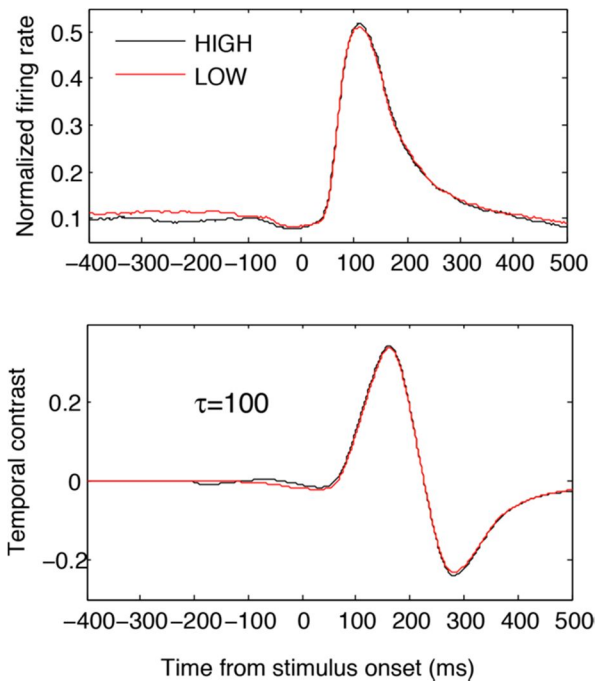

Figure 47. **Temporal contrast**. Averaged spike density from HIGH (black trace) and LOW (red trace) plotted as time from stimulus onset (ms), upper panel. All the trials were normalized with the maximum firing rate within a cell. The detection contrast computed using 100ms tau (lower panel). In this case, the detection gain is 5ms; earlier detection occurred for HIGH condition compared to LOW condition.

In Figure 48, the same analysis was performed as done in Figure 47 (lower panel, detection gain) with wider range of analysis window width from 1 to 250ms with 1ms step. As results, throughout all ranges of analysis widths, the detection occurred earlier (indicated by positive values in y-axis) in HIGH compare to LOW expectation condition. Note that at the tau of 200ms, the detection gain was the highest.

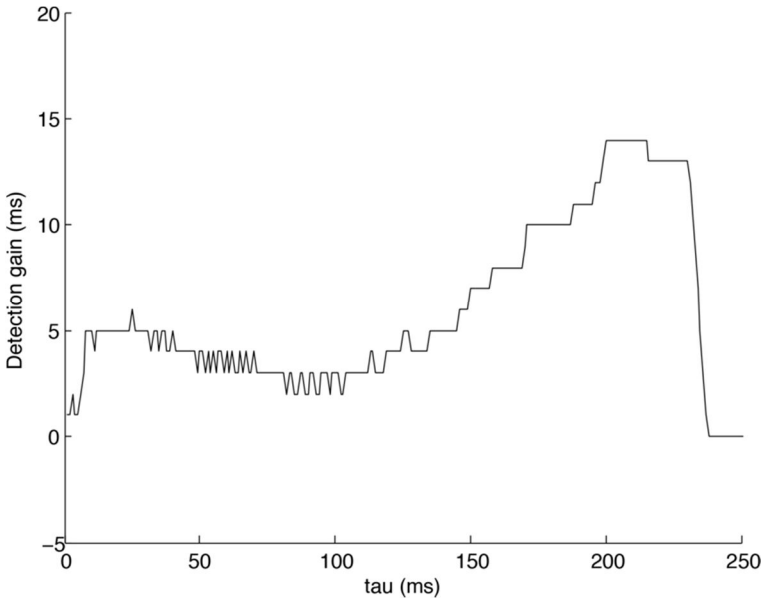

Figure 48. **Detection gain (ms) with ranges of analysis window**. Detection gain (ms, y-axis) was computed with variable tau (x-axis) of detection contrast.

Discussion

1. Role of suppression during pre-target period

To summarize, we found that saccade latency was significantly reduced in the HIGH with respect to LOW conditions on all stimulus contrasts tested (32%, 16%, 8%). For V1 activity, in HIGH condition, spontaneous discharge of V1 was

significantly suppressed compared to LOW condition prior to target onset, on both contralateral and ipsilateral hemispheres. As our main results, detection facilitation occurred earlier in HIGH compared to LOW over a wide range of analysis window width. Overall, our results demonstrate that single neurons in V1 are modulated by temporal expectation of upcoming target, which eventually influences saccadic reaction time.

1.1 Suppression as a top-down contextual gating

The suppression of spike density started hundreds of milliseconds prior to target onset on both hemispheres (Figure 46A, B). Such a time course of suppression was not likely due to the stimulus driven process but may imply slow process of 'top-down contextual gating' from temporal expectation of upcoming target that was previously suggested by Lee et al., (2013). During the experiment, the fixation duration for HIGH expectation was either 400ms during the earlier phase of the experiments, and 700ms for later sessions. Therefore, the subject was in direct control of fixation duration waiting until the target appears for making a saccadic eye movement.

One of the distinctive results in our experiment was the increase in temporal contrast with the suppression on the contralateral side, which would enhance information on upcoming target stimulus (Figure 47) for HIGH expectation condition,

thus, shortening detection latency as reported previously (Coull & Nobre, 1998)

1.2 Suppression on both hemispheres

An intriguing result from our experiment is that the temporal expectation effect was also reflected in the ipsilateral side where stimulus-driven visual response was absent (Figure 46A). This substantiates that the temporal expectation as a feed-back signal is more globally manifested within V1, which is contrasted with the pattern of activity change accompanying spatial attention effect where response strength is increased to the response confined to the RF (Fries, Reynolds, Rorie, & Desimone, 2001; Fries, Womelsdorf, Oostenveld, & Desimone, 2008; Ghose & Maunsell, 2002). Consistent with this, the global and spatially non-selective (central and peripheral regions) modulation of V1 gamma activity from expectation effect was reported previously (Lima, Singer, & Neuenschwander, 2011). The study reported by Lima et al (2011) focused on the frequency power and coherence of gamma responses between LFP and spike activity implementing much different experimental paradigm from ours. In their study, the monkeys had to release a lever to the time of fixation point change where the timing of this fixation point change was cued by visual stimulus with fixed (high expectation) or variable (low expectation) changes between plaids and gratings. The behavioral protocols they used required longer period of time for a trial that they measured the response change of the stimulus constantly presented on both peripheral and central visual fields while

monkeys internally perceived the temporal expectation toward the initiation of fixation point change. The 'global' and 'spatially non-selective' effect stated by this study meant to be restricted to one hemisphere, whereas our study put an emphasis of 'global' as it's meant to be on both hemispheres.

Implications of the studies

The local field potential, the signal that was examined in addition to spike activity in the above studies, has been attempted to link with sensory stimuli and growing number of studies have tried to find relationship between LFP and cell activity. The signal is known to be involved in cognitive processes such as attention, memory and perception and even suggested to be useful for the control of cortical motor prostheses (Spinks, Kraskov, Brochier, Umilta, & Lemon, 2008). In the mean time, the non-invasive fMRI BOLD signal and its relationship with spike activity and LFP is on-to-spot among neuroscientists. However, the mechanism generating LFP signal is not known and finding out what's under the local circuitry and what role the signal takes in the course of neural network will be a huge impact in this field of study.

Single cell recording consumes a lot of time and many complicated processes, and above all, it is invasive. It means there is a problem that we can only

look at the results from limited experimental paradigms. Subjects with higher intelligence than primates can hardly be involved in this type of study. Even though all different signals complement with their own merits, being able to answer such questions asked in this thesis and revealing the mechanisms underlying the relationship between those signal processing in terms of local circuitry may allow us disclose brain activity more deeply and thoroughly. Although there are many issues to concern, working on this notion will finally bring a superb improvement in technology and science itself; in which I believe will happen someday soon.

In study 2, the role of V1 activity upon the processes in superior colliculus (SC) where executes saccadic eye movements has been hypothesized to take a significant functional part in perceptual decision process with the underlying local circuit such as horizontal connection that would facilitate or inhibit the cell activity by means of surround interaction. V1 encodes sensory information and it is probably the most well-understood part among the brain regions. However, in electrophysiology, it is sill questionable whether V1 cell activity reflects perceptual state, such as binocular rivalry, or other tasks involved in perceptual decision-making processes (Gail, 2004). In order to answer the question, I think there should be neither starting nor ending point in the context of perception and cognition. It may take variety of experimental techniques depending on questions. However, what was revealed from these studies provides more detailed and rigorous sketch in neural circuitry, even though further studies should be continued in a near future.

References

Allman, J., Miezin, F., & McGuinness, E. (1985). Direction- and velocity-specific responses from beyond the classical receptive field in the middle temporal visual area (MT). *Perception, 14*(2), 105-126.

Anastassiou, C. A., Perin, R., Markram, H., & Koch, C. (2011). Ephaptic coupling of cortical neurons. *Nat Neurosci, 14*(2), 217-223. doi: 10.1038/nn.2727

Angelucci, A., & Bressloff, P. C. (2006). Contribution of feedforward, lateral and feedback connections to the classical receptive field center and extra-classical receptive field surround of primate V1 neurons. *Prog Brain Res, 154*, 93-120. doi: 10.1016/S0079-6123(06)54005-1

Bair, W., Cavanaugh, J. R., & Movshon, J. A. (2003). Time course and time-distance relationships for surround suppression in macaque V1 neurons. *J Neurosci, 23*(20), 7690-7701.

Bair, W., Cavanaugh, J. R., Smith, M. A., & Movshon, J. A. (2002). The timing of response onset and offset in macaque visual neurons. *J Neurosci, 22*(8), 3189-3205.

Baluch, F., & Itti, L. (2011). Mechanisms of top-down attention. *Trends in neurosciences, 34*(4), 210-224.

Benucci, A., Frazor, R. A., & Carandini, M. (2007). Standing waves and traveling waves distinguish two circuits in visual cortex. *Neuron, 55*(1), 103-117.

Berens, P., Keliris, G. A., Ecker, A. S., Logothetis, N. K., & Tolias, A. S. (2008). Feature selectivity of the gamma-band of the local field potential in primate primary visual cortex. *Front Neurosci, 2*(2), 199-207. doi:

10.3389/neuro.01.037.2008

Boch, R., Fischer, B., & Ramsperger, E. (1984). Express-saccades of the monkey: reaction times versus intensity, size, duration, and eccentricity of their targets. *Exp Brain Res, 55*(2), 223-231.

Bokil, H., Andrews, P., Kulkarni, J. E., Mehta, S., & Mitra, P. P. (2010). Chronux: a platform for analyzing neural signals. *J Neurosci Methods, 192*(1), 146-151.

Bompas, A., Sumner, P., Muthumumaraswamy, S. D., Singh, K. D., & Gilchrist, I. D. (2015). The contribution of pre-stimulus neural oscillatory activity to spontaneous response time variability. *NeuroImage, 107C*, 34-45. doi: 10.1016/j.neuroimage.2014.11.057

Bosman, C. A., Womelsdorf, T., Desimone, R., & Fries, P. (2009). A microsaccadic rhythm modulates gamma-band synchronization and behavior. *The journal of neuroscience, 29*(30), 9471-9480.

Brainard, D. H. (1997). The psychophysics toolbox. *Spatial vision, 10*, 433-436.

Bringuier, V. (1999). Horizontal Propagation of Visual Activity in the Synaptic Integration Field of Area 17 Neurons. *Science, 283*(5402), 695-699. doi: 10.1126/science.283.5402.695

Burns, S. P., Xing, D., & Shapley, R. M. (2010). Comparisons of the dynamics of local field potential and multiunit activity signals in macaque visual cortex. *J Neurosci, 30*(41), 13739-13749. doi: 10.1523/JNEUROSCI.0743-10.2010

Burt, P., & Sperling, G. (1981). Time, distance, and feature trade-offs in visual apparent motion. *Psychol Rev, 88*(2), 171.

Buzsaki, G., Anastassiou, C. A., & Koch, C. (2012). The origin of extracellular fields and currents--EEG, ECoG, LFP and spikes. *Nature reviews. Neuroscience,*

13(6), 407-420. doi: 10.1038/nrn3241

Buzsaki, G., & Draguhn, A. (2004). Neuronal oscillations in cortical networks. *Science, 304*(5679), 1926-1929. doi: 10.1126/science.1099745

Cardin, J. A., Carlen, M., Meletis, K., Knoblich, U., Zhang, F., Deisseroth, K., . . . Moore, C. I. (2009). Driving fast-spiking cells induces gamma rhythm and controls sensory responses. *Nature, 459*(7247), 663-667. doi: 10.1038/nature08002

Carpenter, R. (2001). Express saccades: is bimodality a result of the order of stimulus presentation? *Vision Res, 41*(9), 1145-1151.

Carpenter, R. H. (1988). *Movements of the eyes (2nd rev*: Pion Limited.

Cavanaugh, J. R., Bair, W., & Movshon, J. A. (2002). Selectivity and spatial distribution of signals from the receptive field surround in macaque V1 neurons. *J Neurophysiol, 88*(5), 2547-2556. doi: 10.1152/jn.00693.2001

Chen, M., Liu, Y., Wei, L., & Zhang, M. (2013). Parietal cortical neuronal activity is selective for express saccades. *The Journal of neuroscience : the official journal of the Society for Neuroscience, 33*(2), 814-823. doi: 10.1523/JNEUROSCI.2675-12.2013

Coull, J. T., & Nobre, A. C. (1998). Where and when to pay attention: the neural systems for directing attention to spatial locations and to time intervals as revealed by both PET and fMRI. *The Journal of neuroscience : the official journal of the Society for Neuroscience, 18*(18), 7426-7435.

Cravo, A. M., Rohenkohl, G., Wyart, V., & Nobre, A. C. (2013). Temporal expectation enhances contrast sensitivity by phase entrainment of low-frequency oscillations in visual cortex. *The Journal of neuroscience : the*

official journal of the Society for Neuroscience, 33(9), 4002-4010. doi: 10.1523/JNEUROSCI.4675-12.2013

Das, A., & Gilbert, C. D. (1995). Long-range horizontal connections and their role in cortical reorganization revealed by optical recording of cat primary visual cortex. *Nature, 375*(6534), 780-784.

Dick, S., Kathmann, N., Ostendorf, F., & Ploner, C. J. (2005). Differential effects of target probability on saccade latencies in gap and warning tasks. *Experimental brain research. Experimentelle Hirnforschung. Experimentation cerebrale, 164*(4), 458-463. doi: 10.1007/s00221-005-2266-1

Dorris, M. C., & Munoz, D. P. (1995). A neural correlate for the gap effect on saccadic reaction times in monkey. *J Neurophysiol, 73*(6), 2558-2562.

Dorris, M. C., Pare, M., & Munoz, D. P. (1997). Neuronal activity in monkey superior colliculus related to the initiation of saccadic eye movements. *J Neurosci, 17*(21), 8566-8579.

Dorris, M. C., Pare, M., & Munoz, D. P. (2000). Immediate neural plasticity shapes motor performance. *J Neurosci, 20*(1), 1-5.

Drewes, J., & VanRullen, R. (2011). This is the rhythm of your eyes: the phase of ongoing electroencephalogram oscillations modulates saccadic reaction time. *The Journal of neuroscience : the official journal of the Society for Neuroscience, 31*(12), 4698-4708. doi: 10.1523/JNEUROSCI.4795-10.2011

Edelman, J. A., & Keller, E. L. (1998). Dependence on target configuration of express saccade-related activity in the primate superior colliculus. *Journal of Neurophysiology, 80*(3), 1407-1426.

Everling, S., Krappmann, P., Spantekow, A., & Flohr, H. (1997). Influence of pre-target cortical potentials on saccadic reaction times. *Exp Brain Res, 115*(3), 479-484.

Fischer, B., & Boch, R. (1983). Saccadic eye movements after extremely short reaction times in the monkey. *Brain Res, 260*(1), 21-26.

Fischer, B., & Breitmeyer, B. (1987). Mechanisms of visual attention revealed by saccadic eye movements. *Neuropsychologia, 25*(1A), 73-83.

Fischer, B., & Ramsperger, E. (1984). Human express saccades: extremely short reaction times of goal directed eye movements. *Experimental brain research. Experimentelle Hirnforschung. Experimentation cerebrale, 57*(1), 191-195.

Fregnac, Y., Baudot, P., Chavane, F., Marre, O., Monier, C., Pananceau, M., & Sadoc, G. (2009). Multiscale functional imaging: reconstructing network dynamics from the synaptic echoes recorded in a single visual cortex neuron. *Bull Acad Natl Med, 193*(4), 851-862.

Fries, P., Reynolds, J. H., Rorie, A. E., & Desimone, R. (2001). Modulation of oscillatory neuronal synchronization by selective visual attention. *Science, 291*(5508), 1560-1563.

Fries, P., Womelsdorf, T., Oostenveld, R., & Desimone, R. (2008). The effects of visual stimulation and selective visual attention on rhythmic neuronal synchronization in macaque area V4. *The journal of neuroscience, 28*(18), 4823-4835.

Frohlich, F., & McCormick, D. A. (2010). Endogenous electric fields may guide neocortical network activity. *Neuron, 67*(1), 129-143. doi: 10.1016/j.neuron.2010.06.005

Gail, A. (2004). Perception-related Modulations of Local Field Potential Power and Coherence in Primary Visual Cortex of Awake Monkey during Binocular Rivalry. *Cerebral Cortex, 14*(3), 300-313. doi: 10.1093/cercor/bhg129

Galindo-Leon, E. E., & Liu, R. C. (2010). Predicting stimulus-locked single unit spiking from cortical local field potentials. *J Comput Neurosci, 29*(3), 581-597. doi: 10.1007/s10827-010-0221-z

Gaucher, Q., Edeline, J. M., & Gourevitch, B. (2012). How different are the local field potentials and spiking activities? Insights from multi-electrodes arrays. *J Physiol Paris, 106*(3-4), 93-103. doi: 10.1016/j.jphysparis.2011.09.006

Ghose, G. M., & Maunsell, J. H. (2002). Attentional modulation in visual cortex depends on task timing. *Nature, 419*(6907), 616-620.

Gilbert, C. D., & Wiesel, T. N. (1989). Columnar specificity of intrinsic horizontal and corticocortical connections in cat visual cortex. *The journal of neuroscience, 9*(7), 2432-2442.

Goense, J. B., & Logothetis, N. K. (2008). Neurophysiology of the BOLD fMRI signal in awake monkeys. *Curr Biol, 18*(9), 631-640. doi: 10.1016/j.cub.2008.03.054

Goris, R. L., Movshon, J. A., & Simoncelli, E. P. (2014). Partitioning neuronal variability. *Nat Neurosci, 17*(6), 858-865.

Gray, C. M., & Singer, W. (1989). Stimulus-specific neuronal oscillations in orientation columns of cat visual cortex. *Proceedings of the National Academy of Sciences, 86*(5), 1698-1702.

Grinvald, A., Lieke, E. E., Frostig, R. D., & Hildesheim, R. (1994). Cortical point-spread function and long-range lateral interactions revealed by real-time

optical imaging of macaque monkey primary visual cortex. *J Neurosci, 14*(5 Pt 1), 2545-2568.

Guan, S., Liu, Y., Xia, R., & Zhang, M. (2012). Covert attention regulates saccadic reaction time by routing between different visual-oculomotor pathways. *J Neurophysiol, 107*(6), 1748-1755. doi: 10.1152/jn.00082.2011

Hafed, Z. M., Lovejoy, L. P., & Krauzlis, R. J. (2011). Modulation of microsaccades in monkey during a covert visual attention task. *The journal of neuroscience, 31*(43), 15219-15230.

Haider, B., Duque, A., Hasenstaub, A. R., Yu, Y., & McCormick, D. A. (2007). Enhancement of visual responsiveness by spontaneous local network activity in vivo. *J Neurophysiol, 97*(6), 4186-4202. doi: 10.1152/jn.01114.2006

Haider, B., Hausser, M., & Carandini, M. (2013). Inhibition dominates sensory responses in the awake cortex. *Nature, 493*(7430), 97-100. doi: 10.1038/nature11665

Haider, B., Krause, M. R., Duque, A., Yu, Y., Touryan, J., Mazer, J. A., & McCormick, D. A. (2010). Synaptic and network mechanisms of sparse and reliable visual cortical activity during nonclassical receptive field stimulation. *Neuron, 65*(1), 107-121. doi: 10.1016/j.neuron.2009.12.005

Hamm, J. P., Dyckman, K. A., Ethridge, L. E., McDowell, J. E., & Clementz, B. A. (2010). Preparatory activations across a distributed cortical network determine production of express saccades in humans. *J Neurosci, 30*(21), 7350-7357. doi: 10.1523/JNEUROSCI.0785-10.2010

Hasenstaub, A., Sachdev, R. N., & McCormick, D. A. (2007). State changes rapidly modulate cortical neuronal responsiveness. *The Journal of neuroscience : the official journal of the Society for Neuroscience, 27*(36), 9607-9622. doi:

10.1523/JNEUROSCI.2184-07.2007

Haslinger, R., Pipa, G., Lima, B., Singer, W., Brown, E. N., & Neuenschwander, S. (2012). Context matters: the illusive simplicity of macaque V1 receptive fields. *PLoS ONE, 7*(7), e39699. doi: 10.1371/journal.pone.0039699

Henry, C. A., Joshi, S., Xing, D., Shapley, R. M., & Hawken, M. J. (2013a). Functional characterization of the extraclassical receptive field in macaque V1: contrast, orientation, and temporal dynamics. *J Neurosci, 33*(14), 6230-6242. doi: 10.1523/JNEUROSCI.4155-12.2013

Henry, C. A., Joshi, S., Xing, D., Shapley, R. M., & Hawken, M. J. (2013b). Functional characterization of the extraclassical receptive field in macaque V1: contrast, orientation, and temporal dynamics. *The Journal of neuroscience : the official journal of the Society for Neuroscience, 33*(14), 6230-6242. doi: 10.1523/JNEUROSCI.4155-12.2013

Horton, J. C., & Hoyt, W. F. (1991). The representation of the visual field in human striate cortex. A revision of the classic Holmes map. *Archives of ophthalmology, 109*(6), 816-824.

Ichida, J. M., Schwabe, L., Bressloff, P. C., & Angelucci, A. (2007). Response facilitation from the "suppressive" receptive field surround of macaque V1 neurons. *J Neurophysiol, 98*(4), 2168-2181. doi: 10.1152/jn.00298.2007

Isa, T. (2002). Intrinsic processing in the mammalian superior colliculus. *Curr Opin Neurobiol, 12*(6), 668-677.

Jancke, D., Chavane, F., Naaman, S., & Grinvald, A. (2004). Imaging cortical correlates of illusion in early visual cortex. *Nature, 428*(6981), 423-426.

Jia, X., Xing, D., & Kohn, A. (2013). No consistent relationship between gamma

power and peak frequency in macaque primary visual cortex. *The Journal of neuroscience : the official journal of the Society for Neuroscience, 33*(1), 17-25. doi: 10.1523/JNEUROSCI.1687-12.2013

Jin, Z., & Reeves, A. (2009). Attentional release in the saccadic gap effect. *Vision research, 49*(16), 2045-2055. doi: 10.1016/j.visres.2009.02.015

Jones, H., Grieve, K., Wang, W., & Sillito, A. (2001). Surround suppression in primate V1. *J Neurophysiol, 86*(4), 2011-2028.

Jones, J. P., & Palmer, L. A. (1987). An evaluation of the two-dimensional Gabor filter model of simple receptive fields in cat striate cortex. *J Neurophysiol, 58*(6), 1233-1258.

Kajikawa, Y., & Schroeder, C. E. (2011). How local is the local field potential? *Neuron, 72*(5), 847-858. doi: 10.1016/j.neuron.2011.09.029

Kapadia, M. K., Ito, M., Gilbert, C. D., & Westheimer, G. (1995). Improvement in visual sensitivity by changes in local context: parallel studies in human observers and in V1 of alert monkeys. *Neuron, 15*(4), 843-856.

Katzner, S., Nauhaus, I., Benucci, A., Bonin, V., Ringach, D. L., & Carandini, M. (2009). Local origin of field potentials in visual cortex. *Neuron, 61*(1), 35-41. doi: 10.1016/j.neuron.2008.11.016

Kim, T., & Freeman, R. D. (2014). Selective stimulation of neurons in visual cortex enables segregation of slow and fast connections. *Neuroscience, 274C*, 170-186. doi: 10.1016/j.neuroscience.2014.05.041

Kim, T., Kim, H. R., Kim, K., & Lee, C. (2012). Modulation of v1 spike response by temporal interval of spatiotemporal stimulus sequence. *PLoS ONE, 7*(10), e47543. doi: 10.1371/journal.pone.0047543

Kingstone, A., & Klein, R. M. (1993a). Visual offsets facilitate saccadic latency: does predisengagement of visuospatial attention mediate this gap effect? *Journal of Experimental Psychology: Human Perception and Performance, 19*(6), 1251.

Kingstone, A., & Klein, R. M. (1993b). What are human express saccades? *Perception & Psychophysics, 54*(2), 260-273.

Kraut, M. A., Arezzo, J. C., & Vaughan, H. G. (1985). Intracortical generators of the flash VEP in monkeys. *Electroencephalography and Clinical Neurophysiology/Evoked Potentials Section, 62*(4), 300-312.

Lashgari, R., Li, X., Chen, Y., Kremkow, J., Bereshpolova, Y., Swadlow, H. A., & Alonso, J. M. (2012). Response properties of local field potentials and neighboring single neurons in awake primary visual cortex. *The Journal of neuroscience : the official journal of the Society for Neuroscience, 32*(33), 11396-11413. doi: 10.1523/JNEUROSCI.0429-12.2012

Lee, J., Kim, H. R., & Lee, C. (2010). Trial-to-trial variability of spike response of V1 and saccadic response time. *J Neurophysiol, 104*(5), 2556-2572. doi: 10.1152/jn.01040.2009

Lee, J., Kim, K., Chung, S., & Lee, C. (2013). Suppression of spontaneous activity before visual response in the primate V1 neurons during a visually guided saccade task. *The Journal of neuroscience: the official journal of the Society for Neuroscience, 33*(9), 3760.

Levitt, J. B., & Lund, J. S. (2002). The spatial extent over which neurons in macaque striate cortex pool visual signals. *Vis Neurosci, 19*(4), 439-452.

Lima, B., Singer, W., & Neuenschwander, S. (2011). Gamma responses correlate with temporal expectation in monkey primary visual cortex. *J Neurosci,*

31(44), 15919-15931. doi: 10.1523/JNEUROSCI.0957-11.2011

Liu, J., & Newsome, W. T. (2006). Local field potential in cortical area MT: stimulus tuning and behavioral correlations. *J Neurosci, 26*(30), 7779-7790. doi: 10.1523/JNEUROSCI.5052-05.2006

Liu, Y. J., Hashemi-Nezhad, M., & Lyon, D. C. (2011). Dynamics of extraclassical surround modulation in three types of V1 neurons. *J Neurophysiol, 105*(3), 1306-1317. doi: 10.1152/jn.00692.2010

Logothetis, N. K., Kayser, C., & Oeltermann, A. (2007). In vivo measurement of cortical impedance spectrum in monkeys: implications for signal propagation. *Neuron, 55*(5), 809-823. doi: 10.1016/j.neuron.2007.07.027

Maier, A., Aura, C. J., & Leopold, D. A. (2011). Infragranular sources of sustained local field potential responses in macaque primary visual cortex. *The Journal of neuroscience : the official journal of the Society for Neuroscience, 31*(6), 1971-1980. doi: 10.1523/JNEUROSCI.5300-09.2011

Martinez-Conde, S., Macknik, S. L., & Hubel, D. H. (2000). Microsaccadic eye movements and firing of single cells in the striate cortex of macaque monkeys. *Nat Neurosci, 3*(3), 251-258.

Maunsell, J. H., & Van Essen, D. C. (1983). Functional properties of neurons in middle temporal visual area of the macaque monkey. I. Selectivity for stimulus direction, speed, and orientation. *J Neurophysiol, 49*(5), 1127-1147.

Mitzdorf, U. (1987). Properties of the evoked potential generators: current source-density analysis of visually evoked potentials in the cat cortex. *International Journal of Neuroscience, 33*(1-2), 33-59.

Mitzdorf, U., & Singer, W. (1978). Prominent excitatory pathways in the cat visual

cortex (A 17 and A 18): a current source density analysis of electrically evoked potentials. *Exp Brain Res, 33*(3-4), 371-394.

Munoz, D., Dorris, M., Pare, M., & Everling, S. (2000). On your mark, get set: brainstem circuitry underlying saccadic initiation. *Canadian journal of physiology and pharmacology, 78*(11), 934-944.

Nassi, J. J., & Callaway, E. M. (2009). Parallel processing strategies of the primate visual system. *Nat Rev Neurosci, 10*(5), 360-372. doi: 10.1038/nrn2619

Nauhaus, I., Busse, L., Carandini, M., & Ringach, D. L. (2009). Stimulus contrast modulates functional connectivity in visual cortex. *Nat Neurosci, 12*(1), 70-76. doi: 10.1038/nn.2232

Nauhaus, I., Busse, L., Ringach, D. L., & Carandini, M. (2012a). Robustness of traveling waves in ongoing activity of visual cortex. *J Neurosci, 32*(9), 3088-3094. doi: 10.1523/JNEUROSCI.5827-11.2012

Nienborg, H., & Cumming, B. G. (2014). Decision-related activity in sensory neurons may depend on the columnar architecture of cerebral cortex. *J Neurosci, 34*(10), 3579-3585. doi: 10.1523/JNEUROSCI.2340-13.2014

Nobre, A. C. (2001). Orienting attention to instants in time. *Neuropsychologia, 39*(12), 1317-1328.

Okun, M., Naim, A., & Lampl, I. (2010). The subthreshold relation between cortical local field potential and neuronal firing unveiled by intracellular recordings in awake rats. *The Journal of neuroscience : the official journal of the Society for Neuroscience, 30*(12), 4440-4448. doi: 10.1523/JNEUROSCI.5062-09.2010

Oswal, A., Ogden, M., & Carpenter, R. H. (2007). The time course of stimulus

expectation in a saccadic decision task. *J Neurophysiol, 97*(4), 2722-2730.

Ozen, S., Sirota, A., Belluscio, M. A., Anastassiou, C. A., Stark, E., Koch, C., & Buzsaki, G. (2010). Transcranial electric stimulation entrains cortical neuronal populations in rats. *The Journal of neuroscience : the official journal of the Society for Neuroscience, 30*(34), 11476-11485. doi: 10.1523/JNEUROSCI.5252-09.2010

Palmer, C., Cheng, S. Y., & Seidemann, E. (2007). Linking neuronal and behavioral performance in a reaction-time visual detection task. *J Neurosci, 27*(30), 8122-8137.

Pelli, D. G. (1997). The VideoToolbox software for visual psychophysics: Transforming numbers into movies. *Spatial vision, 10*(4), 437-442.

Polat, U., Mizobe, K., Pettet, M. W., Kasamatsu, T., & Norcia, A. M. (1998). Collinear stimuli regulate visual responses depending on cell's contrast threshold. *Nature, 391*(6667), 580-584. doi: 10.1038/35372

Pratt, J., Bekkering, H., Abrams, R. A., & Adam, J. (1999). The gap effect for spatially oriented responses. *Acta psychologica, 102*(1), 1-12.

Pratt, J., Lajonchere, C. M., & Abrams, R. A. (2006). Attentional modulation of the gap effect. *Vision research, 46*(16), 2602-2607.

Priebe, N. J., & Ferster, D. (2008). Inhibition, spike threshold, and stimulus selectivity in primary visual cortex. *Neuron, 57*(4), 482-497.

Quiroga, R. Q., & Panzeri, S. (2009). Extracting information from neuronal populations: information theory and decoding approaches. *Nature Reviews Neuroscience, 10*(3), 173-185.

Radman, T., Su, Y., An, J. H., Parra, L. C., & Bikson, M. (2007). Spike timing

amplifies the effect of electric fields on neurons: implications for endogenous field effects. *The Journal of neuroscience : the official journal of the Society for Neuroscience, 27*(11), 3030-3036. doi: 10.1523/JNEUROSCI.0095-07.2007

Rasch, M. J., Gretton, A., Murayama, Y., Maass, W., & Logothetis, N. K. (2008). Inferring spike trains from local field potentials. *J Neurophysiol, 99*(3), 1461-1476. doi: 10.1152/jn.00919.2007

Ray, S., & Maunsell, J. H. (2011). Network rhythms influence the relationship between spike-triggered local field potential and functional connectivity. *J Neurosci, 31*(35), 12674-12682. doi: 10.1523/JNEUROSCI.1856-11.2011

Reulen, J. P. (1984). Latency of visually evoked saccadic eye movements. II. Temporal properties of the facilitation mechanism. *Biol Cybern, 50*(4), 263-271.

Reuter-Lorenz, P. A., Hughes, H. C., & Fendrich, R. (1991). The reduction of saccadic latency by prior offset of the fixation point: an analysis of the gap effect. *Perception & Psychophysics, 49*(2), 167-175.

Richmond, B. J., Optican, L. M., Podell, M., & Spitzer, H. (1987). Temporal encoding of two-dimensional patterns by single units in primate inferior temporal cortex. I. Response characteristics. *J Neurophysiol, 57*(1), 132-146.

Robinson, D. A. (1963). A method of measuring eye movemnent using a scieral search coil in a magnetic field. *Bio-medical Electronics, IEEE Transactions on, 10*(4), 137-145.

Rodman, H. R., & Albright, T. D. (1987). Coding of visual stimulus velocity in area MT of the macaque. *Vision Res, 27*(12), 2035-2048.

Rohenkohl, G., Cravo, A. M., Wyart, V., & Nobre, A. C. (2012). Temporal expectation improves the quality of sensory information. *The Journal of neuroscience : the official journal of the Society for Neuroscience, 32*(24), 8424-8428. doi: 10.1523/JNEUROSCI.0804-12.2012

Rohrer, W. H., & Sparks, D. L. (1993). Express saccades: the effects of spatial and temporal uncertainty. *Vision Res, 33*(17), 2447-2460.

Rolfs, M., & Vitu, F. (2007). On the limited role of target onset in the gap task: support for the motor-preparation hypothesis. *J Vis, 7*(10), 7 1-20. doi: 10.1167/7.10.7

Rudolph, M., Pospischil, M., Timofeev, I., & Destexhe, A. (2007). Inhibition determines membrane potential dynamics and controls action potential generation in awake and sleeping cat cortex. *The Journal of neuroscience : the official journal of the Society for Neuroscience, 27*(20), 5280-5290. doi: 10.1523/JNEUROSCI.4652-06.2007

Rutishauser, U., Ross, I. B., Mamelak, A. N., & Schuman, E. M. (2010). Human memory strength is predicted by theta-frequency phase-locking of single neurons. *Nature, 464*(7290), 903-907. doi: 10.1038/nature08860

Saslow, M. G. (1967). Effects of components of displacement-step stimuli upon latency for saccadic eye movement. *Journal of the Optical Society of America, 57*(8), 1024-1029.

Sayer, R., Friedlander, M., & Redman, S. (1990). The time course and amplitude of EPSPs evoked at synapses between pairs of CA3/CA1 neurons in the hippocampal slice. *The journal of neuroscience, 10*(3), 826-836.

Sceniak, M. P., Hawken, M. J., & Shapley, R. (2001). Visual spatial characterization of macaque V1 neurons. *J Neurophysiol, 85*(5), 1873-1887.

Sceniak, M. P., Ringach, D. L., Hawken, M. J., & Shapley, R. (1999). Contrast's effect on spatial summation by macaque V1 neurons. *Nat Neurosci, 2*(8), 733-739.

Schiller, P. H., Sandell, J. H., & Maunsell, J. H. (1987). The effect of frontal eye field and superior colliculus lesions on saccadic latencies in the rhesus monkey. *J Neurophysiol, 57*(4), 1033-1049.

Schölvinck, M. L., Saleem, A. B., Benucci, A., Harris, K. D., & Carandini, M. (2015). Cortical State Determines Global Variability and Correlations in Visual Cortex. *The journal of neuroscience, 35*(1), 170-178.

Schroeder, C., Tenke, C., Givre, S., Arezzo, J., & Vaughan, H. (1991). Striate cortical contribution to the surface-recorded pattern-reversal VEP in the alert monkey. *Vision Res, 31*(7), 1143-1157.

Schroeder, C. E., & Lakatos, P. (2009). Low-frequency neuronal oscillations as instruments of sensory selection. *Trends in neurosciences, 32*(1), 9-18.

Schroeder, C. E., Mehta, A. D., & Givre, S. J. (1998). A spatiotemporal profile of visual system activation revealed by current source density analysis in the awake macaque. *Cerebral cortex, 8*(7), 575-592.

Series, P., Lorenceau, J., & Fregnac, Y. (2003). The "silent" surround of V1 receptive fields: theory and experiments. *J Physiol Paris, 97*(4-6), 453-474. doi: 10.1016/j.jphysparis.2004.01.023

Smith, F. W., & Muckli, L. (2010). Nonstimulated early visual areas carry information about surrounding context. *Proc Natl Acad Sci U S A, 107*(46), 20099-20103. doi: 10.1073/pnas.1000233107

Sparks, D., Rohrer, W., & Zhang, Y. (2000). The role of the superior colliculus in

saccade initiation: a study of express saccades and the gap effect. *Vision Res, 40*(20), 2763-2777.

Spinks, R. L., Kraskov, A., Brochier, T., Umilta, M. A., & Lemon, R. N. (2008). Selectivity for grasp in local field potential and single neuron activity recorded simultaneously from M1 and F5 in the awake macaque monkey. *J Neurosci, 28*(43), 10961-10971. doi: 10.1523/JNEUROSCI.1956-08.2008

Super, H. (2006). Figure-ground activity in V1 and guidance of saccadic eye movements. *J Physiol Paris, 100*(1-3), 63-69.

Supèr, H., van der Togt, C., Spekreijse, H., & Lamme, V. A. (2003). Internal state of monkey primary visual cortex (V1) predicts figure–ground perception. *The journal of neuroscience, 23*(8), 3407-3414.

Tinsley, C. J., & Everling, S. (2002). Contribution of the primate prefrontal cortex to the gap effect. *Progress in Brain Research, 140*, 61-72. doi: 10.1016/S0079-6123(02)40042-8

Todorović, D. (2010). Context effects in visual perception and their explanations. *Review of Psychology, 17*(1), 17-32.

Vinje, W. E., & Gallant, J. L. (2002). Natural stimulation of the nonclassical receptive field increases information transmission efficiency in V1. *J Neurosci, 22*(7), 2904-2915. doi: 20026216

Walker, G. A., Ohzawa, I., & Freeman, R. D. (1999). Asymmetric suppression outside the classical receptive field of the visual cortex. *J Neurosci, 19*(23), 10536-10553.

Wang, Y., Jin, J., Kremkow, J., Komban, S. J., Lashgari, R., & Alonso, J. M. (2013). *Vertical organization of spatial phase in cat primary visual cortex.* Paper

presented at the Society for Neuroscience, San Diego.

Weiss, S. A., & Faber, D. S. (2010). Field effects in the CNS play functional roles. *Frontiers in neural circuits, 4*, 15. doi: 10.3389/fncir.2010.00015

Xing, D., Yeh, C.-I., Burns, S., & Shapley, R. M. (2012). Laminar analysis of visually evoked activity in the primary visual cortex. *Proceedings of the National Academy of Sciences, 109*(34), 13871-13876.

Xing, D., Yeh, C. I., & Shapley, R. M. (2009). Spatial spread of the local field potential and its laminar variation in visual cortex. *J Neurosci, 29*(37), 11540-11549. doi: 10.1523/JNEUROSCI.2573-09.2009

국문초록

원숭이 1차시각피질의 신경활동: 맥락에 따른 활동수준조절과 안구운동 발생에서의 역할

서울대학교 사회과학 대학원
심리학과 생물심리 전공
김 가 연

1차시각피질(V1)은 중추 시각처리의 주요 피질영역이다. V1의 신경활동은 수용장 내에 제시되는 자극으로 유발되지만, 다양한 맥락들이 역동적으로 반응을 조절한다. 시각처리의 역동절 조절 현상과 그 신경적 기반을 이해하는 것은 중요하지만, V1 내의 정확한 신경 기전은 완전히 알려져 있지 않다.

본 논문에서는 세 개의 실험을 통해서 지각적, 인지적 과정에 관련된 맥락들이 V1 세포 활동을 역동적으로 조절하는 현상을 다루었다. 특히 도약안구운동의 발생에 즈음한 V1 세포활동의 조절에 초점을 맞추고, 과제를 수행하는 마카크 원숭이에서 단일 혹은 복수의 세포활동과 국소전위(LFP)를 채집, 분석하였다.

실험1에서는, 수용장 내의 자극에 대한 세포의 반응이 수용장 바깥

에 제시되는 자극에 의해서 조절되는 방식을 살폈다. RF 내외에 Gabor 자극을 제시하고 이에 따라 유발되는 활동전위와 국소전위의 특성을 분석하였다. 알려진 바대로, 수용장 외부의 자극은 그 자체로는 세포의 활동전위를 유발하지 않지만, 국소전위 반응을 일으켰다. 수용장외부 자극에 의해서 유발되는 이 역치하(subthreshold) 국소전위는 수용장 중심과 자극이 제시된 외부 위치와의 거리에 따라 그 정도는 감소하고 전위 발생의 잠재기는 증가하였다. 수용장 내외 자극간 시간차를 0-100ms 사이에서 조절함으로써, 수용장 내부자극에 대한 세포 반응이 외부자극에 의해서 조절되는 정도가 역차하의 국소전위변화의 조절 정도와 유의미한 상관을 보였으며, 역차하의 국소전위 신호가 수용장 외 자극의 시간차에 따라 활동전위 반응이 조절되는 것을 예측한다는 결과를 얻었다.

실험2에서는 V1의 활동조절을 간격도약과제(gap saccade task)를 사용하여 살폈다. 응시점이 사라지고 도약표적이 나타나기까지 시간적 간격을 주면 도약잠재기가 짧아지는 소위 간격효과를 보인다. 응시점은 도약표적에 반응하는 V1세포의 수용장 외부의 자극이므로, 본 실험에서는 V1 내의 시각 표상 간의 상호작용의 예로서 이를 다루었다. 시각탐지과제에서 원숭이가 보는 모니터의 응시점과 시각탐지 자극 간의 시간 간격이 커질수록 자극 탐지에 대한 반응 시간이 단축되는 간격효과를 관찰하였으며, 이에 수반하여 시각자극에 대한 V1 세포의 활동수준이 유의미하게 일찍, 그리고

강하게 변하는 것을 관찰하였다. 또한, 탐지표적자극이 제시되기 전후의 V1의 활동이 급속 및 정규 도약운동의 발생과 관련이 있음을 발견하였으며, 이는 응시점과 시각탐지 자극간의 시각표상에서의 상호작용으로 인해 시각탐지 자극이 나오는 시점에서의 V1 상태가 변하며, 이러한 변화가 결국 시각행동에 기여하는 것임을 시사한다.

실험3에서는 V1의 세포활동을 조절하는 상위 수준의 과정을 표적자극의 제시 시점에 대한 기대 수준을 직접 조작하여 살폈다. 이를 위해 응시점의 색에 따라 표적이 나타나는 시점의 예측 가능성을 달리하여 원숭이가 시각표적이 나타나는 시간에 대한 기대 수준을 달리할 수 있도록 훈련시켰다. 높은 기대 조건의 반응시간이 낮은 기대 조건의 반응시간보다 유의미하게 단축되었으며, 기대효과가 행동으로 나타나는 것을 관찰하였다. 기대효과의 결과로 V1 활동수준이 시각 탐지 자극이 나타나기 전의 수백 밀리세컨드 전부터 강하게 감소하는 것을 관찰하였으며, 이러한 활동 감소 패턴이 V1 의 양반구 에서 모두 나타났다. 이는 시각표적이 나타나는 시점에 대한 기대수준에 따라 V1 세포의 활동수준이 변하며, 이것이 시각행동을 조절함을 시사하는 결과이다.

주요어: 시각피질, 국소장-전위, 단세포 신경활동측정, 도약안구 운동, 반응시간, 자발적 변산성

학번 : 2009-20135